

GUIDANCE OF REGENERATING PERIPHERAL AXON SUBTYPES USING
MOLECULAR CUES

by

Sanjay Anand

APPROVED BY SUPERVISORY COMMITTEE:

Dr. Mario Romero-Ortega, Chair

Dr. Robert L. Rennaker II

Dr. Shalini Prasad

Dr. Michael P. Kilgard

Copyright 2017

Sanjay Anand

All Rights Reserved

This work is dedicated to all my loved ones. Without their support none of this
would be possible.

GUIDANCE OF FUNCTIONAL PERIPHERAL AXON SUBTYPES USING
MOLECULAR CUES

by

SANJAY ANAND, BS

DISSERTATION

Presented to the Faculty of
The University of Texas at Dallas
in Partial Fulfillment
of the Requirements
for the Degree of

DOCTOR OF PHILOSOPHY IN
BIOMEDICAL ENGINEERING

THE UNIVERSITY OF TEXAS AT DALLAS

May 2017

ACKNOWLEDGMENTS

Many individuals have contributed to this work, and without their help and support I would not be where I am today. This work is a small contribution to the growing field of science, and I hope that the compiled information will help others in the field.

I am very thankful to my advisor, Dr. Mario Romero-Ortega, who encouraged and supported me during the course of my training. From the beginning he assigned me as the lead for the DARPA project and got me off to a running start. As my mentor, he ensured that I receive comprehensive guidance in research, teaching, and communication skills. He has constantly pushed me to become a better version of myself and helped me to identify my limitations and improve upon them.

I would also like to thank my committee members for their guidance during my time here. Our multiple meetings enabled me to better understand my data and improve myself as a student. During the course of this work, a lot of individuals worked with me towards the accomplishment of this dissertation. Drs. Ed Keefer and Jonathan Cheng were immensely helpful in teaching me about electrophysiology and surgical skills for which I am truly thankful. My undergraduates Dianna Nguyen, Martin Tran, Nang Su Lwin Myint, Michael Tran, and Elaine Ramirez spent a lot of time and effort in helping me with data collection. Also, Vidhi Desai deserves a special thanks for being an awesome friend and spending countless hours with me in that tiny electrophys room. Also, the great friends I have made over the years, Swarup Dash, Srikanth Vasudevan, Ashwin Nair, Aswini Kanneganti, Nesreen Alsmadi, Geetanjali Bendale, and Eileen Shimizu have made this journey very entertaining and less stressful.

Finally, I would like to thank my family and wife who was with me from the beginning of this journey. Their support throughout helped to keep the stress of graduate life in check. My parents always supported me in everything I have done and I am forever grateful. My wife, Chandni Jindal, constantly supported me in my ups and down with her positive attitude and I am lucky to have her in my life.

November 2016

GUIDANCE OF FUNCTIONAL PERIPHERAL AXON SUBTYPES USING MOLECULAR CUES

Sanjay Anand, PhD
The University of Texas at Dallas, 2017

Supervising Professor: Mario Romero-Ortega, PhD

There are approximately 1.9 million amputees in the USA, and approximately 185,000 new amputations occur every year. Recent progress in robotic limbs provides the possibility of interfacing with the peripheral nerve to replicate natural sensory and motor functions of the human hand. While robotic prosthesis has advanced significantly, providing up to 22 degrees of freedom equipped with multiple sensors for position, temperature, and pressure, eliciting naturalistic sensation has yet to be achieved. Electrodes interfaced at the somatic peripheral nerves are intended to decode motor intent and elicit sensation through selective stimulation of sensory axons. However, current peripheral nerve interfacing technology elicits unnatural sensations through fascicular stimulation of mixed modality axon bundles. In addition, recording motor intent is more difficult due to the sparse arrangement of motor neurons. Therefore, peripheral nerve interfacing technology that selectively records motor activity and elicits naturalistic sensory percepts remains a challenge. This dissertation takes a unique approach to this problem by evaluating the use of molecular cues to selectively guide regenerating motor and

sensory axons into Y-shaped conduits to modulate the sensory to motor ratio of regenerative neural interfaces.

In Chapter 2 we tested the efficacy of single neurotrophic factors (NTFs) in modulating the sensory/motor axon ratio in using a Y-shaped nerve conduit. The functionality of the regenerated segments was confirmed by evoked compound nerve action potentials in 97% of the nerve fascicles. Retrograde labeling of ventral motor neurons showed that glial derived neurotrophic (GDNF) induced a 3-fold increase in motor neurons compared to bovine serum albumin (BSA) compartment, while sensory neuron regeneration showed no difference. The sensory/motor ratio however was not significantly altered by single molecular attractants.

In Chapter 3 we evaluated the response of regenerating axons using motor axon guidance molecules brain-derived neurotrophic factor (BDNF)/GDNF in one compartment and sensory axon attractants nerve growth factor (NGF) or pleiotrophin (PTN) in the adjacent arm. The combination of BDNF/GDNF versus PTN showed a significant ($p < 0.05$) change in the sensory/motor axon ratio between the nerve fascicles. In Chapter 4 we evaluated the effectiveness of Semaphorin3A, a nociceptive sensory axons molecular repellent, in combination with BDNF, an attractant for mechanoreceptors, in one regenerative chamber compared to an adjacent one containing NGF, an attractant for nociceptive axons. Sema3A significantly reduced the number of small myelinated axons compared to the BDNF only compartment, but also affected the NGF chamber, indicating cross-diffusion of the repellent to the other arm. In summary, this body of work supports the notion that molecular attractant cues are able to influence the regeneration of functional sensory/motor axons in nerve fascicles using a Y-conduit *in vivo*, in a nerve amputee model. Furthermore, chemorepellent molecules were shown to induce

an inhibitory effect on small myelinated axons for the first time in a peripheral nerve regeneration paradigm. Together, this work contributes to establish the feasibility of molecularly guided regenerative peripheral neural interfaces, and to define the potential of this technology towards achieving intuitive motor control and conveying natural feel to amputee users of advanced bionic limbs.

TABLE OF CONTENTS

ACKNOWLEDGMENTS	v
ABSTRACT.....	vii
LIST OF FIGURES	xiii
LIST OF TABLES	xviii
CHAPTER 1 INTRODUCTION	1
1.1 Organization and function of the PNS	8
1.2 Guidance of axons using molecular cues during development.....	9
1.3 Role of NTFs in survival and growth after peripheral nerve injury	12
1.4 Specificity of neurotrophins in axon regeneration and guidance.....	13
1.5 Research objective and dissertation organization	15
CHAPTER 2 ELECTROCOMPETENT REGENERATION OF BIFURCATED NERVE FASCICLES USING SINGLE GUIDANCE CUES	17
2.1 Introduction.....	17
2.2 Materials and Method	21
2.2.1 Microencapsulation of neurotrophic factors	21
2.2.2 DRG bioactivity assay.....	22
2.2.3 DRG <i>in vitro</i> immunocytochemistry	23
2.2.4 Y-tube nerve guide fabrication.....	25
2.2.5 Y-tube implantation into the transected sciatic nerve	26
2.2.6 Modeling MP-NTF release in Y-shaped conduits.....	29
2.2.7 Retrograde labeling and quantification of motor and sensory neurons.....	33
2.2.8 Compound Nerve Action Potentials (CNAP)	33
2.2.9 Histology	34
2.2.10 Quantification of retrograde labelled motor and sensory neurons	35
2.2.11 EM morphometric analysis	35
2.2.12 Statistical analysis	36
2.3 Results.....	36

2.3.1	Bifurcated nerve regeneration is comparable among all groups.	36
2.3.2	Regenerated nerve fascicles show electrical competency	39
2.3.3	Effect of single guidance cues on motor and sensory neuron regeneration.....	42
2.3.4	Single NTFs effect on axon morphology without distal end-organ targets 46	
2.4	Discussion	53
2.4.1	Regeneration in the absence of distal targets	54
2.4.2	NTF enrichment of sensory and motor neurons.....	54
2.4.3	NTF effect in sensory/motor ratio	56
2.4.4	Future directions.....	57
CHAPTER 3 MODULATION OF SENSORY/MOTOR RATIO USING MOLECULAR GUIDANCE CUES		58
3.1	Introduction.....	58
3.2	Materials and Method	61
3.2.1	PLGA encapsulation of NTFs and bioactivity test.....	61
3.2.2	Y-tube implantation to the heterogeneous mixed sciatic nerve	61
3.2.3	Analysis of the regenerated Y-Nerve	64
3.2.4	Statistical analysis	65
3.3	Results.....	65
3.3.1	Y-nerve regeneration in the presence of multiple NTFs	65
3.3.2	CNAP shows electrically competent Y-nerve regeneration.....	67
3.3.3	Effect of different combination of NTFs in motor and sensory regeneration.....	68
3.3.4	Normal axonal morphology maintained by combinations of NTFs.....	73
3.4	Discussion	79
3.4.1	Selectivity using combination of NTFs.....	80
3.4.2	Regenerative capacity of NTFs in combination.....	81
CHAPTER 4 SEMAPHORIN 3A INHIBITS SMALL DIAMETER AXONS IN A CHOICE ASSAY WITH BDNF AND NGF MOLECULAR ATTRACTANTS		83
4.1	Introduction.....	83
4.2	Materials and Method	85

4.2.1	PLGA encapsulation of Sema3A	85
4.2.2	<i>In vitro</i> Y-template fabrication.....	86
4.2.3	Sema3A-MP bioactivity assay	87
4.2.4	DRG choice assay quantification	88
4.2.5	Y-tube implantation and analysis	88
4.2.6	Statistical analysis	89
4.3	Results.....	90
4.3.1	Axonal turning in the presence of Sema3A <i>in vitro</i>	90
4.3.2	Sema3A retains functionality of the regenerated nerves.....	92
4.3.3	Sema3A does not modulate the S/M neuron ratio.....	92
4.3.4	Axon morphology analysis in the presence of Sema3A	95
4.3.5	Sema3A shows inhibitor effect of myelinated axons less than 1µm	97
4.4	Discussion	99
4.4.1	Reduced sprouting in the presence of Sema3A.....	100
4.4.2	Limited specificity with two attractants	102
4.4.3	Conclusion.....	102
CHAPTER 5	104
5.1	Summary of thesis contribution	104
5.2	Additional considerations for improved enticement of axon subtype regeneration.....	105
BIBLIOGRAPHY	107
BIOGRAPHICAL SKETCH	123
CURRICULUM VITAE		

LIST OF FIGURES

Figure 2.1. PTN microparticles formulation and release over time. A) SEM image of the PTN microparticles (Scale 2 μ m). B) Cumulative PTN release over 28 day time period.	22
Figure 2.2. PTN-MP bioactivity assay show neurite outgrowth from DRG explants. A & B) Representative images of DRG explants exposed to recombinant PTN and PTN-MP. B) Comparison of axonal length (mean \pm SEM) for recombinant PTN, PTN-MP, BSA-MP, and media only control (CTR (-)). Significance indicated by * ($P < 0.05$) and *** ($P < 0.001$). (Figure prepared with the help of Nesreen Alsmadi)	24
Figure 2.3. Fabrication steps of PEUU Y-conduit. A) Y-shaped molds prepared from dental wax are dipped multiple time in a solution of PEUU solution (B & C). D) Dental wax was cleared after multiple washes and Y-conduit trimmed to appropriate size. (Figure prepared with the help of Dianna Nguyen).....	26
Figure 2.4. Implantation of Y-conduit and experimental timeline. A) Schematic representation of Y-conduit implant into the sciatic mixed nerve. One arm contains an attractant (NGF, GDNF, BDNF, PTN, or NT-3) and the other BSA control. B) Experimental timeline following Y-conduit implantation. C) Representative image of the Y-conduit implantation with an attractant in one arm and BSA control in the other. The ends of the conduit are closed using 1.5% agarose.	28
Figure 2.5. Diffusion of PLGA microparticles loaded with NTF and BSA over a 30 day time period. The top arm represents PTN-MP release and BSA-MP release in the bottom arm. Arrow heads at each time point indicates approximate position of nerve regeneration. (Figure prepared with the help of Lokesh Patil)	31
Figure 2.6. Concentration gradient across the length of the Y-conduit arm for the BSA-MP (Top) and PTN-MP (Bottom).	32
Figure 2.7. Comparable Y-nerve regeneration using NTF-MP with no distal targets. A) Representative image of a regenerated Y-nerve and toluidine stained semi thin sections for the BSA arm (a1) and PTN arm (a2). B) Similar regenerated nerve diameter across the experimental groups. Data presented as mean \pm SEM. No statistical significance observed.	38
Figure 2.8. H&E staining of the two nerve-cap segments distally attached to the regenerated nerve arm.	39
Figure 2.9. CNAP measurements show activation of different fiber composition at 45 days. (A) Setup for measuring CNAP. Bipolar hook electrodes provided stimulus pulses and the response recorded distally from the regenerated arms. (B) CNAP response at threshold	

stimulus and three times threshold for maximum axon activation. (C) Representative recording showing the stimulus artifact followed by three distinct peaks with different velocity ranges. CV measurements separated by fast (> 30 m/s), medium ($5 < x \leq 30$ m/s) and slow (≤ 5 m/s). (Figure prepared with the help of Vidhi Desai).....	41
Figure 2.10. Limited enrichment of VMN by NGF, PTN, and NT-3. A) Schematic of FG labelling at distal regenerated nerve end. B) Schematic representation of the VMN location in the spinal cord and FG+ cells located ipsilateral. Arrows show positively labelled motor neurons. C) FG+ motor neuron quantification show GDNF attracted a significant number compared to BSA control and PTN. * indicates $P < 0.05$; data presented as mean \pm SEM. Scale bar = 100 μ m.	43
Figure 2.11. Sensory neuron counts and perikarya size distribution. (A & B) Schematic of DRG soma size distribution and representative image of FG+ cells of varying size (indicated by arrows and arrow head). (C) FG+ sensory neuron count shows overall reduction in the number of regenerated sensory neurons. (D-F) Perikarya size distribution for small, medium, and large. Data presented as mean \pm SEM. Scale bar = 50 μ m. (Figure prepared with the help of Martin Tran).....	45
Figure 2.12. Ratio of FG+ sensory and motor neurons using single attractants show no difference compared to the BSA arm.	46
Figure 2.13. Representative SEM images of the regenerated Y-nerve arms showing myelinated and unmyelinated axons. Scale bar = 10 μ m.	48
Figure 2.14. Unmyelinated and myelinated axon count show NTF influence. (A) NGF showed significantly higher number of unmyelinated axon compared to BSA arm. (B) Myelinated axon count showed no significant difference. * indicates $P \leq 0.05$; one-way ANOVA followed by Bonferroni's multiple comparison. Data presented as mean \pm SEM. (Figure prepared with the help of Dianna Nguyen).....	49
Figure 2.15. Myelin thickness and fiber diameter were comparable among NTFs. Data presented as mean \pm SEM.	50
Figure 2.16. Scatter plots of g-ratio as a function of axon diameter for different NTFs. Dotted lines represents divisions of myelinated axons as small, medium, and large. Similar trends for NTF and BSA arms observed.	52
Figure 3.1. Schematic representation of the experimental groups. A) Y-conduit sutured to the mixed sciatic nerve with PLGA loaded NTFs in each of the arms. B) Mixed sciatic nerve attached to the proximal end of the Y-conduit with the arms sutured to the sural and tibial nerve targets. C) Y-conduit with 2 mm segment of muscle and skin attached to the distal arms of the Y-conduit.	63

Figure 3.2. Representative images of the implantation of experimental groups. A) Tibial and sural branch sutured to the distal arms of the Y-conduit. B) Muscle and skin segments attached to the distal lumen of the arms. C) Y-conduit loaded with NTF-MP in the individual arms and ends closed with 1.5% agarose.....	64
Figure 3.3. Representative images of the regenerated nerves. A & B) Regenerated nerves for the control groups consisting of nerve-target and end-organ target. C) NTF-MP group in combination versus non-selective BSA control. D & E) NTF-MP for motor enrichment versus sensory enrichment.	66
Figure 3.4. H&E staining of muscle and skin capped ends of the regenerated nerve. Muscles are stained deep pink in the upper image and skin cells pale pink (center region).	67
Figure 3.5. BDNF/GDNF (B/G) combination did not significantly increase the number of regenerated VMN. Numbers on the “Y” diagram in the x-axis represent animals per arm quantified. Data presented at the mean \pm SEM.....	70
Figure 3.6. DRG size distribution comparable in all experimental groups. A) Schematic representation of DRG location and size distribution. B-D) Percent cell size distribution for FG+ cells located in the L4 and L5 DRG categorized into small, medium, and large. Data presented as mean \pm SEM.	72
Figure 3.7. Sensory/motor ratio is modulated when combination of B/G versus PTN is used in the choice assay. Data presented as mean \pm SEM. * indicates $P < 0.05$; Bonferroni’s post test.	73
Figure 3.8. Representative EM images of for the motor and sensory compartment show normal axon morphology. Scale bar = 10 μ m.	75
Figure 3.9. Axonal count from motor and sensory compartment for each group. A) Unmyelinated and B) myelinated axon count. Data presented as mean \pm SEM. * indicates $P < 0.05$	76
Figure 3.10. Fiber diameter (axon + myelin) for the individual arms of the regenerated arm. Data presented as mean \pm SEM. * indicates $P < 0.05$	77
Figure 3.11. Scatter plots of g-ratio as a function of axon diameter. Individual points represent the g-ratio measured for each myelinated axon. (C, F, I, L, O) Linear regression of the best fit per arm per group. The equation for each line presented within the scatter plot...	78
Figure 3.12. Sensory/motor ratio for BDNF/GDNF arm versus PTN showing difference in the percent of motor neuron attracted.	79

Figure 4.1. <i>In vitro</i> Y-template PDMS mold. The 6.0mm holes contain NTF-MP mixed in collagen and the cell chamber (bottom hole) is where the DRG will be place. The canals serve as a pathway for the regenerating axons.....	87
Figure 4.2. Schematic representation of Y-conduit containing attractants and repellent to increased efficacy in axon subtype enrichment.	89
Figure 4.3. Sema3A induced inhibition on DRG neurite outgrowth. A) Bright field image of the DRG axonal extension in the NGF (a1) and Sema3A (a2) chamber. B & C) Normalized axonal length and change in axon turning from the NGF and Sema3A compartments. ** indicates significant difference between the chambers ($P \leq 0.01$). Data present at mean \pm SEM.	91
Figure 4.4. FG+ motor neuron counts unaffected by Sema3A repellent and shows individual arms having similar attractive property. Data present as mean \pm SEM.....	93
Figure 4.5. DRG perikarya size distribution. A) Schematic representation of small, medium, and large cell distribution located in the DRG. B-D) FG+ cell size distribution quantified from the L4 and L5 DRG categorized into small, medium, and large. Data present as mean \pm SEM. (Figure prepared with the help of Michael Tran)	94
Figure 4.6. Sensory/motor neuron ratio show Sema3A was not effective in altering the ratio in the presence of dual choice molecular attractants.....	95
Figure 4.7. Representative EM images from the regenerated arms of the Y-nerve. Arrows designate small myelinated fibers more evident in the group without Sema3A. Scale bar = 10 μ m.	96
Figure 4.8. Unmyelinated and myelinated axon count. A& B) No difference observed in the unmyelinated and myelinated axon count. Data present as mean \pm SEM.	97
Figure 4.9. Scatter plots of g-ratio as a function of axon diameter. (A-B, D-E) G-ratio versus axon diameter for each regenerated arm (n =3 animals per group). Sema3A group shows limited number of small diameter (< 1 μ m) compared to the BDNF vs. NGF group. (C & F) Linear regression and equation (below scatter plots) for the individual groups. (Figure prepared with the help of Elaine Ramirez.)	98
Figure 4.10. Percent distribution of myelinated axon diameter less than 1 μ m. BDNF+Sema3A show significant decrease compared to BDNF only arm. * indicates significant difference between the chambers ($P \leq 0.05$, Bonferroni). Data present at mean \pm SEM.	99
Figure 5.1. Schematic of dual choice guidance based regenerative neural interface.	105

LIST OF TABLES

Table 1.1. Classifications of peripheral nerve fibers based on function, diameter, and conduction velocity.....	9
Table 1.2. Neurotrophic and growth promoting factors after peripheral nerve injury.	13
Table 2.1. Summary of the NTFs with the receptor and function	19
Table 2.2. Dimension and diffusivity values for protein release from PLGA microparticles in collagen.	29
Table 2.3. CNAP peaks incidences observed within the velocity ranges. ‘+’ indicates one peaks observed within the range. (#) indicates number of animals used to obtain CNAP response.....	42
Table 3.1. CNAP peaks incidences observed within the velocity ranges. ‘+’ indicates one peaks observed within the range. (#) indicates number of animals used to obtain CNAP response.....	68
Table 4.1. CNAP peaks incidences observed within the velocity ranges. ‘+’ indicates one peaks observed within the range. (#) indicates number of animals used to obtain CNAP response.....	92

CHAPTER 1

INTRODUCTION

There are approximately 1.9 million amputees in the USA, and this number increases by 150,000 amputation surgeries every year, from which 10% comprised of mostly trauma related to upper limb [1], [2], and a total of 1,458 were related to the military personnel in 2013 [3]. The Defense Advanced Research Projects Agency (DARPA) started an initiative focused on providing war veterans who suffered limb loss with robotic prostheses to improve their quality of life.

Individuals suffering from spinal cord injuries, brain injuries, neurodegenerative diseases, and limb amputation require sophisticated robotic devices capable of providing fast, intuitive, reliable and bidirectional flow of information between the user and the device [4]–[6]. Prosthetic devices have advanced from the traditional mechanical hooks performing simple open/close tasks to more advanced anthropomorphic robotic hands capable of complex movements with as many as 22 degrees of freedom. Despite much progress, current prostheses are controlled through surface electromyogenic (EMG) signals and operated by visual or surrogate sensory control [7]. While force and movement sensors placed on advanced robotic limbs have the potential to offer a closed-loop control if interfaced with the nervous system of the user [8], the current robotic hand sensory technology compares poorly to the estimated 17,000 touch sensing receptors on the hand that provides information about small slips and skin deformation [9]. Furthermore, establishing a reliable neuron-electrode interface with both motor and sensory axons, in order to provide natural control and feel of the robotic limb to the users, remains a formidable challenge

Most recent efforts have been directed towards providing intuitive and natural closed-loop communication between the user and the robotic devices by interfacing with the nervous system. The feasibility of recording from hundreds of cortical neurons in relation to limb movement was demonstrated more than 40 years ago by Evarts and his colleagues, who showed an increase in cortical neuron activity prior to EMG activation in the limb [10]. This was further extended using multielectrode arrays to record from neuronal populations in the cortex to control computer interface devices in humans [11]. However, the absence of proprioceptive feedback required visual dependency resulting in poor coordination, declining accuracy of the prosthesis and exhausting the patient. In addition, no current device can integrate pain and mechanoreception required for a natural “feel” of the robotic prosthetic device.

Commercially available prostheses are normally controlled through two channel electromyogenic (EMG) signals converted to mechanical commands and operated under visual or surrogate sensory control [6], [8]. However, one in five users reject the prostheses with more than 89% reporting the device a hindrance to daily functional activities [12]. Reasons for dissatisfaction include limited range of motion, slow maneuverability, lack of comfort, and fatigue due to the weight of the device. In addition, individuals indicate a lack of embodiment with the prostheses, further increasing the chances of device rejection [13].

Recent efforts to enhance an amputee’s sense of embodiment focuses on providing closed-loops systems consisting of multiple sensors in addition to cosmetic appearance. To address such needs, researchers at Northwestern University in Chicago developed a new technique termed targeted muscle reinnervation (TMR) by redirecting the intact residual nerve from the amputated

stump to denervated remnant muscles. This technique enabled the individual to control a prosthesis with six degrees of freedom by extracting the remnant muscle electromyogram (EMG). Furthermore, limited sensory feedback provided through stimulation of the skin at the target site [14]–[19]. The realization that sensory feedback is critical for performance of simple tasks and patient adoption has motivated the integration of advanced sensors on the robotic prosthesis and artificial skin with temperature, humidity, and pressure sensors [20].

Brain computer interface for prosthetic limbs: Electrode-neuron interfaces in the primary motor cortex of paralyzed patients have been shown to be successful in translating such intention into machine control [21], [22]. Intracortical multielectrode arrays are very sensitive in decoding motor planning information from the motor cortex. However, surgical implantation is highly invasive. Furthermore, arguably cortical interfaces are less suitable for sensory-modality specific stimulation, as this information is generated in distal target organs (skin, tendon, and muscle) and modified in the spinal cord and thalamus before reaching the sensory cortex for interpretation. Most current neural interfaces are designed as microneedle arrays for intact brain or nerve tissue penetration. The rigid electrode materials cause mechanical damage to the softer nerve tissue, as a result of both tissue micromotion and tethering forces imposed by the outside connectors. The resulting cellular damage occurs at the entire neuronal columns of approximately 200-300 μm around the electrode [23]. The result is one of limited functionality (weeks to months) and continued signal deterioration. Such limitation obligates the daily re-calibration of electrodes and the eventual loss of signal.

Peripheral nerve interfacing: In order to interface both sensory and motor neurons, several types of peripheral nerve interfaces have been proposed in the last 30 years, ranging from non-invasive extra-neural cuff to invasive intra-neural and regenerative based electrodes [24]. Sensitivity and selectivity for both recording and stimulation is regulated by multitude of parameters, which include electrode design, material, implantation strategies, and stimulation parameters among others [25]. Human volunteer studies have demonstrated that direct stimulation of single afferent units from the median nerve above the elbow, gives rise to a clear sensation of mechanical deformation after direct electrical stimulation. Thus, the use of peripheral microelectrode arrays is a reasonable alternative to develop bi-directional neurointerfaces. Indeed, K. Horch and R. Norman at Utah University have demonstrated that silicon microelectrode arrays (100 needle electrodes) can be inserted into a peripheral nerve, from where motor information can be recorded and decoded directly [26], [27]. However, the Utah microelectrode needle array produces insertion and micromotion related injuries to the limb nerves, reducing greatly their ability to provide long-term neural recording or stimulation. In addition, insertion electrode arrays cannot control the type of neurons to be contacted, since most peripheral nerves have a mixture of motor, sensory and autonomic axons. Abnormal sensations were also evoked when using longitudinally implanted intrafascicular electrodes (LIFEs), which in addition to conveying grip force and joint position, evoked “electrical” paresthesia including tingling and burning sensations [28], [29].

Pioneering studies with cuff electrodes in amputees that stimulated the residual nerves elicited some normal sensations including digit flexion and vibration, but also evoked abnormal

paresthesia including fist clenching and tingling sensation [30]. A recent study by Tan et al. reported patients feeling natural sensations of pulsing pressure, tactile touch, tapping, and/or vibration by varying the pulse width of stimulation. However, constant stimulation intensity pulse trains with varying frequency range evoked “electrical” paresthesia in 96% of the 151 trials [30]. With the current paradigms, the difficulty in discriminating motor from the different sensory submodalities is limited due to the physiological characteristics and anatomical structure of the PNS.

There are important and well recognized challenges in fabricating an effective neurointerface including achieving stable connectivity at the neural-electrode interface in order to control the prosthetic device by either stimulating or recording from motor and/or sensory neurons. Such a neurointerface must withstand continuous use through heavy recording/stimulating cycles, without damaging the nerve tissue or compromising the neuron-electrode interface that is needed for long-term functionality of the prosthetic device. While early neural interface designs have demonstrated the feasibility to decode the neural discharge patterns involved in motor planning in humans, reliable long-term neuron-electrode interface of the nervous system remains a challenge.

An additional challenge is the desire to achieve selective neural interface for the control of artificial limbs, which requires the ability to access volitional information from motor neurons, and safely stimulating specific sensory modalities of sensory axons to convey needed

proprioception for precise motor control and/or other modalities (i.e., pain, light touch, mechanoreception).

Regenerative Electrode Arrays

SIEVE: Regenerative peripheral nerve electrode interfaces were first proposed more than 25 years ago, and are based on the innate capacity of peripheral nerves to spontaneously regrow after injury [31]. These “sieve” electrodes integrate recording-stimulating electrodes via holes (40 μm diameter) implanted between the severed ends of the nerve [32]. However, the transverse placement of a sieve electrode constitutes a micro perforated barrier that compromises the regeneration process, delaying and impeding the elongation of some growing axons. In addition, the rigid structure of the sieve and the lead connectors results in compressive axonopathy due to the inability to accommodate the increase in axon size (from 1 μm to 14 μm) as axons mature and undergo remyelination. The spatially restrictive nature of sieve electrodes most likely explains the resulting decline of target tissue reinnervation and loss of regenerated nerve fibers following implantation of the electrode [32].

REMI: It has been demonstrated that peripheral nerves can be induced to regenerate through commercially available electrode arrays and be effectively interfaced, even after long-term injuries. In recent experiments we implanted 16-microelectrode arrays in both acute and six-month chronic injured nerves. The monolithic nerve guide/electrode array device was placed in the sciatic nerve by suturing proximal and distal nerve stumps. This study also showed that peripheral nerves, whether acutely injured or implanted after months of chronic amputation,

could be interfaced by enticing them to grow in close proximity to electrodes placed in a tridimensional open regenerative multielectrode interface (REMI), which [33]. Subsequent studies demonstrated that the number of active recording sites, the amplitude and firing rate increased from 7 to 15 days post-implantation, in agreement with an increasing number of regenerating axons across the REMI, despite immature myelination. Indeed, the number of animals exhibiting spike activity increased 33% from 7 to 15 days following REMI implantation with a corresponding increase in firing rate of 243% [34]. Together, these studies demonstrate that regenerating axons depolarize spontaneously. Most peripheral nerves include mixed motor fibers and multiple sensory axon sub-modalities (i.e., limb position, skin deformation). We have previously demonstrated peripheral neural interfacing in freely moving animals with acute and chronic nerve injuries. More recently, we obtained compelling evidence that REMI interfacing can record specifically from both motor and sensory sub-modality axons in animals in which the interfaced nerves are allowed to reinnervate their original target organs in the skin and muscle [35].

However, the fact that most peripheral nerves consist of mixed motor fibers and multiple sensory sub modalities (i.e., limb position, skin deformation), a situation exacerbated in nerve regeneration, makes the recording of motor axons and the selective electrical stimulation of specific sensations highly unreliable. Despite such limitation, developmental, anatomical, molecular, and electrophysiological evidence exists that suggests motor and sensory modalities can be selectively activated by molecular signals.

1.1 Organization and function of the PNS

Normal peripheral nerves contain a mixed population of motor and sensory axons. In the rat sciatic nerve there are approximately 15 times more sensory fibers compared to motor [36]. For example, the human hand is populated by an estimated 17,000 touch sensing receptors that provide information regarding small slips, skin deformation, limb position, etc. and contribute to roughly 20 distinct modalities conveyed by several types of nerve fibers [9], [37]. In the glabrous skin of the palms, the A δ afferents are rapid adapting (RA) neurons that innervate Pacinian and Meissner's corpuscles which are vibration receptors that encode texture [9], [38]. Conversely, the highest spatial acuity of mammalian touch receptors proposed to represent object features such as edges and curvature involve A β afferents that innervate Merkel cells. Early physiological studies classified axons in the peripheral nerves based on axon diameter (AD) and conduction velocity (CV) (Table 1.1). In a mixed population of axons, two biophysical properties presents a challenge in attempts to selectively activate one specific population of axons without concomitant activation of the neighboring population [39], [40]. The axon distance between the electrode and diameter of the nerve fiber determine the time of activation. Axons close to the electrode require less current to activate. Additionally, large myelinated axons (i.e., motor and proprioceptive) are depolarized with smaller currents than the small diameter fibers as described by the current-diameter relationship [39]. Thus, efforts of stimulate naturalistic sensation is challenging as the mixed nature of the nerve results in paresthesia from the indiscriminate stimulation.

Table 1.1. Classifications of peripheral nerve fibers based on function, diameter, and conduction velocity [4], [37].

Fiber Type	Function	Diameter (μm)	Conduction Velocity (m/s)
<i>Myelinated</i>			
$A\alpha$	Motor efferents; Proprioception	12-22	60-120
$A\beta$	Tactile, proprioceptive	6-12	4-70
$A\gamma$	Gamma-motor efferents	3-5	30-45
$A\delta$	Pain, cold afferents	2-5	10-30
B	Preganglionic autonomic	1-5	3-15
<i>Unmyelinated</i>			
C	Thermal, pain, mechanical	0.3-1.3	0.5-2
C	Postganglionic autonomic	0.3-1.3	0.7-2.3

1.2 Guidance of axons using molecular cues during development

Developing axons are guided to their target using long-range diffusible and short-range surface-bound factors. These factors are presented along the path of the growing axons and can exert an attractive or repulsive force which include netrins [41], semaphorins [42], [43], ephrins and eph receptors [44], [45], slit and robo receptors [46], neurotrophic factors [47], and morphogens [48], [49]. These molecules are tightly controlled both temporally and spatially, thus playing a critical role in orchestrating type-specific axonal navigation and target innervation [50]–[52]. Both attractant and repellent molecules bind to specific receptors on the growth cone, which then

modulates the structure and dynamics of the actin cytoskeleton [48], [53]–[55]. These changes enable the growth cone to either extend towards a specific direction or retract adjusting its trajectory. Based on the fiber type and function, specific molecular cues or neurotrophic factors (NTFs) are able to modulate growth and survival [56]. During development, axon projections are guided towards their end muscle and skin targets by the means of NTFs. Ramon y Cajal first postulated the role of NTFs in the guidance of motor and sensory axons to their targets [57]. This was further confirmed by the “neurotrophic factor hypothesis” by Rita Levi-Montalcini in the 1940’s which stated that after numerous axonal projections reach their target, there is a limited amount of target-derived molecules to promote survival [58]. This led to the discovery of the first nerve growth factor (NGF) in the 1950’s, followed by related members such as brain-derived neurotrophic factor (BDNF), neurotrophin-3 (NT-3), and neurotrophin-4/5, which bind to tropomyosin receptor kinase (Trk)A, TrkB, and TrkC, respectively; and to the common low affinity p75 receptor [59]. Others include glial cell line-derived neurotrophic factor (GDNF) and related molecules neurturin (NRTN), artemin (ARTN), and persephin (PSPN), which bind a two-component receptor complex consisting of a GDNF binding domain (GFR α) and a signal transducing domain (RET) [46]. Specific receptors expressed on the growth cone of the extending axons interact with specific NTFs to guide motor axons from the spinal cord to the muscle and sensory axons from the Dorsal Root Ganglion (DRG) to the skin, tendon, and muscle [50]. Motor axon targeting to the muscle is mediated by GDNF [44] along with NT-3 for muscle spindle innervation by proprioceptive sensory neurons [60]–[62]. Axon innervation to the epidermis of the skin by nociceptive axons is guided by NGF. Sensory mechanoreceptors include two rapid adapting (RA): Meissner and Pacinian, and two slow adapting (SA) receptors: Merkel

and Ruffini Meissner's corpuscles [9], [63], [64]. RA mechanoreceptive axons express the cRet receptor for glial-derived neurotrophic factor (GDNF) [65]. SA mechanoreceptors express TrkB, a receptor for both BDNF and NT4. In mature DRG neurons, BDNF is required for mechanoreceptive neuron function [66], and BDNF overexpression in the skin increases the number of Merkel cells [67]. Conversely, the development of Pacinian corpuscles depends on Ret and GFR α 2, receptors for GDNF and Neurturin, respectively [68]. Nociceptive axons express TrkA, mechanoreceptive neurons express TrkB, and proprioceptive fibers express TrkC. Knock out mice for pro-apoptotic gene Bax, crossed with NGF or TrkA null mice, showed lack of skin innervation by small caliber nociceptive and thermoreceptive axons [69]. Meissner corpuscles are absent in both BDNF and TrkB null mice, and Pacinian corpuscles are dependent on the receptor tyrosine kinase Ret and the GPI-anchored ligand GFR α 2 [65]. NT-3/TrkC null mice lack proprioceptive sensory neurons [55], [70], [71].

Apart from chemoattractants, chemorepulsive cues play a crucial role in creating patterns of somatosensory innervation by restricting growth cone extension and branching [72].

Chemorepellents result in the collapse of the axon growth cone leading to changes in the directional outgrowth or retraction. In the early 1980's, studies revealed the presence of inhibitory diffusible factor from the spinal cord that restricted sensory axon outgrowth toward the ventral spinal cord *in vitro* [42], [73]. Semaphorins, one of the identified repellents, are the most widely characterized for their role in sensory axon development. Sema3A, a member of the Semaphorin family, contribute to the differential patterning of innervating axons at the target. Knock-outs for the Sema3A receptors, PlexinA3 and A4, resulted in misprojections and

disorganized innervation [72]. Another repellent is the contact-mediated action of the ligand Ephrins and their “Eph” receptors. The expression of these factors during development allows for tight coordination of motor and sensory projections, and knock-out of the Eph receptors results in motor-sensory miswiring [45], [52].

1.3 Role of NTFs in survival and growth after peripheral nerve injury

Peripheral nerves intrinsically retain the ability to regenerate following injury and several biological factors including cytokines and growth factors influence the efficacy of regeneration [74]–[76]. Similar to development, trophic factors play a key role during regeneration. Endogenous presence of growth promoting factors are upregulated following injury by Schwann cells and the distal muscle and skin targets. The first evidence of trophic factors in axon regeneration was discovered by Lundborg in 1982, by elucidating the growth promoting capacity of the luminal fluid inside a nerve conduit. Application of the fluid resulted in the neurite outgrowth from DRG cultures *in vitro* [74]. Further studies showed that a multitude of growth factors are present after injury and demonstrated their role in survival and regeneration (Table 1.2). Exogenous application of these NTFs has promoted regeneration after chronic axotomy, increased speed of regeneration, improved functional recovery, and increased neuron survival [77], [78].

Table 1.2. Neurotrophic and growth promoting factors after peripheral nerve injury.

Factors	Regeneration Influence
Neurotrophin-3 (NT-3)	TrkC expressing Proprioceptors [79], [80]
Neurotrophin-4/5 (NT-4/5)	Mechanoreceptors [81]
Nerve growth factor (NGF)	TrkA expressing Nociceptors [82]
Brain-derived neurotrophic factor (BDNF)	TrkB expressing mechanoreceptors [83]
Glial cell derived neurotrophic factor (GDNF)	Ret expressing sensory and motor neurons [84]
Insulin-like growth factors-1/2 (IGF1, IGF2)	Increase speed of regeneration [85]
Pleiotrophin (PTN)	Motor neuron regeneration [86], [87]
Fibroblast growth factor (FGF)	Proliferation of Schwann cell [88]
Vascular endothelial growth factor (VEGF)	Angiogenesis [89]–[91]
Leukemia inhibitory factor (LIF)	Motor pathway regeneration [92]
Ciliary neurotrophic factor (CNTF)	Survival of motor neurons; reinnervation [93]
Interleukin-6 (IL-6)	Enhance nerve regeneration [94]

1.4 Specificity of neurotrophins in axon regeneration and guidance

In addition to promoting survival and regeneration after peripheral nerve injury, recent studies have also proposed the role of NTFs in guiding axonal regeneration and mediating target recognition. Extensive studies with Y-tubes exposing the regenerating axons to different target tissues including nerve, muscle, skin, and fat, have demonstrated a differential effect of tissues

on nerve regeneration. Specifically, when given a choice between nerve, muscle and fat, myelinated axons grew preferentially towards the nerve stump and the muscle compartments [95]–[98]. This was further validated using a nerve transection and repair in rat femoral model where regenerating motor axons preferentially reinnervated the muscle pathway as opposed to the cutaneous [99]. Different Schwann cell phenotype present in the sensory and motor branch showed differential expression of NTFs thereby influencing the directional growth of regenerating axons [100]. Schwann cells in the motor branch upregulate the expression of GDNF and pleiotrophin (PNT), whereas NGF, BDNF and GDNF are overexpressed in the sensory branches [100]. An increased in up-regulation of BDNF, GDNF, and NT-3 expression was also observed at the denervated muscle target [101]. The difference in the expression of the NTFs suggest their role in guiding axon subtypes. This was demonstrated using adenoviral expression of NGF in the sensory branch of the femoral nerve following transection and repair to directing regenerating sensory axon to that branch. This result was validated by calcitonin gene-related peptide (CGRP) positive expressing sensory axons choosing the correct pathway as opposed to entering the motor branch [102]. Furthermore, Romero et al. showed that NGF expression in the dorsal lamina increased the number of regenerating adult nociceptive axons into the spinal cord following injury [103]. These studies demonstrate the role of NTFs to achieve neuron-type selective regeneration in the presence of an intact distal target.

Recently we have demonstrated that compartmentalized diffusion delivery of NGF and NT-3 preferentially entice the growth of TrkA⁺ nociceptive C-fibers and large diameter sensory neurons *in vitro* [104]. This was further showed *in vivo* using a “Y” nerve guide to compare the

natural segregation enticed by mostly motor (tibial) or sensory (sural) axon fibers compared to that enticed by NGF and NT-3 containing chambers. Optical densitometry showed large myelinated axons labeled with N52 antibody were observed growing towards the tibial nerve or NT-3 filled chambers compared to collagen filled compartments. Here we extend our initial observations by evaluating the use of specific NTFs (NGF, NT-3, BDNF, GDNF, and PTN) to modulate the sensory/motor neuron ratio following nerve regeneration without distal targets.

1.5 Research objective and dissertation organization

Achieving a greater concentration of axons from a particular neuron subtype is expected to provide more sophisticated and selective peripheral nerve interfaces. In this work we hypothesize that sensory-motor ratio in regenerated amputated nerves can be influenced in regenerated segments using a Y-shaped nerve conduit with differential presentation of specific molecular guidance cues.

In Chapter 2, single molecular guidance cues will be used to determine if the nerve fascicles regenerating into a Y-shaped nerve conduit are electro-competent, and whether the sensory/motor neuron ratio of the fascicles are altered *in vivo*. The electrical competency will be measured by compound nerve action potential (CNAP), retrograde labeling will be used to evaluate sensory and motor neuron regeneration, and normal axon morphology will be analyzed using electron microscope (EM) analysis.

Chapter 3 will use different combination of molecular attractants to evaluate if the sensory/motor neuron ratio in the regenerated fascicles can be modulated in a choice assay. The specific aim is

to selectively guide the growth of motor and sensory axon subtype into separate compartments. BDNF/GDNF combination growth factors will be used for motor axon while NGF or PTN will guide sensory axon into the adjacent compartment. The effectiveness of difference molecular attractants will be compared to distal nerves in continuity and end organ targets (muscle and skin).

Chapter 4 extends the approach used in Chapter 3 to improve the efficacy sensory/motor neuron ratio by using the chemorepulsive effect of semaphorin 3A (sema3A). Sema3A in combination with a BDNF, a chemoattractive cue, will limit the regeneration of NGF⁺ axons and guide this sensory subpopulation towards the adjacent compartment containing NGF. This study will aim to increase sensory/motor ratio in the NGF compartment.

CHAPTER 2

ELECTROCOMPETENT REGENERATION OF BIFURCATED NERVE FASCICLES USING SINGLE GUIDANCE CUES

2.1 Introduction

Molecular cues guide developing axons to their targets using long-range diffusible and short-range surface-bound factors. These molecules include netrins [41], semaphorins [42], [43], ephrins and eph receptors [44], [45], slit and robo receptors [46], neurotrophic factors [47], and morphogens [48], [49]. These molecules are tightly controlled both temporally and spatially, thus playing a critical role in orchestrating type-specific axonal navigation and target innervation [50]–[52]. Both attractant and repellent molecules bind to specific receptors on the growth cone, which then modulates the structure and dynamics of the actin cytoskeleton [48].

Neurotrophic factors (NTFs) include members of the neurotrophin family such as nerve growth factor (NGF), brain-derived neurotrophic factor (BDNF), neurotrophin-3 (NT-3), and neurotrophin-4/5, which bind to tropomyosin receptor kinase (Trk)A, TrkB, and TrkC, respectively; and to the common low affinity p75 receptor [59], [105]. Others include glial cell line-derived neurotrophic factor (GDNF) and related molecules neurturin (NRTN), artemin (ARTN), and persephin (PSPN), which bind a two-component receptor complex consisting of a GDNF binding domain (GFR α) and a signal transducing domain (RET) [46].

During development, motor axons from the spinal cord and dorsal root ganglia (DRG) sensory neurons that form the somatic peripheral nerves; are guided to specific areas in the muscle and

skin, respectively by their differential expression of NTF receptors [50]. GDNF is essential in muscle targeting by the motor neurons [44], nociceptive axons depend on NGF for innervating the epidermis, BDNF is needed to guide mechanoreceptive fibers to the dermis, and NT-3 is necessary for the innervation of muscle spindles by proprioceptive sensory neurons [60]. Nociceptive axons express TrkA, mechanoreceptive neurons TrkB, and proprioceptive fibers TrkC. Knock out mice for the pro-apoptotic gene Bax, crossed with NGF or TrkA null mice, showed lack of skin innervation by small caliber nociceptive and thermoceptive axons [69]. Meissner corpuscles are absent in both BDNF and TrkB null mice, and Pacinian corpuscles are dependent on the receptor tyrosine kinase Ret and the GPI-anchored ligand GFR α 2 [65]. NT-3/TrkC null mice lack proprioceptive sensory neurons [55], [70], [71].

Following adult peripheral nerve injury, Schwann cells in motor and sensory nerves differentially up-regulate NTFs. Schwann cells in damaged motor branch increase the expression of GDNF and pleiotrophin (PNT), whereas NGF, BDNF and GDNF are overexpressed in injured sensory branches after injury [100]. This differential up-regulation of NTFs have also been reported at the distal target, as BDNF, GDNF, and NT-3 expression increases in the denervated muscle [101]. These NTFs have been shown to enhance nerve regeneration by promoting axon growth across the injury site and improving functional recovery [106]–[109]. NGF enhanced the regeneration of TrkA nociceptive neurons [102], [103]; NT-3 promotes TrkC expressing proprioceptors [62], [110], [111]; BDNF enhance regeneration of TrkB mechanoreceptive fibers and motor neurons [66]; GDNF stimulate outgrowth of RET expressing sensory and motor neuron [106], [112], [113]; and PTN promotes motor neuron regeneration (summarized in Table

2.1) [87]. More recently, the role of such NTFs in guiding axonal regeneration and mediating target recognition has been investigated.

Table 2.1. Summary of the NTFs with the receptor and function

Growth Factor	Cell Types	Receptors	Function	Reference
NGF	Nociceptive C-fibers (small axons)	TrkA; P75	Pain sensation	[102], [103], [114]
NT-3	Proprioceptive fibers (small Ad and large Aa, Ab axons)	TrkC; P75	Proprioception	[62], [110], [111]
PTN	Multiple cell types	ALK, PTP β / ζ , and Syndecan-3	Various	[86], [87]
BDNF	Mechanoreceptive fibers (large axons Aa, Ab axons); Motor	TrkB; P75	Object feature detection	[66], [77]
GDNF	Mechanoreceptive fibers large axons Aa, Ab axons); Motor	cRET	Vibration and surface pressure detection	[106], [112], [113]

We have previously reported that NGF can entice the regeneration of adult nociceptive (calcitonin gene-related peptide; CGRP) central axons [103]. In the injured femoral nerve, sensory axons randomly choose a motor or a sensory branch at the bifurcation, however, the induced expression of NGF in the sensory branch significantly increases the number of nociceptive CGRP-positive neurons choosing this pathway [102]. This study demonstrated that

neuron-type selective regeneration could be achieved by the expression of specific NTFs while a distal target is intact. Furthermore, we have recently demonstrated that NTFs could entice the regeneration of sensory axon subtypes *in vitro* using NGF and NT-3 [104]. We also showed that NT-3 can guide the regeneration path of axons into a separate chamber. Here, we extend our initial observations by evaluating the effect of NGF, BDNF, NT-3, GDNF, and PTN in regenerating nerve fascicles that are electro-competent and determine if the guidance of sensory and motor neurons into separate closed compartments can alter the sensory/motor ratio. A “Y” conduit was sutured to a transected mixed sciatic nerve with luminal neurotrophin-release by microparticles in one arm, and compared to the non-specific bovine serum albumin (BSA) control in the adjacent arm in a closed end conduit with no distal muscle and skin targets. Our results indicate that 97% of the regenerated nerve fascicles were electrically conductive. The recorded CNAPs showed multiples peaks, with conduction velocity ranges from 1-35 m/s. GDNF and BDNF showed preference for motor neurons compared to NGF, NT-3 and PTN. Sensory neuron regeneration was comparable between all groups and sensory subtype breakdown showed no selectivity between the NTFs and BSA arm. Axon morphometric analysis confirmed that the elongated nerve segment has a normal structure and myelination.

These results indicate that individual NTFs are capable of enticing axon subtype regeneration in the absence of distal guidance target. Additionally, the regenerated nerve fascicles maintain their ability to conduct action potentials. A number of regenerative strategies, including regenerative neural interfaces such as the REMI [33], [115] may be able to incorporate specific molecular guidance cues to control axonal regeneration and differentially attract axons into separate

compartmentalized electrode chambers, which in turn could offer a more selective neural interface for the control and feel of robotic prosthetic devices.

2.2 Materials and Method

2.2.1 Microencapsulation of neurotrophic factors

Biodegradable microparticles were made with poly(DL-lactic-co-glycolic acid) (PLGA) using the double emulsion method as reported previously [90]. Briefly, PLGA 50:50 (Lakeshore Biomaterial, St. Louis, MO) was dissolved in dichloromethane (DCM) 200 mg/ml (Sigma-Aldrich, St. Louis, MO), and mixed with aqueous solutions of human recombinant NGF (7S, 13.5 kD; Invitrogen), BDNF (27 kD), NT-3 (13.6kD), GDNF (15 kD), or PTN (15.4kD) (20µg/ml; Preprotech Inc, NJ) or BSA (20 µg/ml; Sigma-Aldrich). This solution was then added to polyvinyl alcohol (20 mg/ml) and emulsified. The MP solution was stirred for 1-2 hours to remove excess DCM, centrifuged at 4000 rpm for 15 minutes to pellet the particles and separated from the supernatant. The resulting MPs were transferred to -20°C for 2 hours, to -80°C overnight, freeze dried for 48 hours and stored at -20°C until used. Loading efficacy was calculated at $67 \pm 5\%$. The particles were evaluated by SEM (Hitachi S-3000 N) and the particle size distribution estimated at 800 nm using a Zeta Pals, Zeta Potential Analyzer (Figure 2.1 A). PTN and NGF release into PBS from MPs was evaluated at 37°C in a shaker incubator at hourly intervals, daily for a week, and weekly after that for 4 weeks, and quantified by ELISA (PTN;TSZ ELISA, HU9951) (Figure 2.1 B). BSA release was quantified using the BCA assay (Thermo Scientific, Rockford, IL) and read at 562 nm.

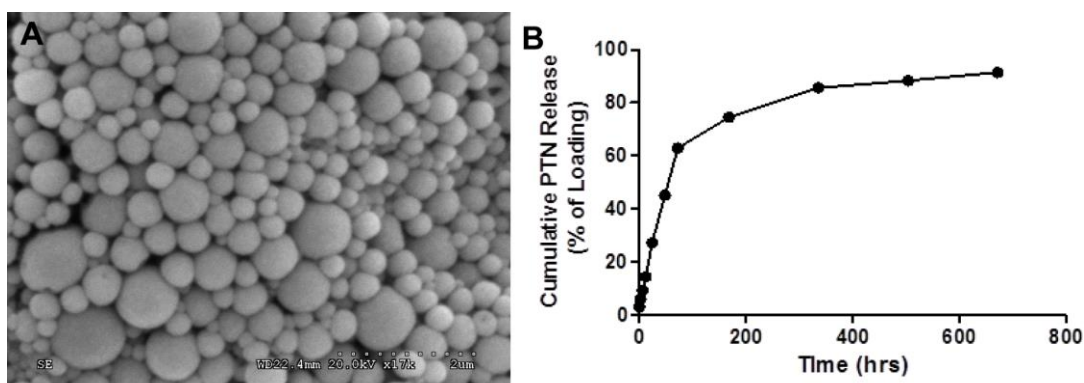


Figure 2.1. PTN microparticles formulation and release over time. A) SEM image of the PTN microparticles (Scale 2 μ m). B) Cumulative PTN release over 28 day time period. (Adapted from Alsmadi 2014.) [116]

2.2.2 DRG bioactivity assay

Neonatal (P0 - P4) mice (CD1) were dissected and whole dorsal root ganglia (DRGs) were collected in L-15 Medium (Leibovitz). The DRGs were cleaned of connective tissue and placed in poly-D-lysine (PDL) coated glass-bottom wells suspended in 10 μ l of atelomeric chicken collagen (85 % type I, 15 % type II; Millipore; Temecula, CA). The explants were incubated at 37°C with 5% CO₂ for 15 minutes to allow gelation before adding 200 μ l of Neurobasal A media (Sigma Aldrich) supplemented with 2% B27, 0.5% penicillin/streptomycin, and 0.75% L-glutamine. NTF MPs were compared to recombinant proteins at previously reported physiological concentrations: NGF, BDNF and PTN were tested at a 100 ng/ml, GDNF at 50 ng/ml and NT-3 at 5 ng/ml. The NTFs and NTF-MPs were added 24 hours after placing the DRGs and cultured for 5 days. Control DRG explants were incubated in BSA-MPs. The DRGs were fixed for 15 minutes in 4% PFA, rinsed and stored at 4°C.

2.2.3 DRG *in vitro* immunocytochemistry

Fixed DRGs were permeabilized in 0.5% PBS-Triton X100 for 5 minutes. Non-specific staining was blocked with 4% normal donkey serum for 1 hour, followed by incubation with a mouse anti- β tubulin III antibody (1:400; Sigma Aldrich) overnight at 4°C. After rinsing, the tissue was incubated for 1 hour with a Cy2-conjugated donkey anti mouse antibody (1:400; Sigma Aldrich, St. Louis, MO). The stained tissue was imaged on a Zeiss confocal microscope (Zeiss Axioplan 2 LSM 510 META). Axonal growth was estimated from 3 DRGs per treatment. Z-stacks were imaged at 20X magnification (20 images each at 15.4 μ m slice thickness) and individual axons were traced and measured from the edge of the DRGs to the axon terminals (Figure 2.2). Compared to control and BSA MP, the average axonal length for PTN and PTN MP was significantly higher ($P \leq 0.001$).

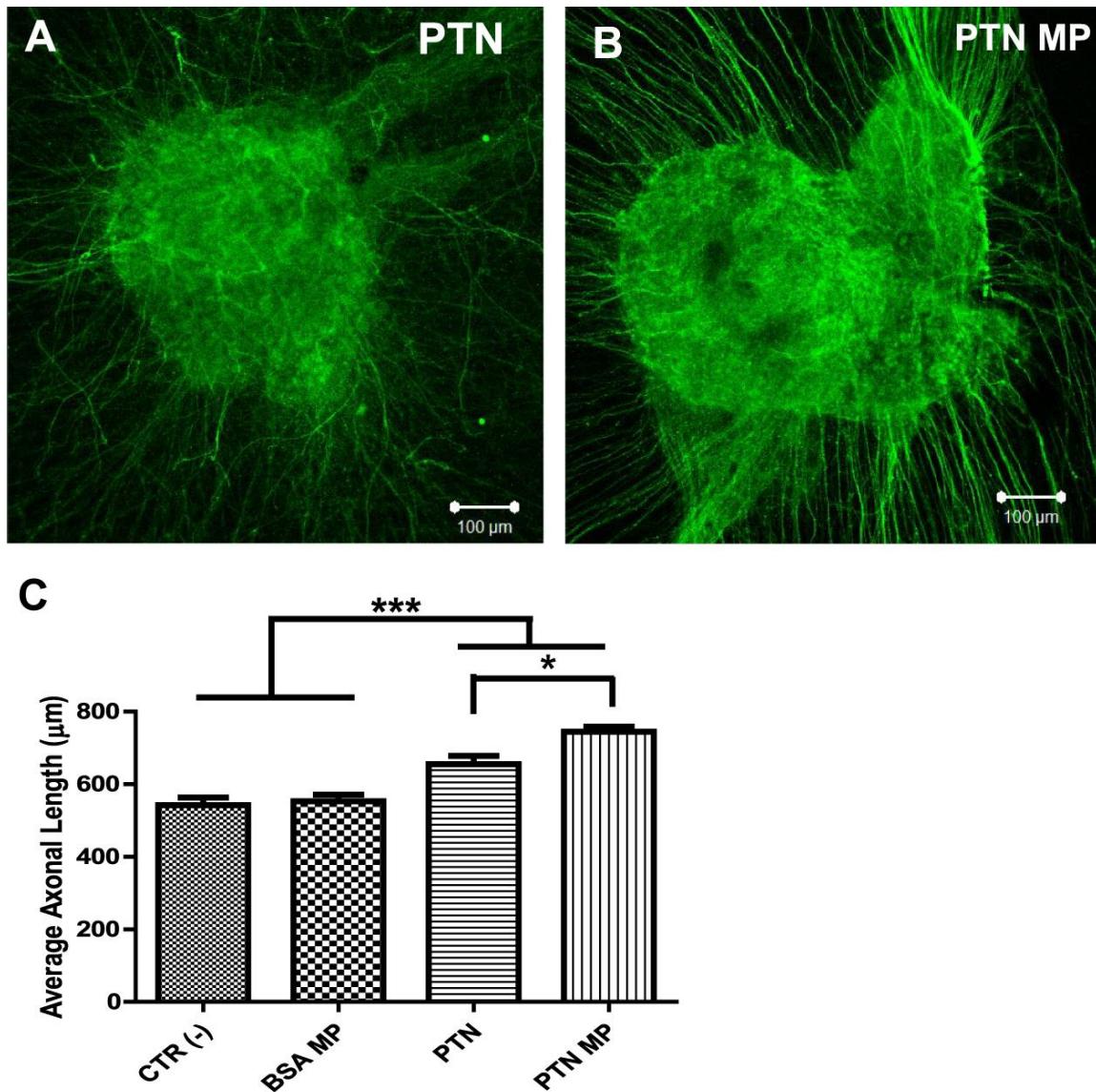


Figure 2.2. PTN-MP bioactivity assay show neurite outgrowth from DRG explants. A & B) Representative images of DRG explants exposed to recombinant PTN and PTN-MP. B) Comparison of axonal length (mean \pm SEM) for recombinant PTN, PTN-MP, BSA-MP, and media only control (CTR (-)). Significance indicated by * ($P < 0.05$) and *** ($P < 0.001$). (Adapted from Alsmadi 2014.) [116]

2.2.4 Y-tube nerve guide fabrication

Biocompatible thermoplastic elastomeric Y-shaped conduits were prepared using molds made with dental wax (Polysciences Inc., Warrington, PA). The molds were dipped-coated 5-6 times into 5% poly(ester urethane urea) in hexafluoro isopropanol solution to achieve a wall thickness of approximate 0.25mm according to previously reported methods [117], [118]. The coated tubes were dried overnight at room temperature, after which the dental wax was removed from the conduits by washing with hexane solution. The Y-conduit common segment measured 5 mm and each of the two arms measured 5-7 mm from the bifurcation, with 1.5mm ID and total length of 10 -12 mm (Figure 2.3).

Y-tube conduits were sterilized with 70% ethanol (15 min) followed by UV light irradiation (20 min). As previously described, collagen type I/III (EMD Millipore, Billerica, MA) was used to fill the lumen of the Y-conduit. The common arm was filled with collagen using a 28g insulin syringe up to the bifurcation and allowed to polymerize at 37 °C for 10 minutes. The "Y" arms were then filled with 10 μ L of NTF-MP or BSA-MP mixed with collagen and polymerized at 37°C for another 10 minutes before implantation.

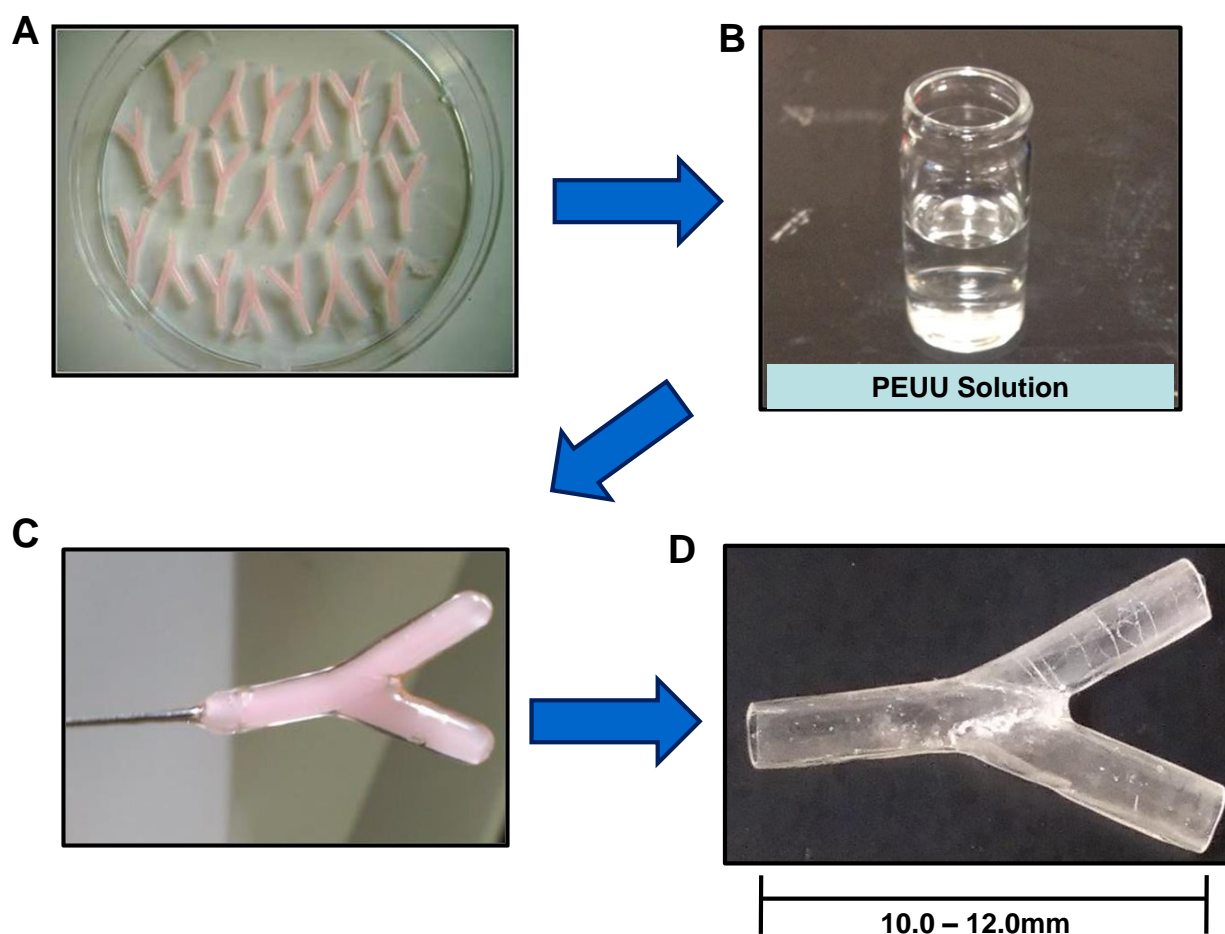


Figure 2.3. Fabrication steps of PEUU Y-conduit. A) Y-shaped molds prepared from dental wax are dipped multiple time in a solution of PEUU solution (B & C). D) Dental wax was cleared after multiple washes and Y-conduit trimmed to appropriate size. (Figure prepared with the help of Dianna Nguyen.)

2.2.5 Y-tube implantation into the transected sciatic nerve

Forty-two adult female Lewis rats were included in the study. All animals received BSA MPs in one arm and the other arms were divided equally into five experimental NTF-MP groups (NGF, NT-3, BDNF, GDNF, and PTN), a positive (2mm nerve segment ligated distally), and a negative (BSA) control; (Figure 2.4 A). Animals were anesthetized with isoflurane (2-2.5%) in 100%

oxygen. Once adequate depth of anesthesia was attained, the sciatic nerve was exposed by muscle-sparing incision between the semitendinosus and the bicep femoris muscles. The exposed sciatic nerve was transected proximal to the trifurcation. A 2 cm segment distal to the transection site was removed to prevent the contribution of other external guidance cues. The proximal nerve segment was attached to the common arm of the Y-conduits using 9.0 nylon sutures. The distal ends of the Y-tube were capped by adding 1.5% agarose (Figure 2.4 C). The muscles were then closed using 4.0 silk suture, and the skin stapled. Prophylactic topical antibiotic ointment was applied to the wound. All animals received antibiotic (cephazolin; 5mg/kg, IM) and pain control (sustained 3-day release Buprenorphine; 0.1 mg/kg, SC) post-surgery. Experimental time for regeneration is set at 45 days and subsequent procedures as described in Figure 2.4 B. All animal procedures were performed in accordance with the guidelines of the Institutional Animal Care and Use Committees of The University of Texas at Arlington and The University of Texas at Dallas.

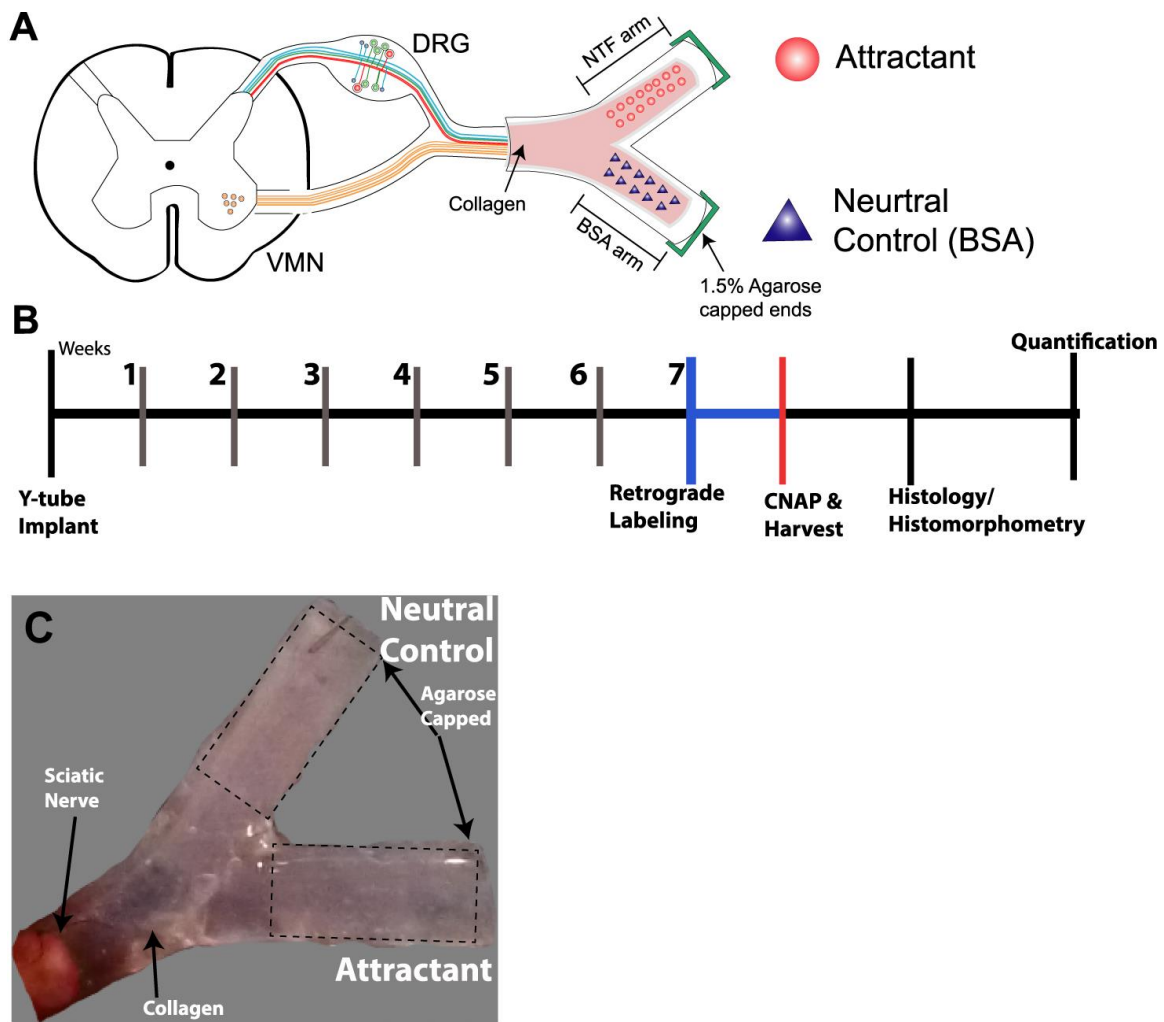


Figure 2.4. Implantation of Y-conduit and experimental timeline. A) Schematic representation of Y-conduit implant into the sciatic mixed nerve. One arm contains an attractant (NGF, GDNF, BDNF, PTN, or NT-3) and the other BSA control. B) Experimental timeline following Y-conduit implantation. C) Representative image of the Y-conduit implantation with an attractant in one arm and BSA control in the other. The ends of the conduit are closed using 1.5% agarose.

2.2.6 Modeling MP-NTF release in Y-shaped conduits.

We estimated the amount of NTF MPs needed to provide sustained release for 30 days in each arm of the Y-conduit with minimal mixing by modeling the protein release and diffusion of the NTF MP as previously reported [119]. Briefly, finite element analysis (COMSOL, Inc.) was used to model the NTF concentration and diffusion in the collagen-filled lumen. One arm of the Y-conduit was modeled for PTN release and another for BSA, according to the parameters specified in Table 2.2.

Table 2.2. Dimension and diffusivity values for protein release from PLGA microparticles in collagen.

Parameter	Value	Description
D_{PTN}	7.6×10^{-12} m ² /s [119]	Diffusivity of PTN in 0.1% collagen
D_{BSA}	2.2×10^{-11} [120]	Diffusivity of BSA in 0.1% collagen
ID	1.5 mm	Channel ID
L	5 mm	Channel length
$V_{microchannel}$	10 μ l	Volume of conduit NTF or BSA-arm
$d_{microparticle}$	2 μ m	Diameter of PLGA microparticles
T_{total}	1.34 ng	Total amount of releasable PTN in the arm

The following equations were used:

$$P = Kt^n \quad \text{[Equation 1]}$$

Percent drug released (P) equals the release constant (K) over time (t). Values of K and n were calculated to be 3.148 and 0.221 from the PTN release data. We estimate PTN diffusivity in

collagen by assuming the molecular structure closely resembles that of NGF in collagen based on their similar molecular weight [120], [121]. NTF diffusion into the collagen-filled lumen is based on Fick's 2nd law [122]:

$$\frac{\partial C}{\partial t} = \nabla \cdot (D \nabla C) + R \quad [\text{Equation 2}]$$

C is the concentration in mol/m³, D denotes the diffusivity in m²/s, and R represents the rate of drug release from the PLGA microparticles in mol/m³s. Since R is the rate of drug release per unit volume, we formulate R to be:

$$R = \frac{M_t}{V} \frac{dP}{dt} \quad [\text{Equation 3}]$$

Where M_t is the moles of drug within a PLGA microparticle of volume V (in m³). The computational domain was discretized using 2nd order Lagrangian tetrahedral volume element. Our model predicts the concentration of the BSA and PTN release throughout the experimental time period. From Day 1 to 10 there is a gradient formation in the conduit arm with higher concentrations at the capped distal end which is impermeable to large molecules (Figure 2.5). The concentration across the length of the arm in the lumen of the conduit is quantified in Figure 2.6. The arrow head located at different days on the figure represents the approximate location of the nerve during regeneration. Assumptions for this model are described below:

- Surface and bulk erosion of the PLGA microparticle and collagen are ignored.
- Diffusivity of the proteins are considered isotropic and constant.
- The size of the PLGA microparticles were limited to 2 μm

- The half-life of the growth factors was not considered as well as axonal uptake during regeneration over time.

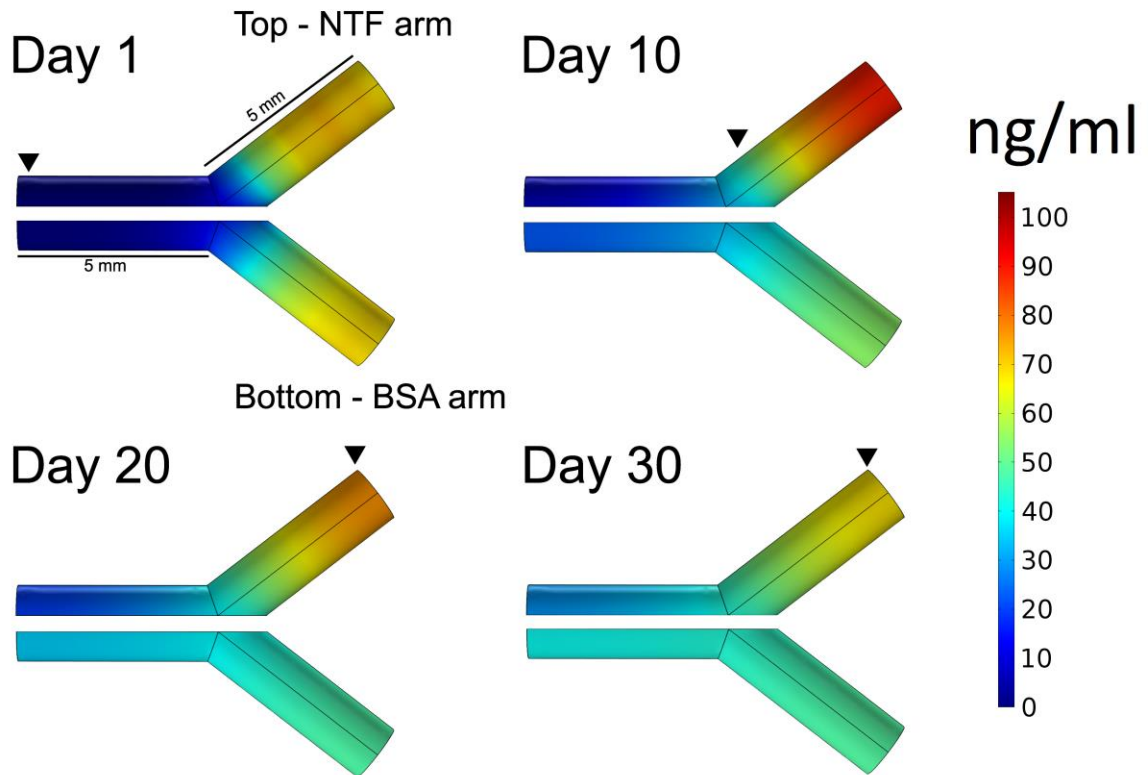


Figure 2.5. Diffusion of PLGA microparticles loaded with NTF and BSA over a 30 day time period. The top arm represents PTN-MP release and BSA-MP release in the bottom arm. Arrow heads at each time point indicates approximate position of nerve regeneration. (Figure prepared with the help of Lokesh Patil)

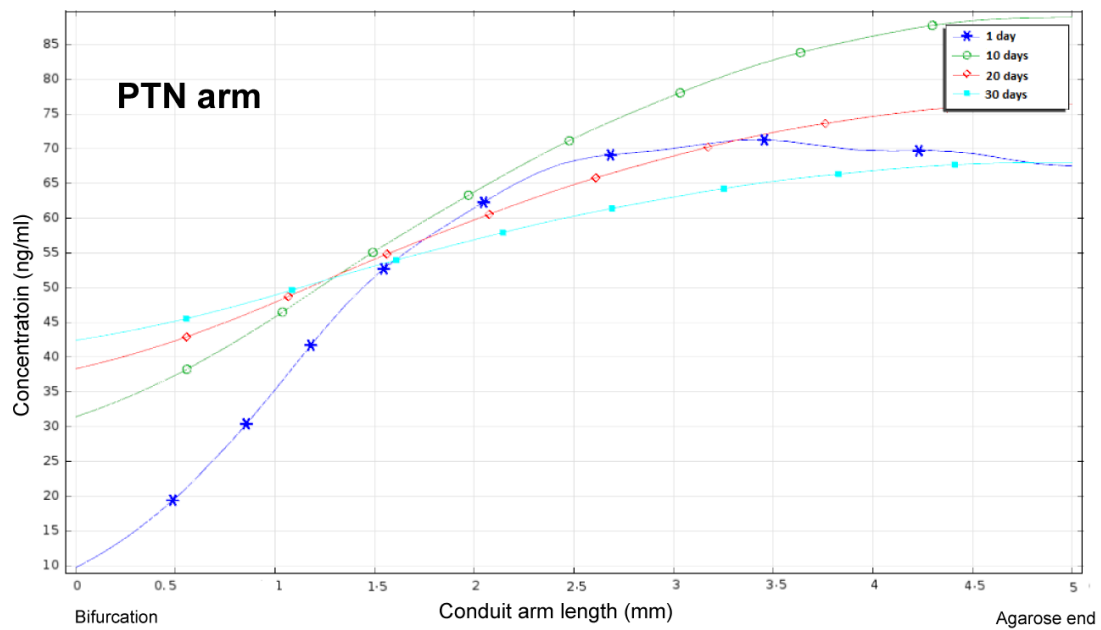
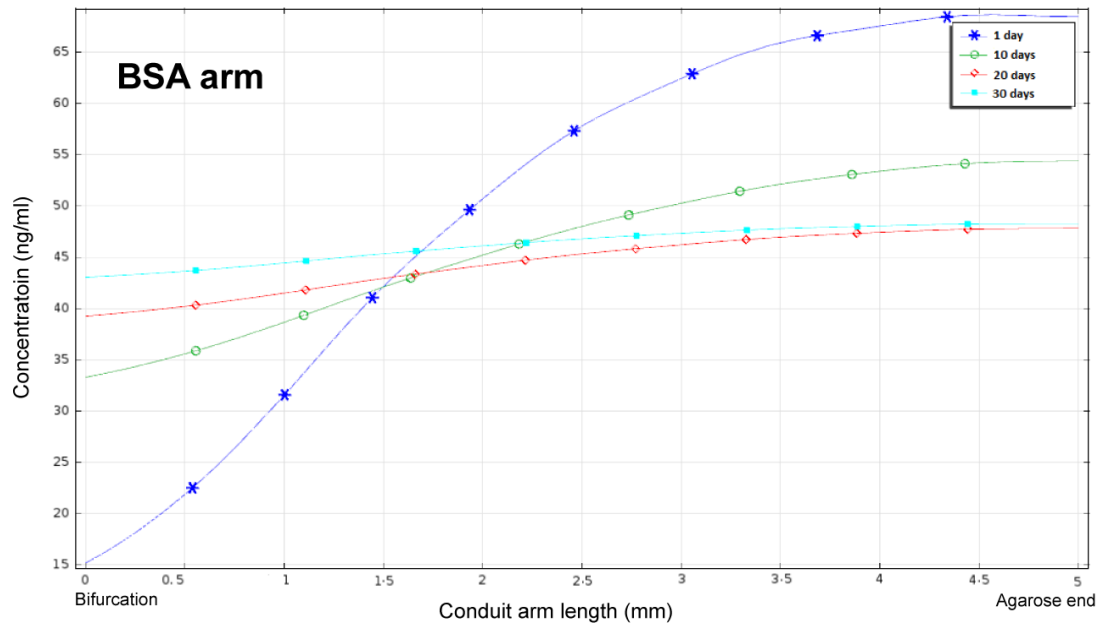


Figure 2.6. Concentration gradient across the length of the Y-conduit arm for the BSA-MP (Top) and PTN-MP (Bottom).

2.2.7 Retrograde labeling and quantification of motor and sensory neurons

The number of motor and sensory neurons that regenerated into each of the "Y" conduit arms was visualized using retrograde labeling from the distal end of the regenerated arms. The number of motor neuron cell bodies visualized in the ventral spinal cord indicated motor axon innervation, and the number of labeled cells in the DRG determined the number of sensory neuron regenerated into each compartment. Briefly, 45 days post implantation, the Y-tube conduit was exposed and the distal edge of the regenerated nerve was isolated by removing a 2 mm tube segment. A reservoir was made around the expose nerve segment using sterilized vaseline. Vaseline was also injected at the bifurcation site to prevent leakage of the retrograde label into the common arm. FluoroGold (FG) and FluoroRuby (FR) (5 μ L of 4%; Fluorochrome LLC, Denver, CO) was applied to the exposed nerve for 1 hour, avoiding cross contamination with the other arm. The exposed nerve segment was rinsed with saline to remove any excess retrograde label and the vaseline removed. The Y-tube was placed back under the muscles and the wound closed as described above.

2.2.8 Compound Nerve Action Potentials (CNAP)

The functionality of the regenerated nerves into the arms of the Y-conduit was confirmed by electrophysiological evaluation. Seven days following the FG-labeling, the entire regenerated nerve was exposed (10-12 mm). Two Pt hooks electrodes (FHC Inc., Bowdoin, ME) were placed in the nerve with one at the sciatic notch, proximal to the implant for stimulation, and the other at the most distal segment of the Y- arm segment (recording). The CNAPs were evoked by stimulating at 0.5-3V using biphasic pulses at 2 Hz, and a pulse width of 30 μ s (A-M Systems,

Sequim, WA). The voltage was determined as three times the amount needed to evoke a CNAP (supramaximal) to ensure activation of all fiber types within the regenerated segment. The response was recorded using Omniplex Data Acquisition System (Plexon Inc., Dallas, TX) at 40 kHz sampling frequency at a bandwidth of 300-8000 Hz.

A custom MATLAB algorithm was used to measure the individual peaks latency of the response and determine their conduction velocity. Using the spike-triggered averaging method, the number of events plus the response was averaged. The latency was measured from the start of the stimulus to the individual response peaks. The conduction velocity for each peak was then calculated based on the distance between the stimulating and recording electrode.

2.2.9 Histology

Following the electrophysiological evaluation (52 days post-implantation), the animals were sacrificed by overdose injection of sodium pentobarbital (120 mg/kg, IP) followed by transcardial perfusion with 4% paraformaldehyde (PFA). The regenerated Y-nerve were harvested and postfixed in 4% PFA/2.5% glutaraldehyde in 0.1 M Cacodylate buffer for EM processing. The spinal cord and the L4 and L5 Dorsal root ganglion were isolated, post fixed and cryoprotected in 30% sucrose prior to OCT embedding for cryosection. The spinal cord tissue was cut in the sagittal plane at 20 μ m thickness and the DRG cross sections at 10 μ m thickness. The sections were mounted onto glass slides serially and stored at -20C until used.

Hematoxylin and Eosin (H&E) staining were performed on nerve-cap segments for signs of necrosis. Following nerve harvest, distal nerve segments were paraffin embedded and cross sections were obtained at 10 μ m thickness. The samples were deparaffinized using xylene and ethanol washes. Hematoxylin was added onto the sample for 4 minutes followed by 3 washes

with dH₂O. Eosin counter stain was added for 2 minutes and then slides washed again with dH₂O three times and were cover slipped.

2.2.10 Quantification of retrograde labelled motor and sensory neurons

All slides were rinsed in PBS to remove the OCT and treated for lipofuscin reduction by incubating the tissue in 750 μ M cupric sulfate/50mM ammonium acetate for 40 minutes as reported elsewhere [123]. The tissue was then rinsed in PBS and cover slipped using immuno-mount (Fisher Scientific, Waltham, MA).

The FG+ and FR+ cells in the spinal cord and DRG were identified with a Zeiss fluorescence microscope using a wide band ultraviolet (UV) excitation filter. To prevent double counting, only positive retrograde labelled cells with a distinct nucleolus were included. Positively labelled DRG were also counted and the area was analyzed using the analyze particle option using ImageJ image processing tool. The DRG soma area was categorized into small ($< 300\mu\text{m}^2$), medium ($300\mu\text{m}^2 < x < 700\mu\text{m}^2$), and large ($700\mu\text{m}^2 \leq$). Multiple counting of motor or sensory neurons were corrected by accounting for section thickness and split nuclei count using methods described by Abercrombie [124].

2.2.11 EM morphometric analysis

A subset of experimental groups (nerve-cap, GDNF, NGF, PTN and respective BSA compartments) were processed for EM (n=3 per group) to evaluate the axon type composition and myelination. The fixed tissue was embedded in plastic and section at 1 μ m thickness using an ultra-microtome. The thin sections were stained with toluidine blue and photographed.

Osmium stained sections were visualized using a JEOL LEM 1200 EX II microscope. Five to six

fields of view per section were imaged (4000x magnification) and analyzed for the number of unmyelinated and myelinated axons, fiber (axon + myelin) diameter, axon diameter, and g-ratio, using ImageJ software.

2.2.12 Statistical analysis

The groups were compared using one-way ANOVA and Bonferroni's ad-hoc multiple comparison test using Prism 6 software (GraphPad Software Inc.). A $p \leq 0.05$ was considered statistically significant. The data is presented as the mean \pm standard error of the mean.

2.3 Results

2.3.1 Bifurcated nerve regeneration is comparable among all groups.

Gross evaluation of the regenerated nerves into the Y-shaped conduits 45 days after implantation demonstrated that nerve growth into the separate chambers were similar among all groups (Figure 2.7). We confirmed that nerves regenerated along the 5 mm common arm and bifurcated into two similar size branches (4-5mm), as it entered into the NTF- or BSA-arms of the Y-conduit (Figure 2.7 A). In all cases the nerves grew into the center of conduit filling about 30-40% of the available cross section area (1.5 mm), before stopping at the agarose-capped end. The nerve diameter between the groups showed no significant difference and the length of the individual regenerated arms were similar as well (4-6 mm) (Figure 2.7 B). Histological analysis confirmed a normal perineurium and endoneurium composition in all treatment groups. The area occupied by axons in the tissue was estimated from a cohort of 3-6 animals per group and showed that axons fibers filled $73.8 \pm 19.3\%$ of the cross sectional area. In all cases a small area

containing collagen devoid of axons was seen primarily at the center of the NTF and BSA arms. No significant differences were observed by the specific NTF treatment compared to BSA at the gross anatomical level.

The distal nerve-cap segments used as non-specific control was histologically analyzed for necrosis using H&E staining. Absence of clustered nuclei staining suggests the tissue did not undergo a necrosis process (Figure 2.8). The pale pink region in the middle of the tissue is indicative of collagen.

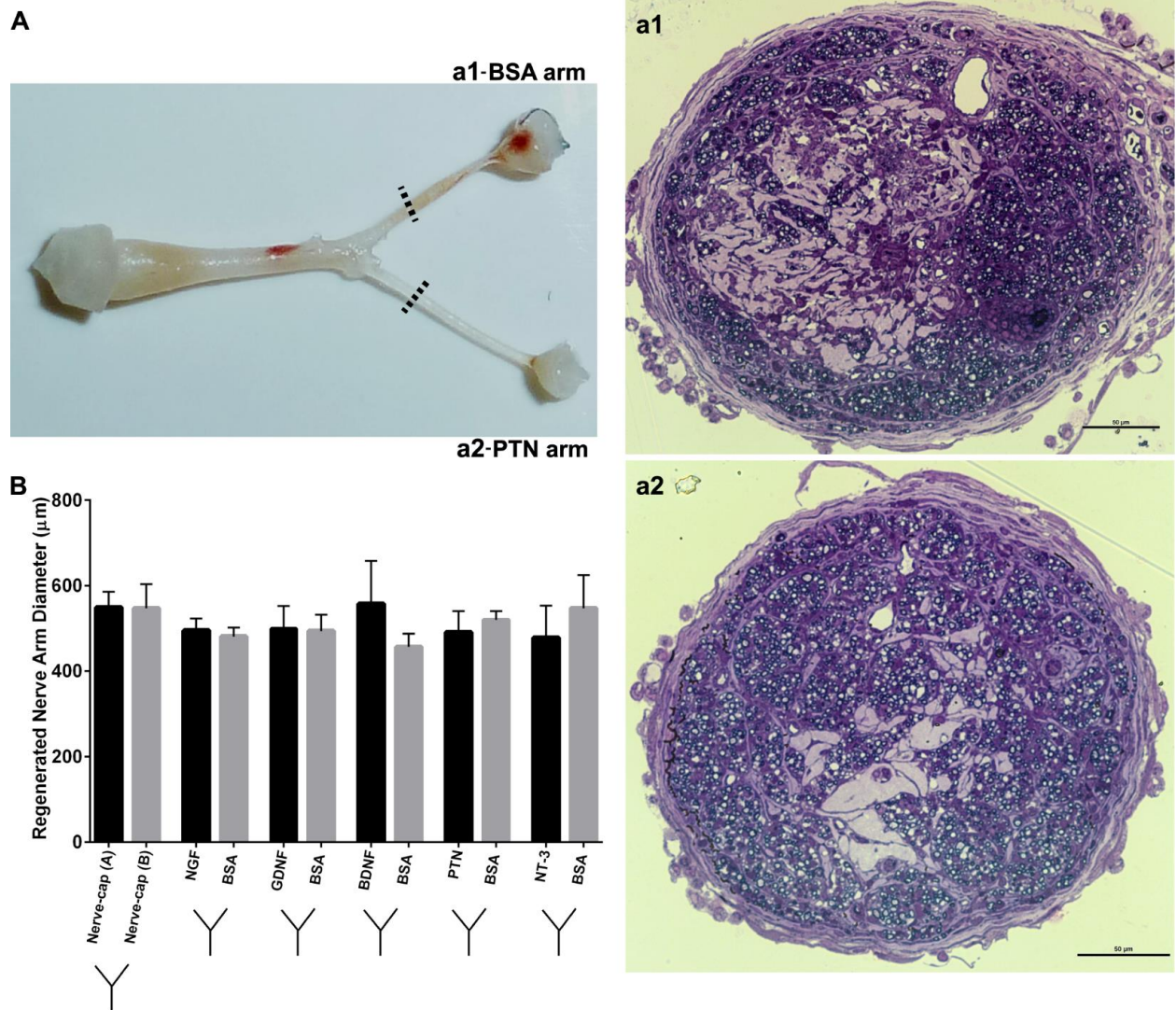


Figure 2.7. Comparable Y-nerve regeneration using NTF-MP with no distal targets. A) Representative image of a regenerated Y-nerve and toluidine stained semi thin sections for the BSA arm (a1) and PTN arm (a2). B) Similar regenerated nerve diameter across the experimental groups. Data presented as mean \pm SEM. No statistical significance observed.

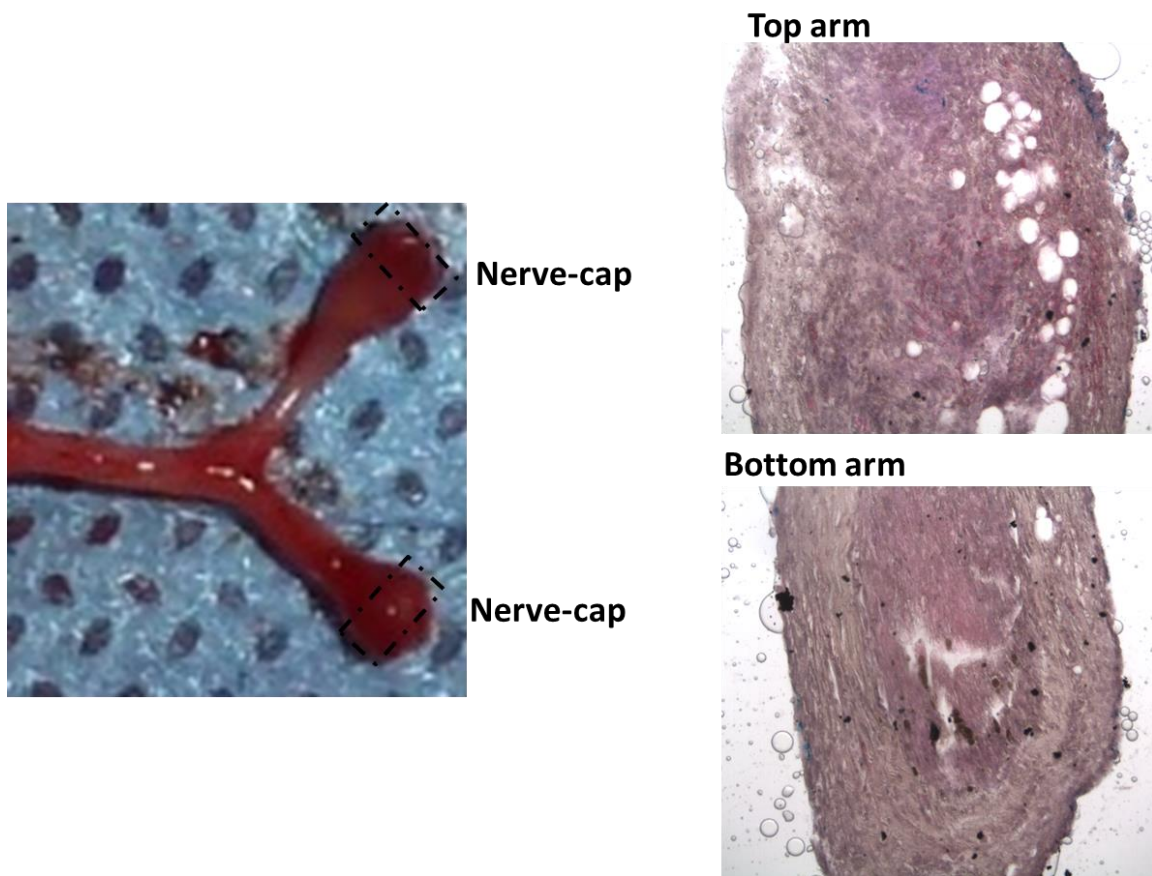


Figure 2.8. H&E staining of the two nerve-cap segments distally attached to the regenerated nerve arm.

2.3.2 Regenerated nerve fascicles show electrical competency

Electrophysiological recordings from the regenerated Y-nerve were obtained by measuring CNAP from the individual regenerated nerve fascicles (Figure 2.9). Multiple peaks were observed following activation of different fiber types and the latency was measured. Conduction velocity (CV) was calculated after spike triggered averaging, and the values were categorized into slow (≤ 5 m/s), medium ($5 < x \leq 30$ m/s), and fast (> 30 m/s) (Figure 2.10 B & C). A peak

was considered a response if the amplitude was 10% or more than the baseline noise level which ranged from -0.003 to +0.003 mV.

The number of peaks observed among the NTF groups ranged from 1-3 peaks and showed no difference between the groups (Figure 2.9 D). Each CNAP response was then categorized based on CV and the incidence peaks were analyzed for each experimental group to identify any indication of NTF selectivity (Table 2.3). Majority of the peaks were in the medium velocity range ($51.6 \pm 17.3\%$) with fast ($27.7 \pm 14.6\%$) and slow ($20.7 \pm 12.3\%$) range peaks have limited number of occurrences. Comparison between the NTF and BSA control groups showed no difference in any CV ranges.

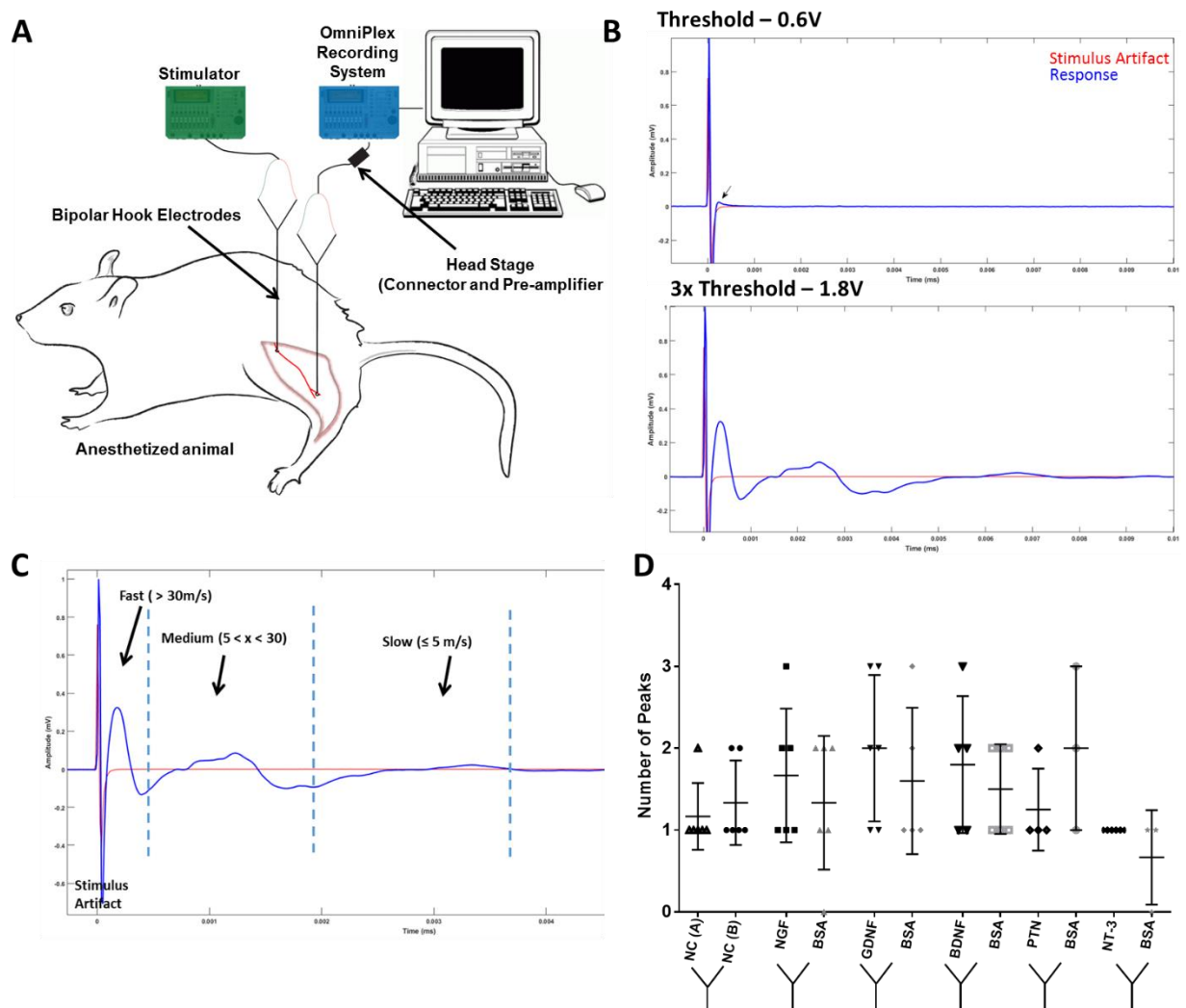


Figure 2.9. CNAP measurements show activation of different fiber composition at 45 days. (A) Setup for measuring CNAP. Bipolar hook electrodes provided stimulus pulses and the response recorded distally from the regenerated arms. (B) CNAP response at threshold stimulus and three times threshold for maximum axon activation. (C) Representative recording showing the stimulus artifact followed by three distinct peaks with different velocity ranges. CV measurements separated by fast (> 30 m/s), medium ($5 < x \leq 30$ m/s) and slow (≤ 5 m/s). (Figure prepared with the help of Vidhi Desai)

Table 2.3. CNAP peaks incidences observed within the velocity ranges. ‘+’ indicates one peaks observed within the range. (#) indicates number of animals used to obtain CNAP response.

	Fast ($>30 \text{ ms}^{-1}$)	Medium ($5 < x < 30$)	Slow ($\leq 5 \text{ ms}^{-1}$)
NC (A) (6)	+++	+++++	++
NC (B) (6)	+++	+++	
NGF (6)	++	+++++	+++++
BSA (6)	+	++++	+++
GDNF (6)	++++	+++++	++
BSA (5)	++	++++	+
BDNF (5)	++	+++++	+++
BSA (5)	+++	++++	+++
PTN (4)	++	+++	+
BSA (3)	++	+	+
NT-3 (4)	++	++++	
BSA (3)		++	

2.3.3 Effect of single guidance cues on motor and sensory neuron regeneration

FluoroGold positive motor neurons were visualized in the spinal cord ipsilateral to the implantation site (Figure 2.10). FluoroRuby traced cell were omitted for quantification due to limited efficiency in retrograde label uptake. An uninjured control was used to determine efficacy and the baseline of the number of ventral motor neurons. A one-way ANOVA analysis showed a significant effect due to treatment ($P \leq 0.05$; $F = 8.824$; $R^2 = 0.74$). The number of

ventral motor neurons (VMN) attracted by the nerve-cap segments were 424 ± 176.4 and 400.3 ± 377.8 respectively which was comparable to the total number of VMN in the uninjured control. The number of VMNs in the PTN (101.3 ± 34.38), NGF (162.5 ± 20.5), and NT-3 (160.0 ± 54.5) were comparable to each other. In sharp contrast to the PTN, NGF, and NT-3 groups, both BDNF (388.5 ± 295.8) and GDNF (476.6 ± 242.6) showed an increased number of attracted motor neurons comparable to the nerve-cap. Comparison of GDNF to its BSA arm (133.7 ± 33.9) revealed a significant increase in the number of VMN ($P \leq 0.05$; Bonferroni's).

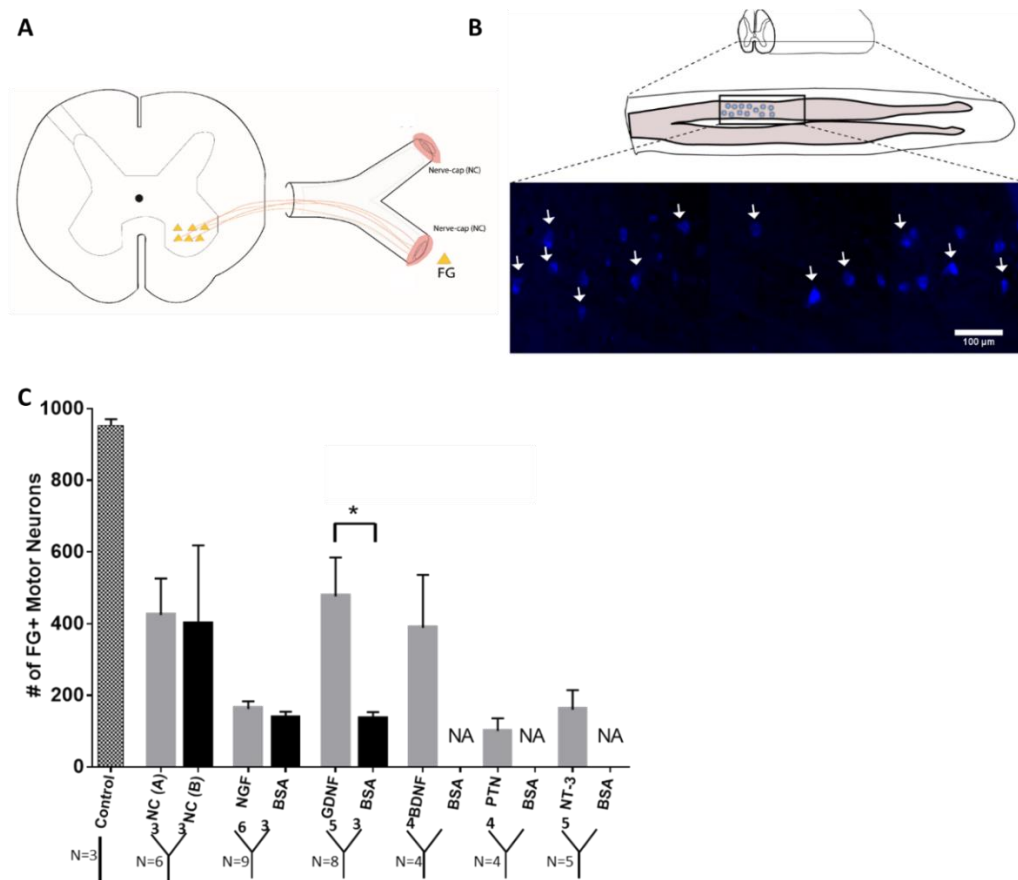


Figure 2.10. Limited enrichment of VMN by NGF, PTN, and NT-3. A) Schematic of FG labelling at distal regenerated nerve end. B) Schematic representation of the VMN location in the spinal cord and FG+ cells located ipsilaterally. Arrows show positively labelled motor neurons. C) FG+ motor neuron quantification shows GDNF attracted a significant number compared to BSA control and PTN. * indicates $P < 0.05$; data presented as mean \pm SEM. Scale bar = 100 μ m.

Positively labelled DRG sensory neurons were counted and separated by perikaryal (cell body) size (Figure 2.11 A & B). Perikaryal size varies greatly and is roughly correlated with the conduction velocity and the sensory modality [125], [126]. Cells with an area less than $300\ \mu\text{m}^2$ were considered small, greater than $700\ \mu\text{m}^2$ was large, and in between were classified as medium. DRG cell count showed greater than 50% reduction when compared to the uninjured control which was in accordance with previous literature (Figure 2.11 C) [127]–[129]. The total number of retrograde traced sensory neurons showed no difference between the NTF and the BSA arms. Due to the low efficacy of FluoroRuby retrograde label, the BSA arms for the BDNF, PTN, and NT-3 were omitted. Analysis of the sensory subtype based on perikaryal size also showed no significant effect in the different size modalities.

Positively labeled VMN and DRG sensory neurons in each compartment of the conduit were used to determine the sensory/motor ratio (Figure 2.12). The S/M ratio for uninjured control was 7.3 ± 0.8 while nerve-cap A and B control showed ratios of 5.5 ± 4.0 and 4.4 ± 1.2 respectively due to the decreased sensory neuron regeneration following injury. The ratios of NGF and GDNF when compared to their respective BSA arms showed no significant effect. However, among the NTF groups, PTN showed the highest S/M ratio of 9.2 ± 5.8 but could not be compared to its respective BSA arm.

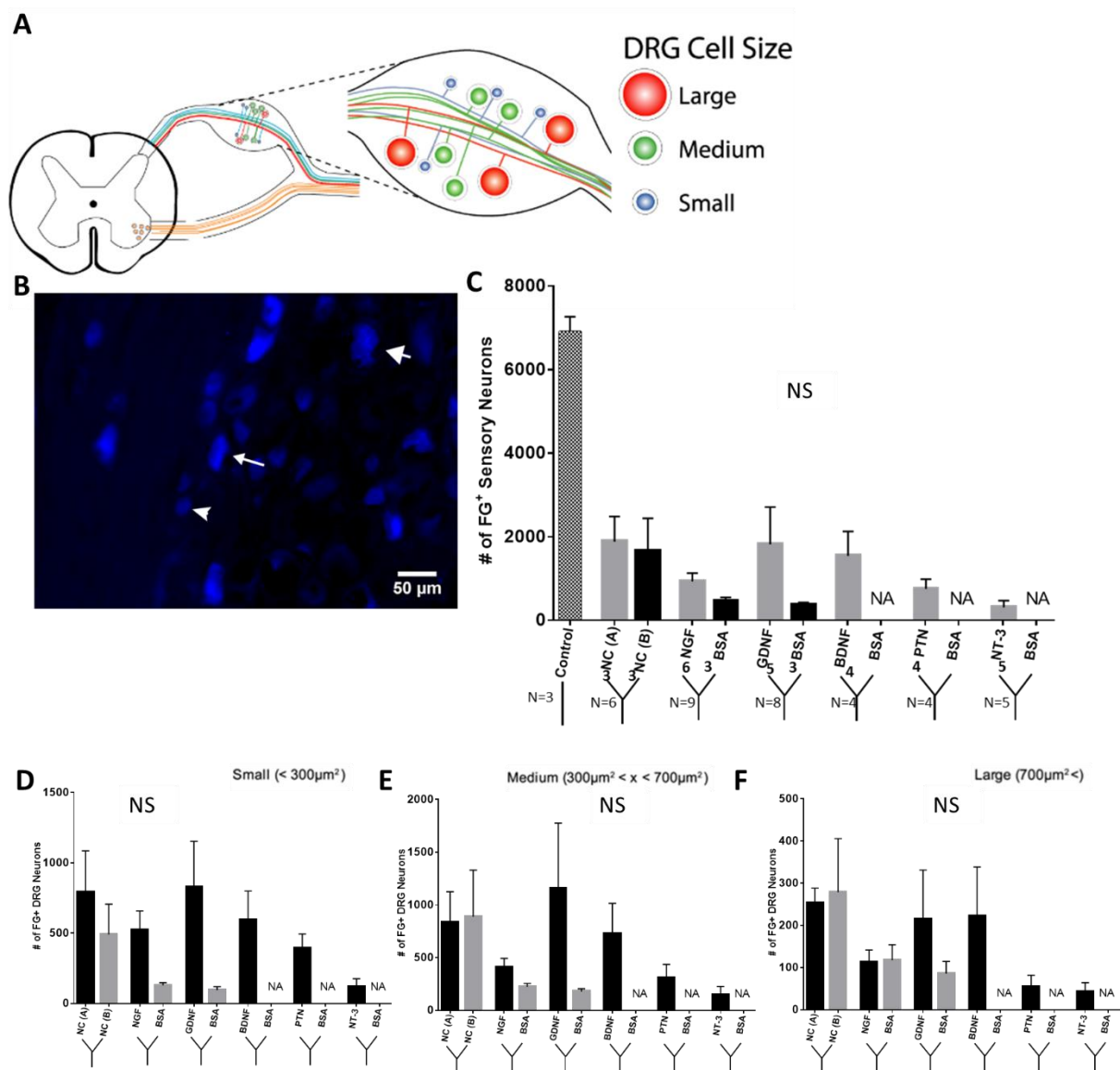


Figure 2.11. Sensory neuron counts and perikarya size distribution. (A & B) Schematic of DRG soma size distribution and representative image of FG+ cells of varying size (indicated by arrows and arrow head). (C) FG+ sensory neuron count shows overall reduction in the number of regenerated sensory neurons. (D-F) Perikarya size distribution for small, medium, and large. Data presented as mean \pm SEM. Scale bar = 50 μ m. (Figure prepared with the help of Martin Tran)

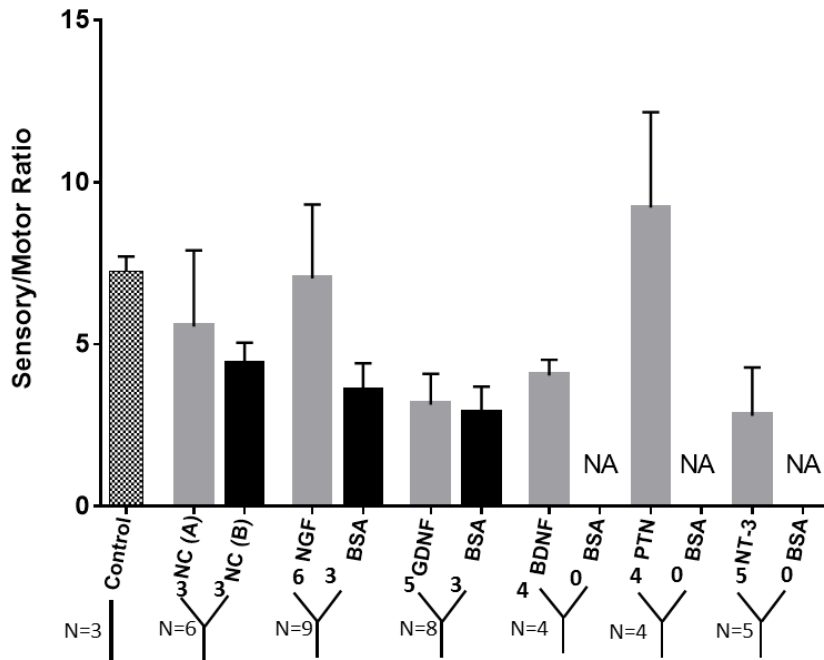


Figure 2.12. Ratio of FG+ sensory and motor neurons using single attractants show no difference compared to the BSA arm.

2.3.4 Single NTFs effect on axon morphology without distal end-organ targets

Axon type composition and myelination were analyzed from a subset of NTF groups (Figure 2.13). Electron microscopic evaluation showed normal myelinated and unmyelinated axons within the regenerated nerve fascicles. A one-way ANOVA showed a significant effect between the NTF groups for unmyelinated axon count ($P \leq 0.05$; $F = 2.89$; $R^2 = 0.61$) (Figure 2.14A). The NGF arm (118.1 ± 44.1) had significantly higher number of unmyelinated axon count compared to PTN (66.3 ± 26.8) ($P \leq 0.05$; Bonferroni's). GDNF and PTN showed no difference in number of unmyelinated axon count when compared to their adjacent BSA arm. Group wise comparison between the nerve-cap and NTFs also showed no difference. Conversely, no significant

difference was observed in the number of myelinated axon count. The nerve-cap groups showed lower number of myelinated axons without reaching significance. Comparison of myelin thickness showed no difference between the NTF groups and their respective BSA control arms (Figure 2.15 A). The fiber diameter for the NTF groups were on average was 1 μm smaller compared to the nerve-cap groups (Figure 2.15 B). No significant effect was observed between the experimental groups.

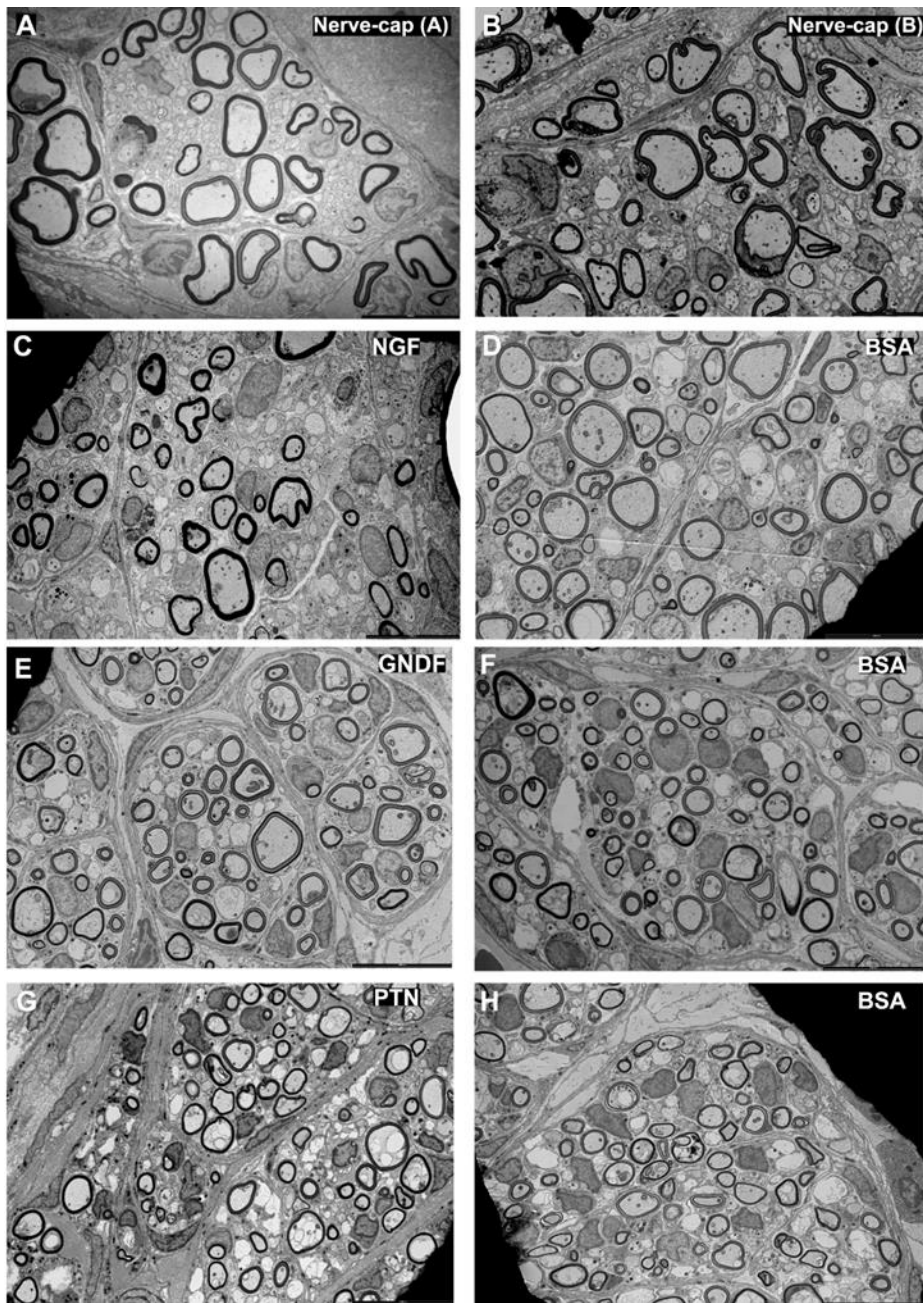


Figure 2.13. Representative SEM images of the regenerated Y-nerve arms showing myelinated and unmyelinated axons. Scale bar = 10 μ m.

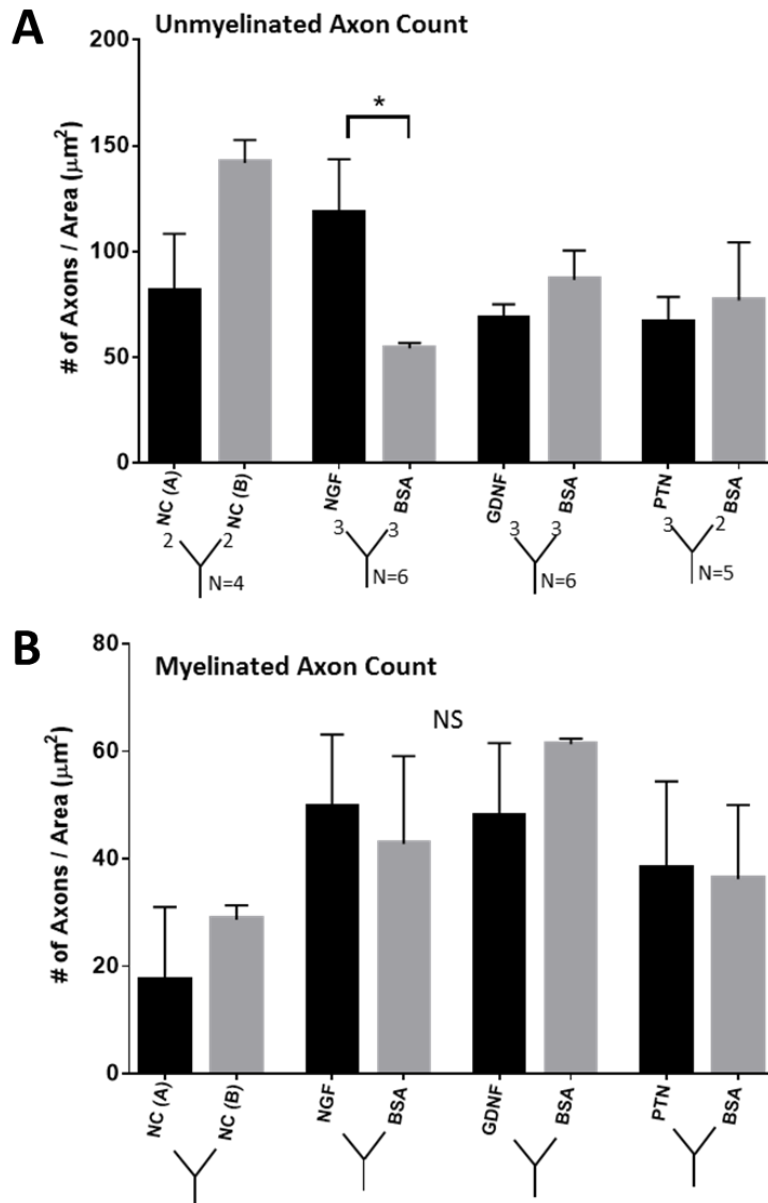


Figure 2.14. Unmyelinated and myelinated axon count show NTF influence. (A) NGF showed significantly higher number of unmyelinated axon compared to BSA arm. (B) Myelinated axon count showed no significant difference. * indicates $P \leq 0.05$; one-way ANOVA followed by Bonferroni's multiple comparison. Data presented as mean \pm SEM. (Figure prepared with the help of Dianna Nguyen)

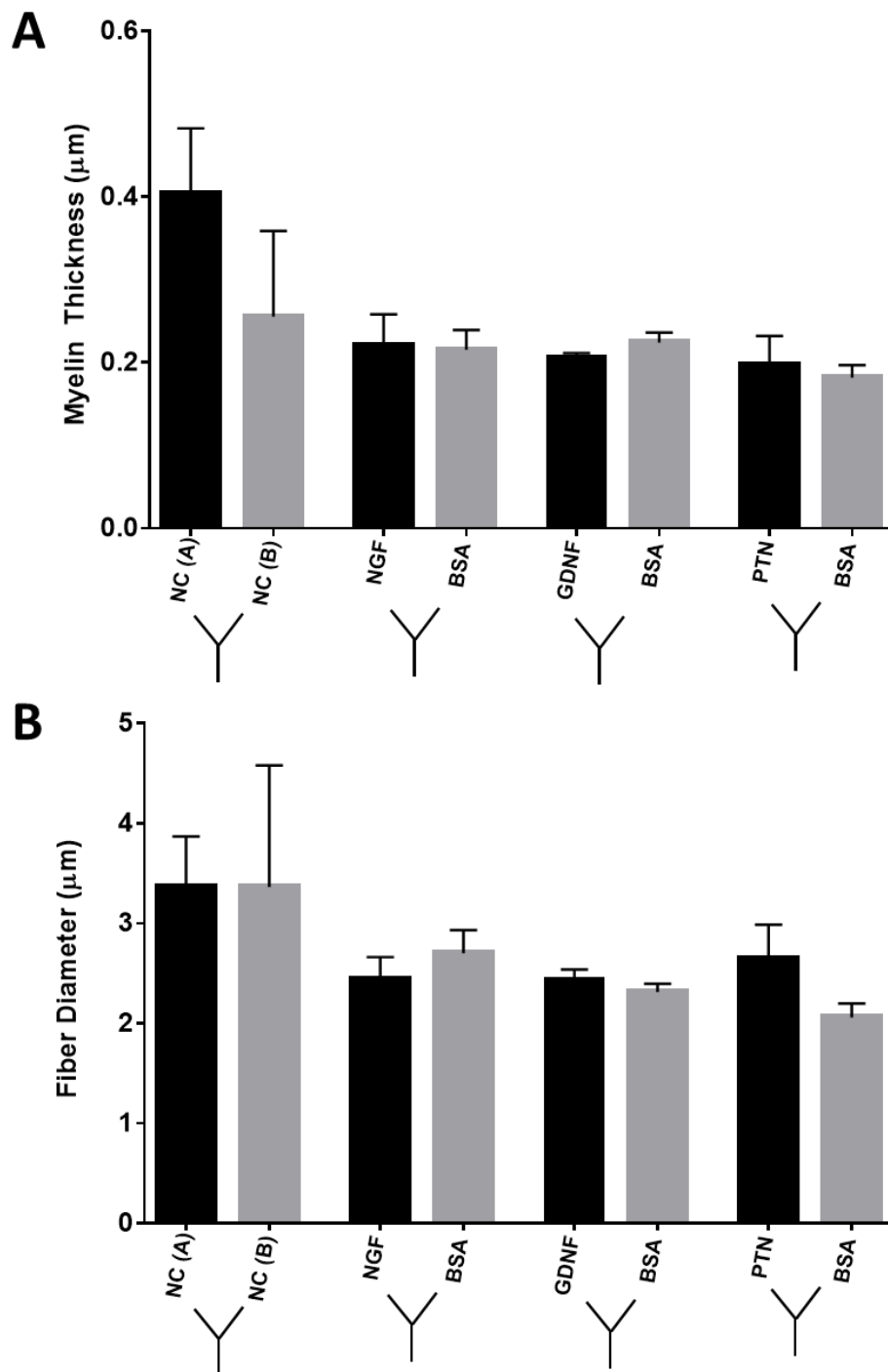


Figure 2.15. Myelin thickness and fiber diameter were comparable among NTFs. Data presented as mean \pm SEM.

Scatter plots of g-ratio as a function of axon diameter was plotted for each experimental group (Figure 2.16). Axon diameter was divided into small myelinated ($\leq 1\ \mu\text{m}$), medium myelinated ($1 < x \leq 4\ \mu\text{m}$), and large ($> 4\ \mu\text{m}$) based on axon size reduction following nerve injury [130]. The nerve-cap A showed a different trend when compared to nerve-cap B, with more myelinated axons and a g-ratio range from 0.4-0.6. Myelinated axons in the small, medium, and large range were also present in the NTF groups, with the majority falling in the medium range with a g-ratio range of 0.6 – 0.8. The smaller myelinated axons ($< 1\ \mu\text{m}$), showed a higher degree of myelination for GDNF and NGF with a g-ratio range from 0.4 – 0.6. Compared to the NTF groups, their adjacent BSA arms showed similar trends, suggesting some degree of cross-diffusion.

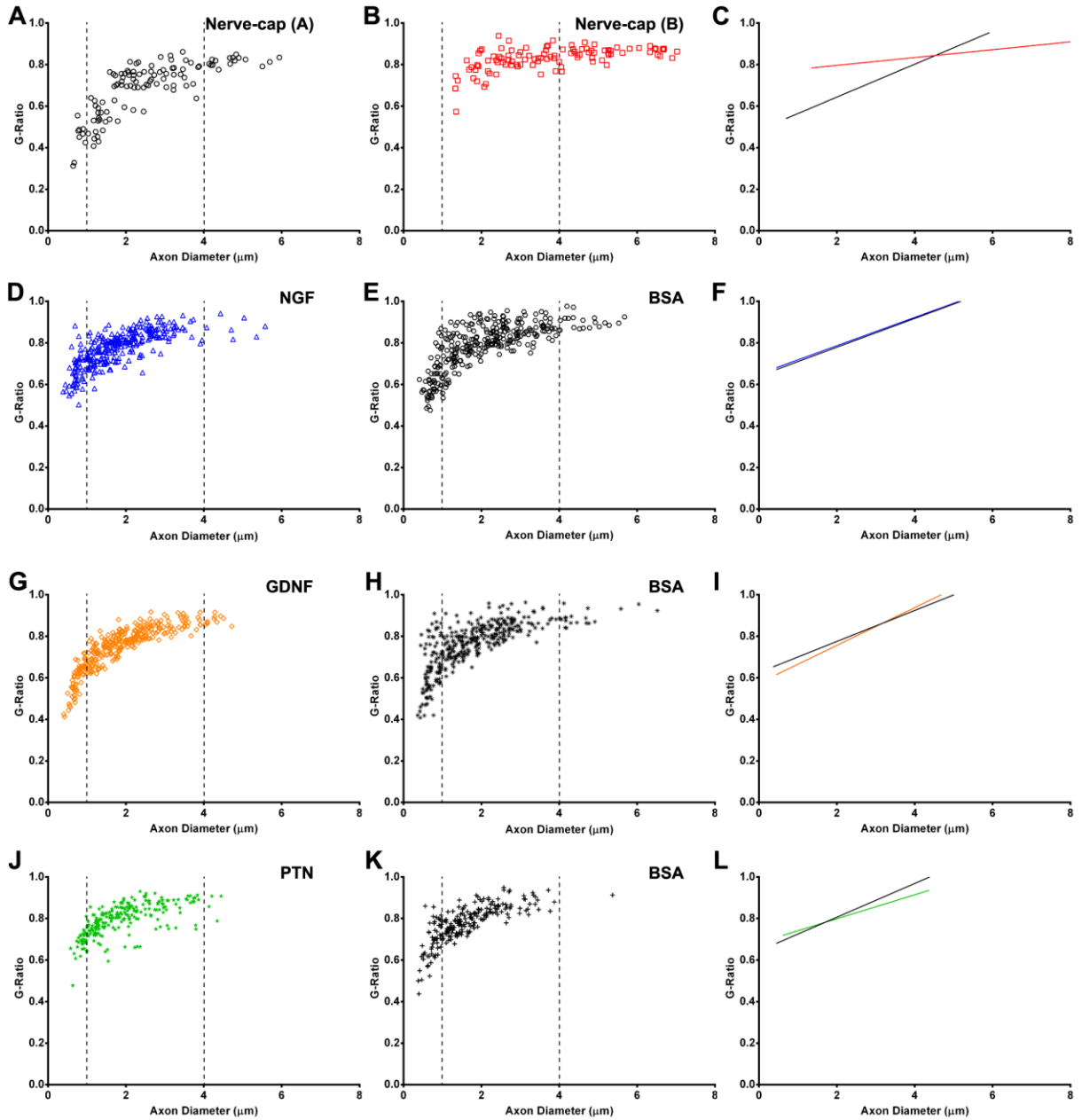


Figure 2.16. Scatter plots of g-ratio as a function of axon diameter for different NTFs. Dotted lines represents divisions of myelinated axons as small, medium, and large. Similar trends for NTF and BSA arms observed.

2.4 Discussion

Peripheral nerves are composed of a mixed population of motor and sensory subtypes [37], and current methods of recording motor activity and eliciting sensory percepts have resulted in concomitant activation of multiple fiber types leading to paresthesia [30], [39], [131], [132]. Regenerative based electrodes have demonstrated their capability in recording motor activity and providing safe stimulation ranges [27], [33], [115], [133]–[135]. In addition, they also offer a new venue to manipulate the pathway of regenerating axons for interfacing. Previously we demonstrated the use of molecular cues to entice axon regeneration for such interfaces [104]. With this in mind, the current study evaluated the effectiveness of single molecular guidance cues (NGF, NT-3, GDNF, BDNF, and PTN) to entice the regeneration of electrocompetent axons and modulate the sensory to motor ratio using NTFs encapsulated in microparticles. The NTF-MP were employed in a compartment of the Y-conduit and compared to a non-selective BSA control in the other compartment. We adapted the mixed sciatic nerve model to investigate the ability of specific NTFs to entice the growth of motor and sensory axon subtypes. Influence in regeneration from the outside environment was minimized using agarose fillings at the distal ends of the Y-conduit. The expression of NTFs in the arms of the Y-conduit established a gradient that persisted throughout the experimental time point. Our results demonstrate successful nerve elongation can be achieved in the absence of distal targets and in the presence of a single NTF. The regenerated nerve fascicles showed electrocompetency in 97% of the cases with different axon composition as represented by multiple peaks in the CNAP. Although successful regeneration was observed, single NTF were shown to be insufficient to modulate the sensory to motor neuron ratio.

2.4.1 Regeneration in the absence of distal targets

Spontaneous regeneration following peripheral nerve injury has been documented previously [136]. During regeneration, the distal nerve and end-organ targets provide a growth permissive environment for the regenerating axon [107], [137], and exogenous application of NTFs in addition to the presence of growth factors secreted by Schwann cells and end-organ enhance regeneration [75], [79], [107]. However, in such paradigms, nerve regeneration was accomplished in continuity with the distal target. In this study, we demonstrated that nerve regeneration can be initiated and sustained over a 45 day time period without a distal target. The single NTFs used in the Y-conduit arms enticed regeneration and sustained axonal growth and maturation. The regeneration bifurcated midway in the conduit and stopped distally, forming bulbous ends. This observation suggests a possible neuroma formation, however animals did not display any signs of discomfort throughout the study. In a similar study, neuroma feature was also observed after nerve regeneration was capped distally [138]. However, the method of capping the distal end has been shown to suppress pain induced through the spontaneous ectopic firing resulting from a neuroma formation [139], [140]. Moreover, the authors were able to demonstrate the maintenance of the regenerated capped nerve over a period of nine months, suggesting its application for neural interfaces can be established chronically.

2.4.2 NTF enrichment of sensory and motor neurons

Continuation from previously reported findings [104], an array of NTFs were tested here to see if the sensory to motor ratio can be modulated in an *in vivo* choice assay. The ability of NTFs to exert a regenerative force in the absence of end organ target and maintain electrical conductivity

ensures the feasibility of the current approach. Semi-quantitative analysis of the CNAP demonstrated multiple peaks within different velocity ranges suggesting the regeneration of multiple neuronal modalities. Comparison of the number of peaks in the NTF compartment was variable and also axon quantification of the area under the curve of the peaks also yield high variability (data not shown). It is believed that the recording setup for CNAP was not sensitive enough to visualize a difference in NTF specificity using bipolar hook electrode.

To determine neuronal composition, retrograde labeling was employed which revealed regeneration of both motor and sensory neurons. Motor neuron regeneration by GDNF and BDNF was comparable to the of nerve-cap control. This is in conjunction with previous studies on their role in enhancing motor neuron regeneration; however this was in continuity to an end target [84], [107], [113]. Conversely, PTNs role in enhancing motor neuron regeneration was not observed in this current study [86], [87], [100], suggesting PTN by itself is not sufficient to initiate motor neuron regeneration. PTN is expressed in Schwann cells, macrophages, and endothelial cells resulting in an adaptive response following injury [141]. It is plausible that PTN plays a key role in promoting synergistic effect only in the presence of distal nerve target. On the contrary, PTN did show a high sensory/motor ratio which suggests PTNs feasibility in generating a sensory rich nerve fascicle arm.

The presence of multiple axon subtypes can be attributed to the expression of receptors present in both motor and sensory axons [59]. After peripheral nerve injury, axons and Schwann cells express the low-affinity p75 receptors. NGF has been shown to induce a growth promoting effect

through this receptor or indirectly by Schwann cells [142], [143]. Similarly, sensory neuron regeneration into the GDNF compartment can be attributed to its receptor (RET, GFR α 1- 3) expressed in large diameter DRG neurons as well as unmyelinated sensory neurons [144]. This could explain the two-fold increase in the sensory count compared to NGF, which was expected to yield a high sensory/motor ratio compared to uninjured control.

The non-selective BSA control arm also included motor and sensory axon subtypes regeneration. Previous studies using BSA as a negative control showed minimal regeneration of axons following peripheral nerve injury and repair [109]. In this study, the BSA was adjacent to the NTF arm and showed a similar trend for g-ratio as a function of axon diameter (Figure 2.16). This suggests that there was cross-diffusion of the NTFs into the bifurcation region resulting in the axonal regeneration into the BSA compartment. Also, it should be noted that the neuronal content in both the BSA arms in the GDNF and NGF groups show similar potency of regeneration for both motor and sensory neurons, which would represent the baseline regeneration level in the paradigm.

2.4.3 NTF effect in sensory/motor ratio

Interfacing a heterogeneous nerve for recording motor activity is known to be challenging as the sensory neurons outnumber motor neurons ~15:1 [36]. In addition, the spatial arrangement of the motor neurons are sparsely organized [145]. In this study, a Y-conduit was used to alter the ratio of a regenerating heterogeneous mixed nerve into two separate compartments. Single NTFs show it is feasible to regenerate nerve fascicles without distal targets, however modulating the sensory to motor ratio could not be achieved (Figure 2.12). Additionally, the overall regenerative potency

between the NTFs were different. GDNF showed comparable regenerative potential to nerve-cap controls in motor and sensory neuron regeneration, whereas NGF and PTN saw a decrease of 50-60%. The BSA control showed a greater than 70% decrease in the total number of regenerated neurons. Even though BSA groups show no difference in the S/M ratio compared to their NTF arms, overall regenerative capacity of the NTFs was better than the BSA treatment.

2.4.4 Future directions

An alternative approach to modulate the ratio would be to apply two different molecular attractants in each of the compartments. Since the influence of a single attractant is not potent enough to entice distinct regeneration, two attractants known to bind to two specific receptors in the regenerating axon might be sufficient to modulate the S/M ratio. Apart from GDNF, we also observed higher number of attracted motor neurons in the BDNF compartment. Axotomized motor neurons express receptors for BDNF (trkB and p75) and has been shown to play a role in motor neuron survival following ventral root avulsion [83], [146], [147]. Evaluation of the synergistic combination of both GDNF and BDNF to enrich motor neurons to a compartment can further improve the efficacy of peripheral nerve interface. Synergistic combination of NTF have demonstrated enhanced regeneration compared to single factors [77]. In addition, using a subtractive method to inhibit axon subtype also provides a venue into altering the S/M ratio.

CHAPTER 3

MODULATION OF SENSORY/MOTOR RATIO USING MOLECULAR GUIDANCE CUES

3.1 Introduction

Peripheral nerves are composed of a heterogeneous mix of axon types consisting of somatic motor and sensory neurons as well as autonomic fibers. Despite being heterogenic, peripheral nerves are somatotopically organized as fascicles targeting individual muscles and skin targets [148]. However, for individuals with amputation, interfacing in the peripheral nerves can be difficult as the somatotopic organization is less evident proximal to the distal injury site. The intrinsic ability of the peripheral nerve to spontaneously regenerate following injury has provided a gateway into interfacing at the residual nerve stump [136]. Regenerative based electrodes have demonstrated the feasibility of interfacing in a mixed nerve to record motor activity and stimulate sensory fibers for a bidirectional flow of information [25], [32]. Recently, we developed a Regenerative Multi-electrode interface (REMI) capable of recording both motor and sensory related activity in chronically injured peripheral nerves [33], [35]. In addition, the REMI has been shown to provide safe physiological stimulation in the mixed nerve. However, the mixed nature of the axonal regeneration provides difficulty in interpreting the nature of the recorded signals and further makes precise sensory stimulation difficult due to concomitant recruitment of axon fibers [35], [39].

During development motor efferent and sensory afferent projections are organized into coordinate and functionally separate pathways. This sensory-motor heterotypic neuron

segregation is the result of the repulsive interaction of ephrin-A ligands and its Eph receptors [45]. Moreover, molecular attractive cues from the distal muscle and skin targets guide extending axons and organize them into intra-nerve fascicles. The distal targets continuously express specific NTFs to promote axon survival and maintenance. However, after injury the connections are lost and the regenerating axons seek its original target with the help of guidance cues. Days following injury, the ventral root and muscle efferent nerve show increased expression of GDNF, PTN, and BDNF, whereas the dorsal root and cutaneous nerve had increased expression of NGF, HGF, VEGF, GDNF, and BDNF [100]. Additionally, the target end-organs play a vital role in the guidance of regenerating axons with differential up-regulation BDNF, GDNF, and NT-3 by the denervated muscle [101], [149]–[152]. Application of these NTFs have been shown to enhance axon regeneration and improve functional recovery, and their recent roles in guiding axonal regeneration has been demonstrated.

NGF is one of the most widely studied NTFs and its application in promoting sensory axon growth has been demonstrated [109]. NGF role in axon guidance was previously reported where induced lentiviral expression of NGF in the sensory branch of the femoral nerve enticed the regeneration of CGRP⁺ axons towards that branch [102]. Similarly, NGF expression in the spinal cord initiated sensory axon regeneration into the dorsal lamina [103], [114]. Additionally, enhanced motor neuron regeneration was also observed in rats where both BDNF and GDNF were exogenously applied. Retrograde labeling following nerve transection and repair showed an increased number of regenerating motor axons using BDNF, GDNF, and both in combination [77], [106], [108], [153]. These studies demonstrate that specific expression of NTFs can induce

neuron-type selective regeneration. Furthermore, we have recently demonstrated the role of NTFs in enticing sensory axon subtype regeneration *in vitro* using NGF and NT-3 [104]. We showed that NGF was able to guide CGRP⁺ axons to one chamber while NT-3 chamber showed large diameter fibers. This was also translated *in vivo* using a “Y” conduit and verified. This initial study was expanded to evaluate a number of NTFs including NGF, BDNF, NT-3, GDNF, and PTN in the absence of a distal target in the previous chapter. We demonstrated that single NTFs are capable of regenerating electrically competent nerve fascicles, however, single attractants were insufficient to alter the sensory/motor (S/M) ratio. Though this study compared a single NTF in one chamber of the Y-conduit versus a control (BSA), multiple NTFs have yet to be incorporated into a single Y-conduit.

This current chapter aims to use the findings from Chapter 2 to determine if one compartment in the Y-conduit can be enriched with motor axons while the other can increase the number of sensory axons. Here we will use the Y-conduit to evaluate if BDNF/GDNF in one compartment versus either NGF or PTN is able to enrich motor and small sensory subtype axons. We hypothesized that the sensory/motor neuron ratio in regenerated nerve fascicles can be modulated by different combinations of molecular attractants in a choice assay.

3.2 Materials and Method

3.2.1 PLGA encapsulation of NTFs and bioactivity test

Microparticles loaded with NTFs were encapsulated using biodegradable PLGA using the double emulsion method as described in Chapter 2. The concentration used for the NTFs are as follows: human recombinant NGF (7S, 13.5 kD; Invitrogen), BDNF (27 kD), NT-3 (13.6kD), GDNF (15 kD), and PTN (15.4kD) (20µg/ml; Preprotech Inc, NJ) or BSA (20 µg/ml; Sigma-Aldrich). The bioactivity of fabricated PGLA microparticles loaded with NTFs were tested on neonatal (P0-P4) mice DRGs as mentioned in the previous chapter. All NTF-MP showed biological activity comparable to the recombinant protein.

3.2.2 Y-tube implantation to the heterogeneous mixed sciatic nerve

Fifty-seven adult female Lewis rats were used in this study. Two control groups were used for the study: 1) the motor related tibial fascicle and the sensory associated sural fascicles of the sciatic nerve which were in continuity to their targets. The presences of NTFs released by end target organs and motor and sensory phenotypic Schwann cells were evaluated. 2) The effect on selectivity of end-target organs using muscle-cap and skin-cap. The NTF-MP groups consisted of BDNF/GDNF (B/G) to enrich motor axons in one arm and the other arm with either NGF or PTN for enticing regeneration of small diameter sensory fibers. The combination of BDNF/GDNF was also compared to BSA control to determine the combinatory effect of multiple NTFs in enticing axon subtype. The animals were divided equally into four experimental groups; n = 12 per group (Figure 3.1). The Y-conduit implantation for the NTF-MP groups were similar to the process described in Chapter 1. For the tibial and the sural branch, the

Y-conduits were filled with collagen prior to implantation. The proximal stump of the sciatic arm was sutured to the end of the Y-conduit (Figure 3.2 A). The distal stumps of the nerve were separated and the tibial branch was sutured to one arm and the sural branch to the other. The end-target group used a 2 mm segment of the bicep femoris muscle suture to one of the arms and a 2 mm segment from the plantar surface of the hind limb was sutured to the other arm (Figure 3.2 B). The distal end of the sciatic nerve was removed to prevent the contribution of other external cues for the NTF and end-target organ groups. The muscles were then closed using 4.0 silk suture, and the skin stapled. Prophylactic topical antibiotic ointment was applied to the wound. All animals received antibiotic (cephazolin; 5mg/kg, IM) and pain control (sustained 3-day release Buprenorphine; 0.1 mg/kg, SC) post-surgery. All animal procedures were performed in accordance with the guidelines of the Institutional Animal Care and Use Committees of The University of Texas at Arlington and The University of Texas at Dallas.

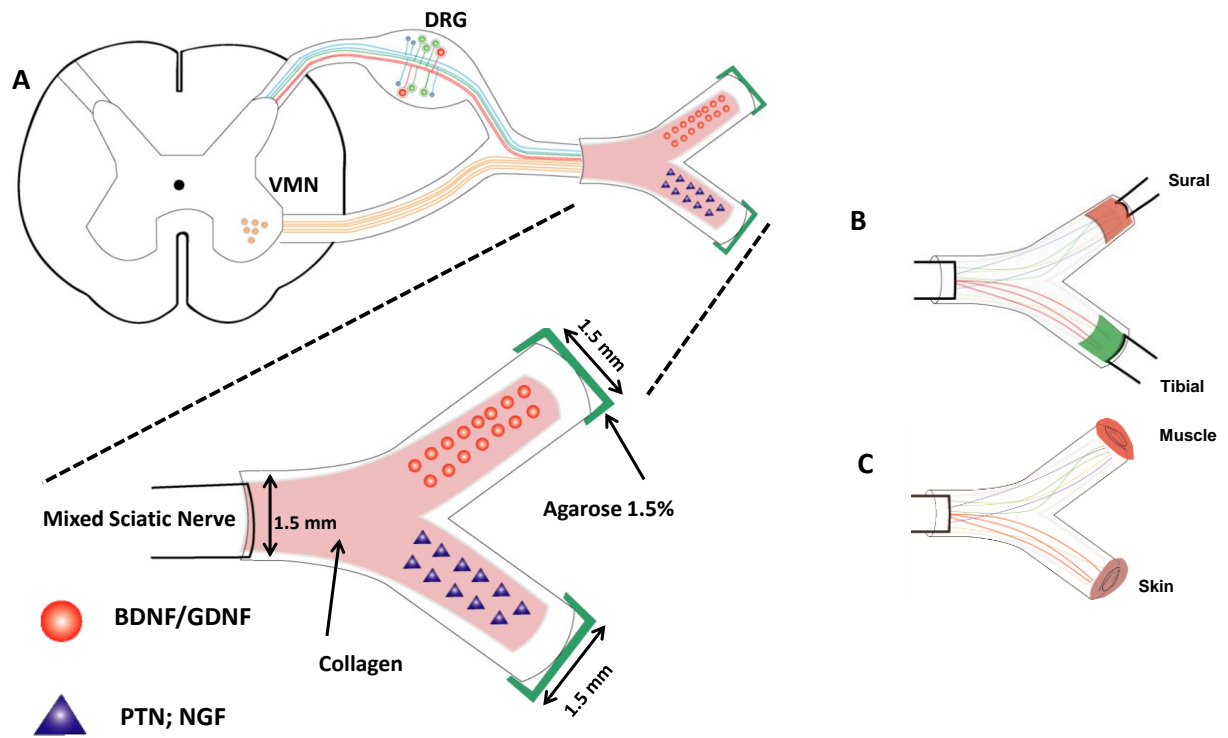


Figure 3.1. Schematic representation of the experimental groups. A) Y-conduit sutured to the mixed sciatic nerve with PLGA loaded NTFs in each of the arms. B) Mixed sciatic nerve attached to the proximal end of the Y-conduit with the arms sutured to the sural and tibial nerve targets. C) Y-conduit with 2 mm segment of muscle and skin attached to the distal arms of the Y-conduit.

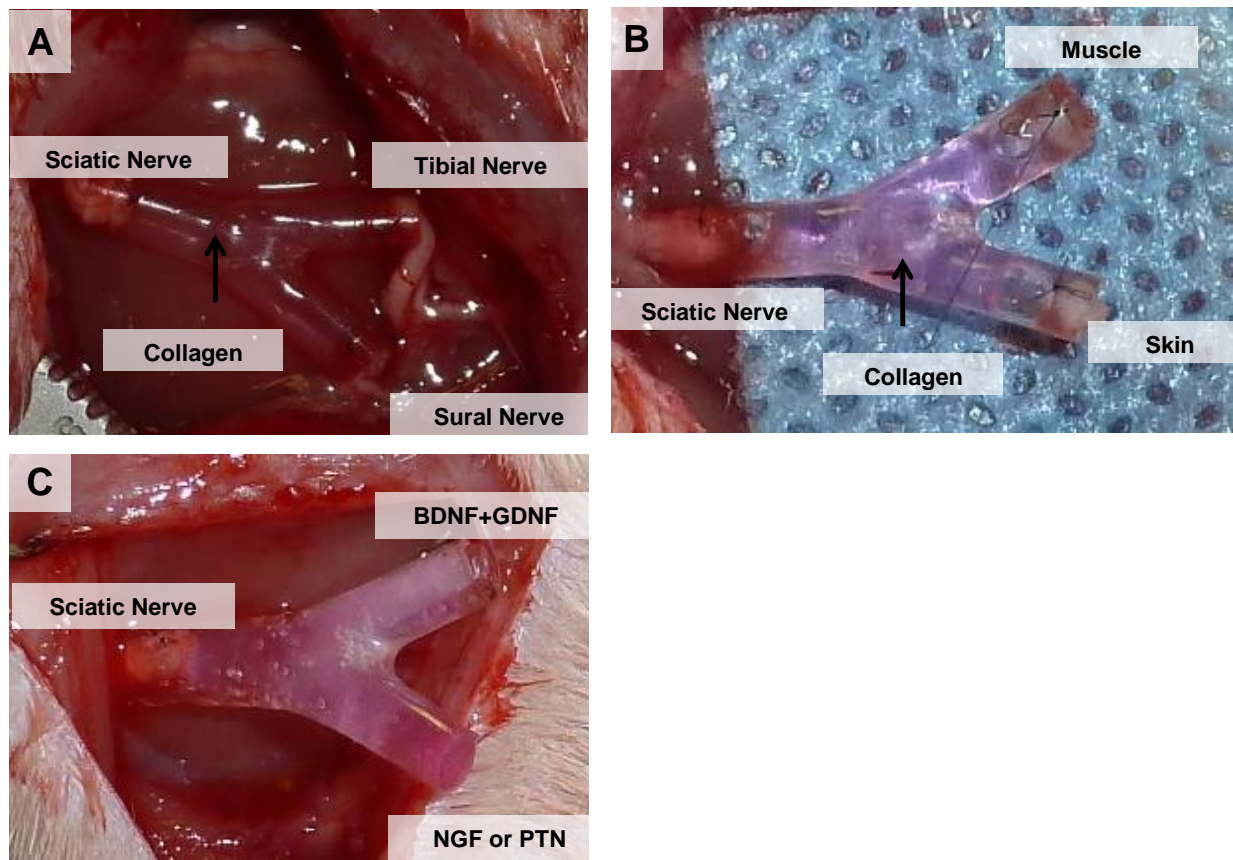


Figure 3.2. Representative images of the implantation of experimental groups. A) Tibial and sural branch sutured to the distal arms of the Y-conduit. B) Muscle and skin segments attached to the distal lumen of the arms. C) Y-conduit loaded with NTF-MP in the individual arms and ends closed with 1.5% agarose.

3.2.3 Analysis of the Regenerated Y-Nerve

Forty-five days post implantation, the number of motor and sensory neuron enrichments into each of the Y-conduit arms was accessed by fluorogold (FG) retrograde labeling similar to the process described in Chapter 2. Seven days post retrograde labeling, the functionality of the regenerated nerve was confirmed using electrophysiological evaluation. Finally, the morphology

of the axons composition (number of myelinated and unmyelinated axon, fiber diameter, axon diameter, and g-ratio) was evaluated using ImageJ software.

3.2.4 Statistical Analysis

The groups were compared using one-way ANOVA and Bonferroni's ad-hoc multiple comparison test using Prism 6 software (GraphPad Software Inc.). A $p \leq 0.05$ was considered statistical significant. The data is presented as the mean \pm standard error of mean.

3.3 Results

3.3.1 Y-nerve Regeneration in the presence of multiple NTFs

Regeneration was confirmed at 45 days post implantation along the 5 mm length of the common arm and then bifurcating into two 4-5 mm branches at the bifurcation as it entered into the different compartments (Figure 3.3). Gross evaluation of the regenerated nerves was similar for all groups that had no distal targets, filling about 30-40% diameter of the Y-conduit. The nerve-target group showed slightly larger diameter on the muscle related tibial branch when compared to mostly sensory sural branch, similar to the pre-implantation anatomical size. Histological analysis confirmed a normal perineurium and endoneurium composition in all treatment groups (data not shown). Moreover, a relative small area devoid of axons was seen primarily within the center of the nerve. Necrosis of the end-target organs distally attached to the Y-conduits was analyzed using H&E (Figure 3.4). Aggregation of blue color nuclei staining were absent from the distal ends. Muscle segments were stained in deep pink and the skin components in light pink.

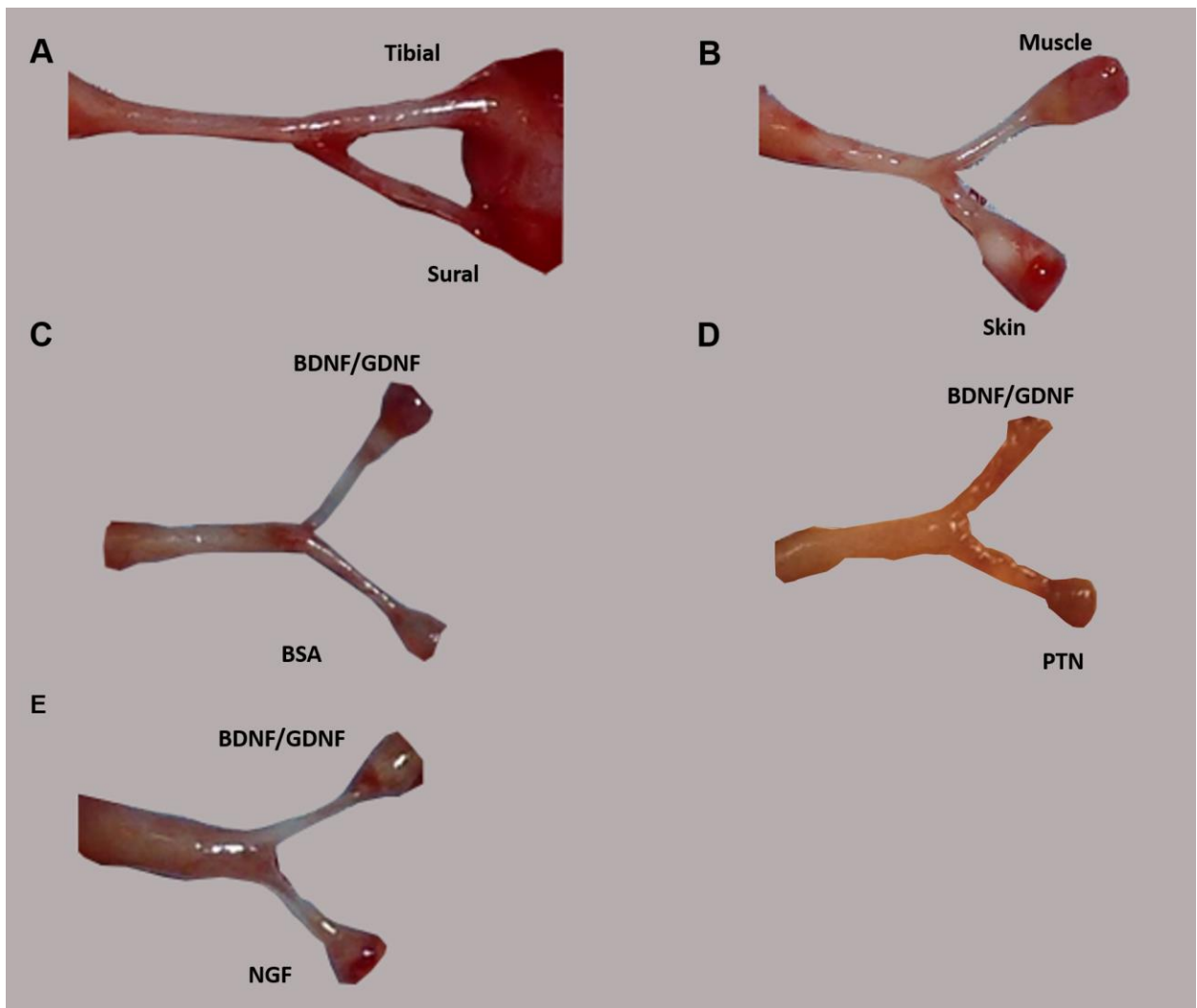


Figure 3.3. Representative images of the regenerated nerves. A & B) Regenerated nerves for the control groups consisting of nerve-target and end-organ target. C) NTF-MP group in combination versus non-selective BSA control. D & E) NTF-MP for motor enrichment versus sensory enrichment.

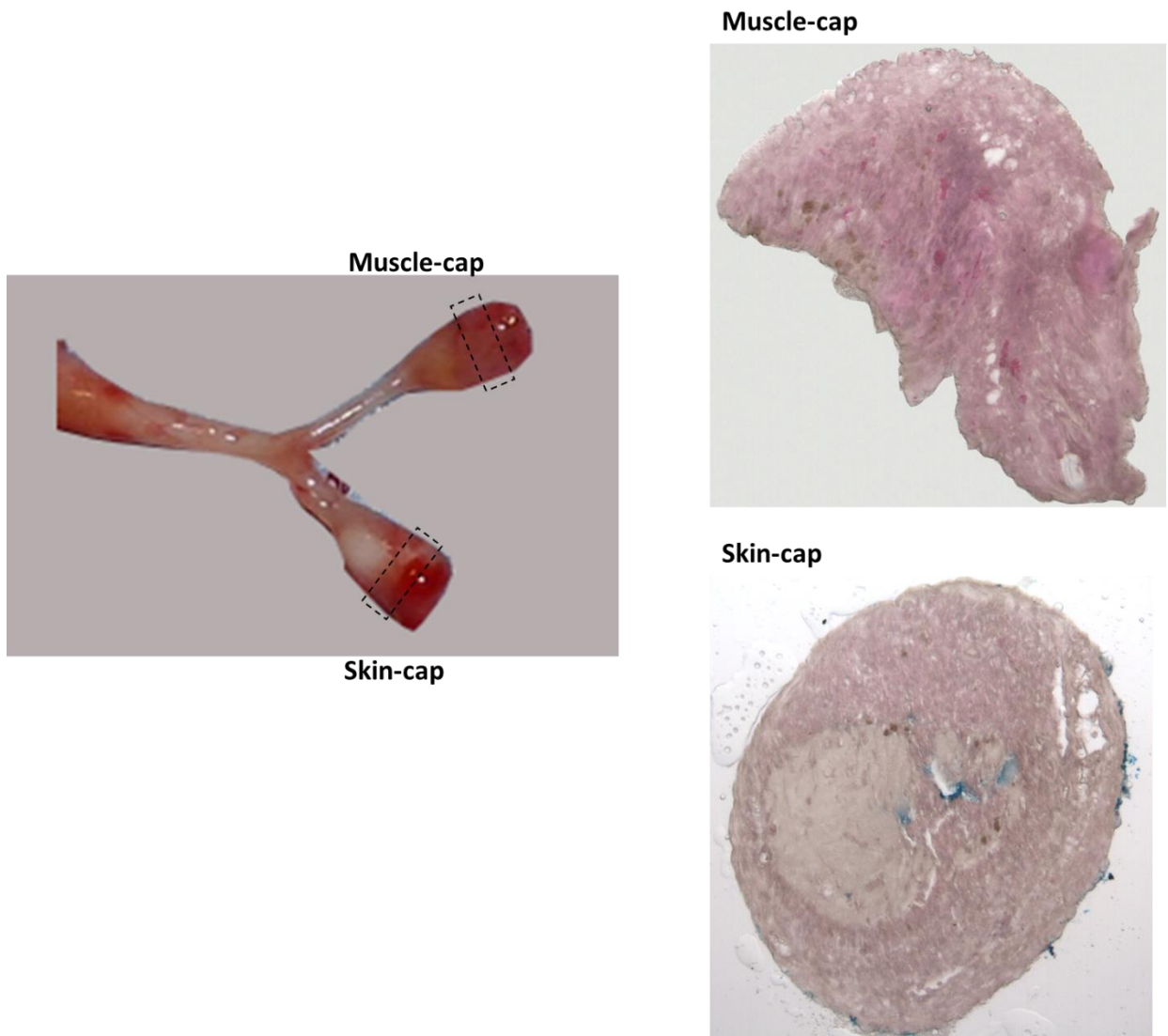


Figure 3.4. H&E staining of muscle and skin capped ends of the regenerated nerve. Muscles are stained deep pink in the upper image and skin cells pale pink (center region).

3.3.2 CNAP shows electrically competent Y-nerve regeneration

Electrically conducting axons were confirmed from all groups using electrophysiology recordings of CNAPs. Distribution of fiber size and myelination produced multiples peaks and the latency was calculated for each peak. Conduction velocity (CV) was calculated following

spike triggered averaging, and the values were categorized into slow (≤ 5 m/s), medium ($5 < x \leq 30$ m/s), and fast (> 30 m/s) (Table 3.1). All experimental groups showed peaks in the three ranges. However, the 45-day initial evaluation showed high variability in the peaks suggesting the axons are still in a state of flux.

Table 3.1. CNAP peaks incidences observed within the velocity ranges. ‘+’ indicates one peaks observed within the range. (#) indicates number of animals used to obtain CNAP response.

	Fast (>30 ms⁻¹)	Medium ($5 < x < 30$)	Slow (≤ 5 ms⁻¹)
Tibial (5)	+++++	++++	+++++
Sural (5)	+++++	+++++	+++++
Muscle (6)	++++	+++++++	++
Skin (6)	+++	+++++	++++
B/G (6)	+++++++	+++	+
BSA (6)	+++	++++	+
B/G (5)	+++++++	++++	+++++++
PTN (5)	++++	+++++++	++++
B/G (4)	+++	+++++++	+++
NGF (3)	+++	+++++	+++++

3.3.3 Effect of different combination of NTFs in motor and sensory regeneration

FluoroGold positive motor neurons were quantified in the ventral spinal cord ipsilateral to the implantation site (Figure 3.5). The presence of multiple NTFs showed an overall reduction in the

number of regenerated motor neurons compared to the nerve-cap in Chapter 2. The motor enrichment compartments (tibial branch, muscle-cap, and B/G arms) showed no significant effect when compared to the sensory enrichment compartment (sural branch, skin-cap, PTN, and NGF) for each experimental group. Preferential motor enrichment was not observed in the motor related tibial branch (207.0 ± 120.8 VMN) when compared to the sensory sural branch (204.5 ± 159.5). Conversely, the muscle-cap attracted more motor neurons (288.4 ± 172.8) when compared to the skin-cap (142.4 ± 71.67) without reaching statistical significance. The B/G compartments had increased number of motor neurons for all experimental groups versus PTN, NGF, or BSA control arm, however, was not statistically significant.

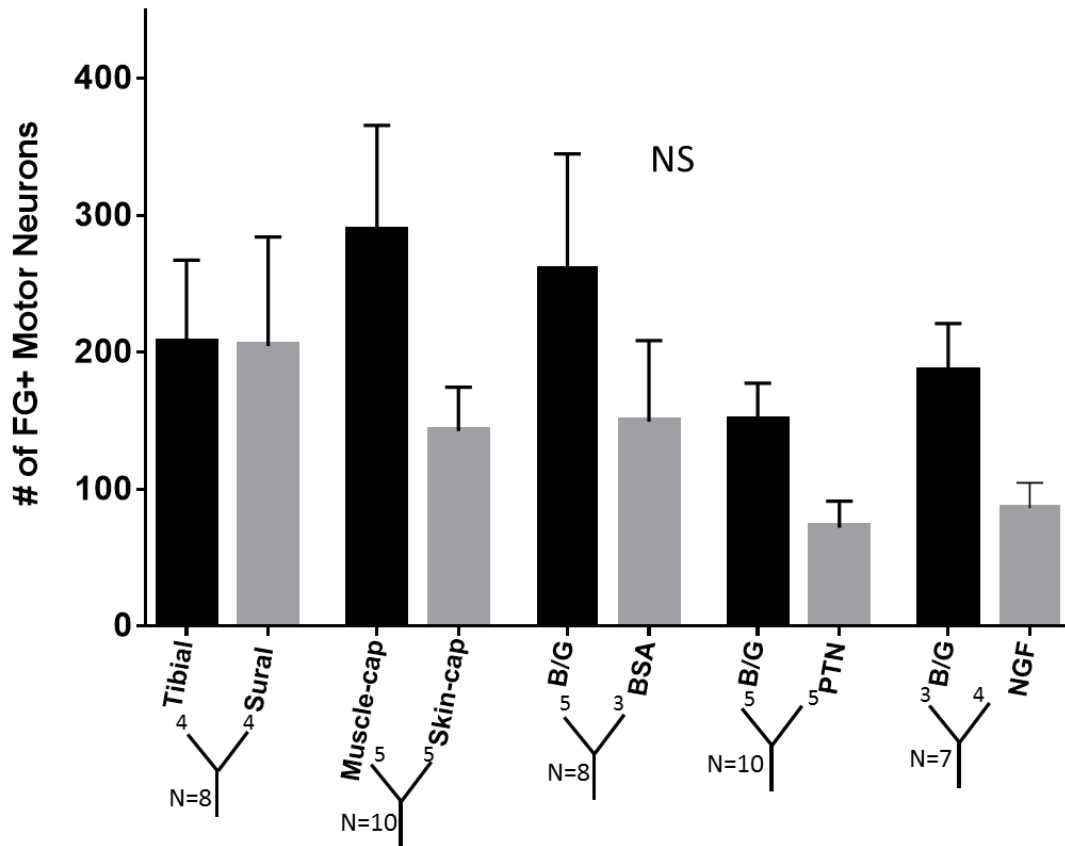


Figure 3.5. BDNF/GDNF (B/G) combination did not significantly increase the number of regenerated VMN. Numbers on the “Y” diagram in the x-axis represent animals per arm quantified. Data presented at the mean \pm SEM.

FG+ sensory neurons in the DRG were categorized based on perikarya (cell body) size.

Perikarya size has been shown to be correlated with specific sensory modality and conduction velocity [125], [126]. Cells with an area less than $300 \mu\text{m}^2$ were considered small, greater than $700 \mu\text{m}^2$ were large, and in between were classified as medium. The overall regenerative capacity using combination of NTF was lower when compared to single NTFs from the previous chapter (Figure 3.6 B). Additionally, there was a greater than 60% reduction in the number of

regenerated sensory neurons after regeneration. The tibial and sural regenerated arms had higher FG+ sensory neuron count compared the other experimental groups. This could result from the increased expression of growth promoting cues in the distal nerve stumps connected to their target organs. The muscle- and skin-cap groups showed comparable sensory neuron regeneration when compared to the NTF arms. Furthermore, the effect of NGF in enriching small caliber sensory neurons was also absent (Figure 3.6 C). The small, medium and large size cell distribution were comparable among all group and showed no significance.

The sensory to motor ratio was determined from positively labeled VMN and DRG sensory neurons from the nerve fascicles (Figure 3.7). A significant effect between the motor and sensory compartment was observed using a one-way ANOVA ($P \leq 0.05$; $F = 3.27$; $R^2 = 0.49$) The tibial motor and sural sensory branch had comparable S/M ratios of 9.3 ± 3.1 and 9.7 ± 3.6 respectively indicating preferential motor reinnervation is effected in this regenerative model. The muscle- and skin-cap showed an inverse ratio, however, the molecular cues from the end target organs was insufficient to induce a significant difference. The B/G combination with BSA and NGF showed no difference in the S/M ratio, however, a significant effect was observed in the B/G (4.4 ± 1.0) combination versus PTN (12.7 ± 0.9).

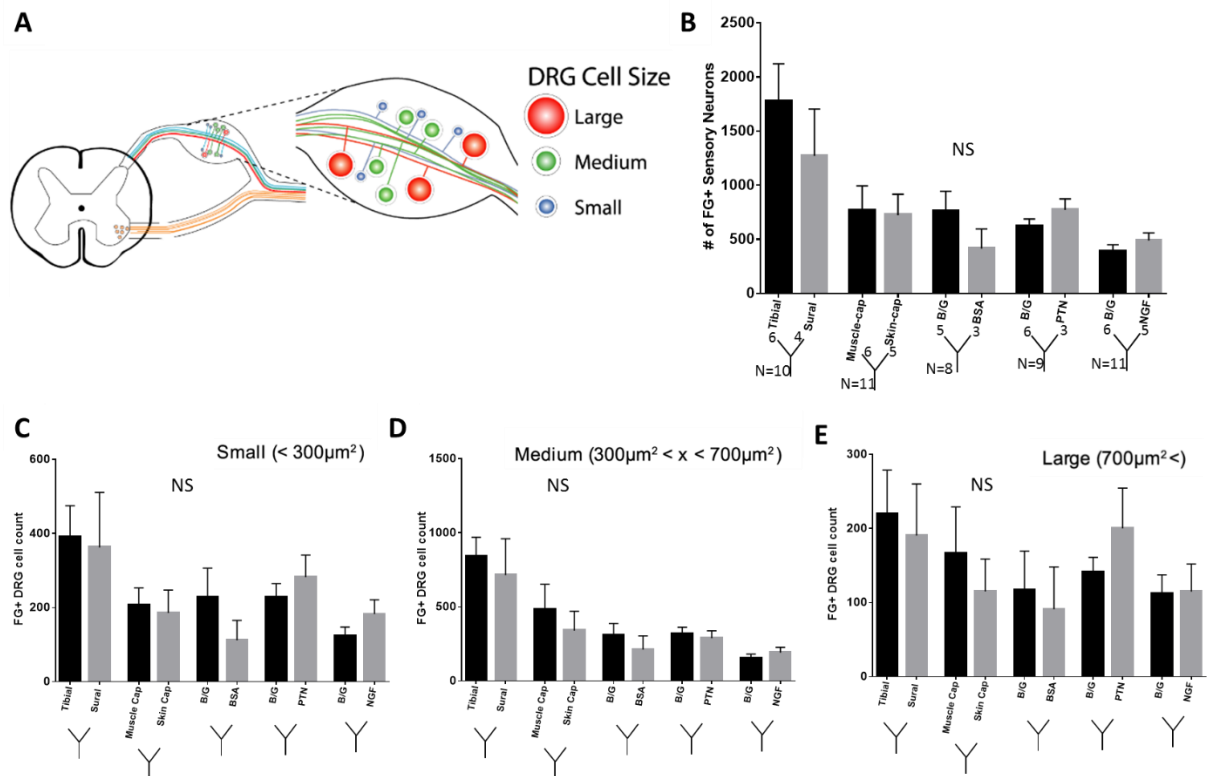


Figure 3.6. DRG size distribution comparable in all experimental groups. A) Schematic representation of DRG location and size distribution. B-D) Percent cell size distribution for FG+ cells located in the L4 and L5 DRG categorized into small, medium, and large. Data presented as mean \pm SEM.

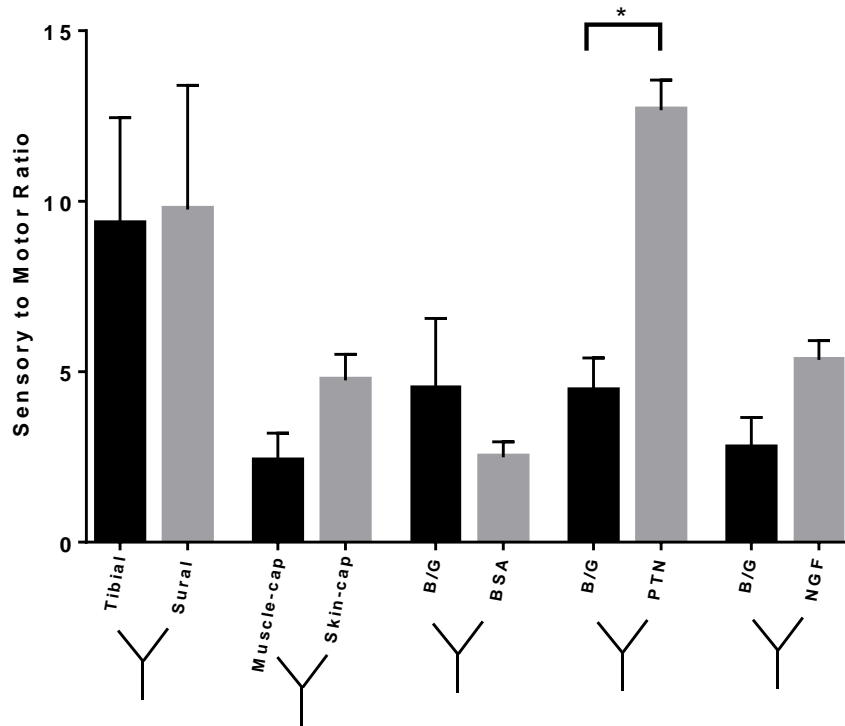


Figure 3.7. Sensory/motor ratio is modulated when combination of B/G versus PTN is used in the choice assay. Data presented as mean \pm SEM. * indicates $P < 0.05$; Bonferroni's post test.

3.3.4 Normal axonal morphology maintained by combinations of NTFs

A small subset of regenerated Y-nerves ($n = 3$ per group) were analyzed for difference in axon type and fiber morphology (Figure 3.8). Electron microscopic evaluation revealed myelinated and unmyelinated axons with normal fascicle formation with perineurium and epineurium structures. The count of myelinated axons showed a significant effect between the experimental groups using a one-way ANOVA ($P \leq 0.05$; $F = 3.09$; $R^2 = 0.67$) (Figure 3.9 A). The skin-cap showed a significantly higher number of unmyelinated axon count (240.0 ± 56.3 ; $P < 0.01$) compared to the muscle-cap (123.4 ± 42.3). All other experimental groups showed no significant differences between the regenerated Y-arms. The number of myelinated axons showed no

difference among the experimental group. However, lower number of myelinated axons were observed in the tibial arm and the B/G arm in the B/G vs. BSA group. This lower number in myelinated axon count is correlated with increase in fiber diameter (Figure 3.10). The mean fiber diameter of the tibial branch was $3.5 \pm 1.3 \mu\text{m}$, which was higher compared to $2.9 \pm 0.9 \mu\text{m}$ in the sural arm without reaching significance. However, the B/G arm had a mean diameter of $3.5 \pm 1.2 \mu\text{m}$ significantly higher when compared to the BSA arm ($2.5 \pm 1.0 \mu\text{m}$) ($P \leq 0.05$, Bonferroni) (Figure 3.10). The regenerated arms of both the B/G vs. PTN group had the lowest mean fiber diameter among all the experimental groups.

The scatter plots of g-ratio as a function of axon diameter was plotted for each experimental groups (Figure 3.11). Linear regression was used to observe the relationship between g-ratio and axon diameter distribution. Axon diameter was divided into small myelinated ($\leq 1 \mu\text{m}$), medium myelinated ($1 \leq x \leq 4 \mu\text{m}$), and large ($> 4 \mu\text{m}$) based on axon size reduction following nerve injury [130]. The tibial and the sural branch show a difference in the steepness of the slope, where the sural arm's steep slope indicates higher degree of myelination. This was also similar in the muscle-cap groups compared to the skin-cap. The number of quantified values for the B/G arm in the B/G vs. BSA group was lower, however myelination was less affected by larger axons with a less steep slope. The slope for B/G vs. PTN was similar with the PTN slope shifter to the right indicating more myelination in the PTN compartment. The B/G versus NGF graph has similar trend suggesting limited guidance or cross-diffusion from the different attractants.

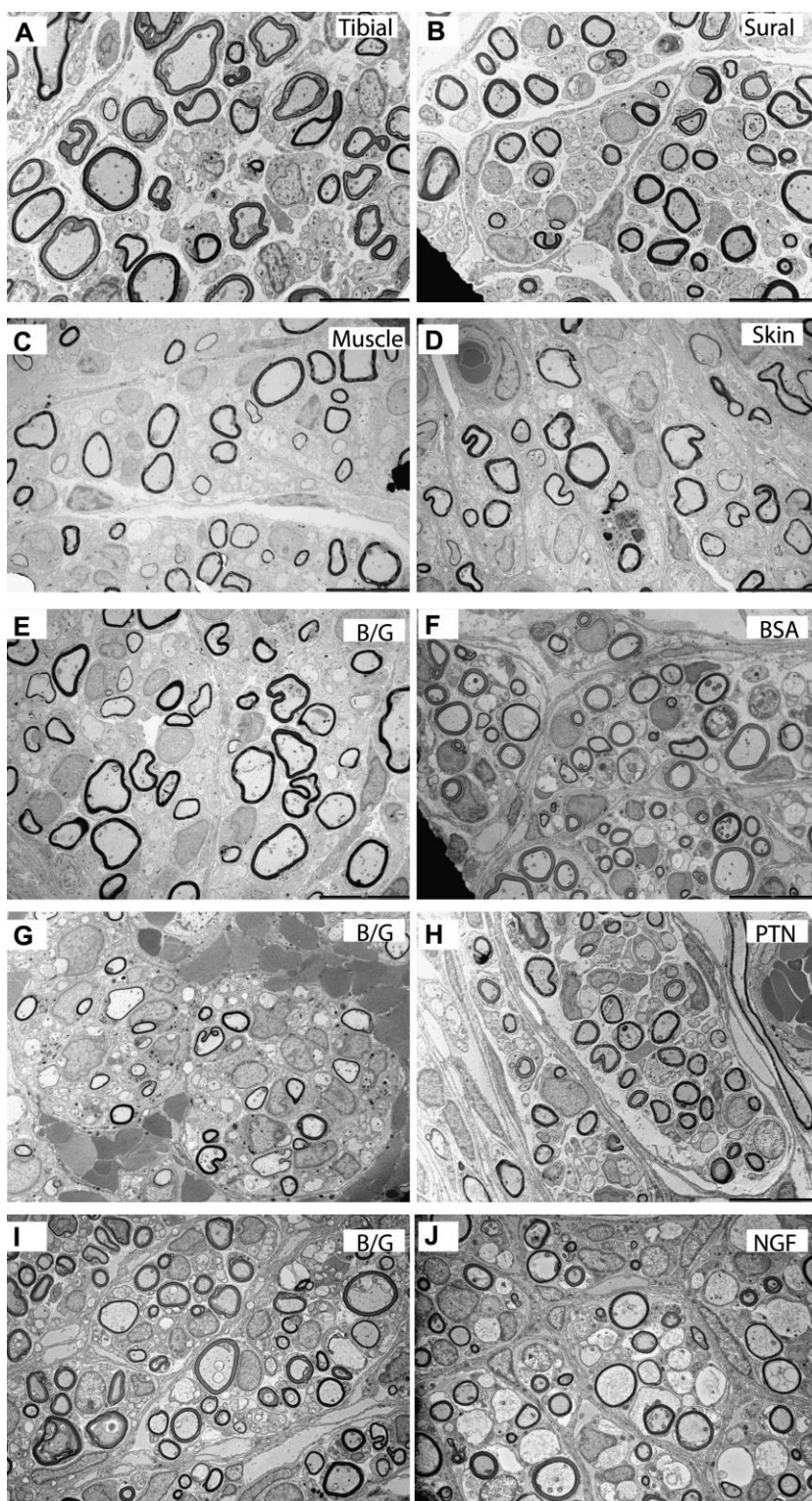


Figure 3.8. Representative EM images of for the motor and sensory compartment show normal axon morphology. Scale bar = 10 μm.

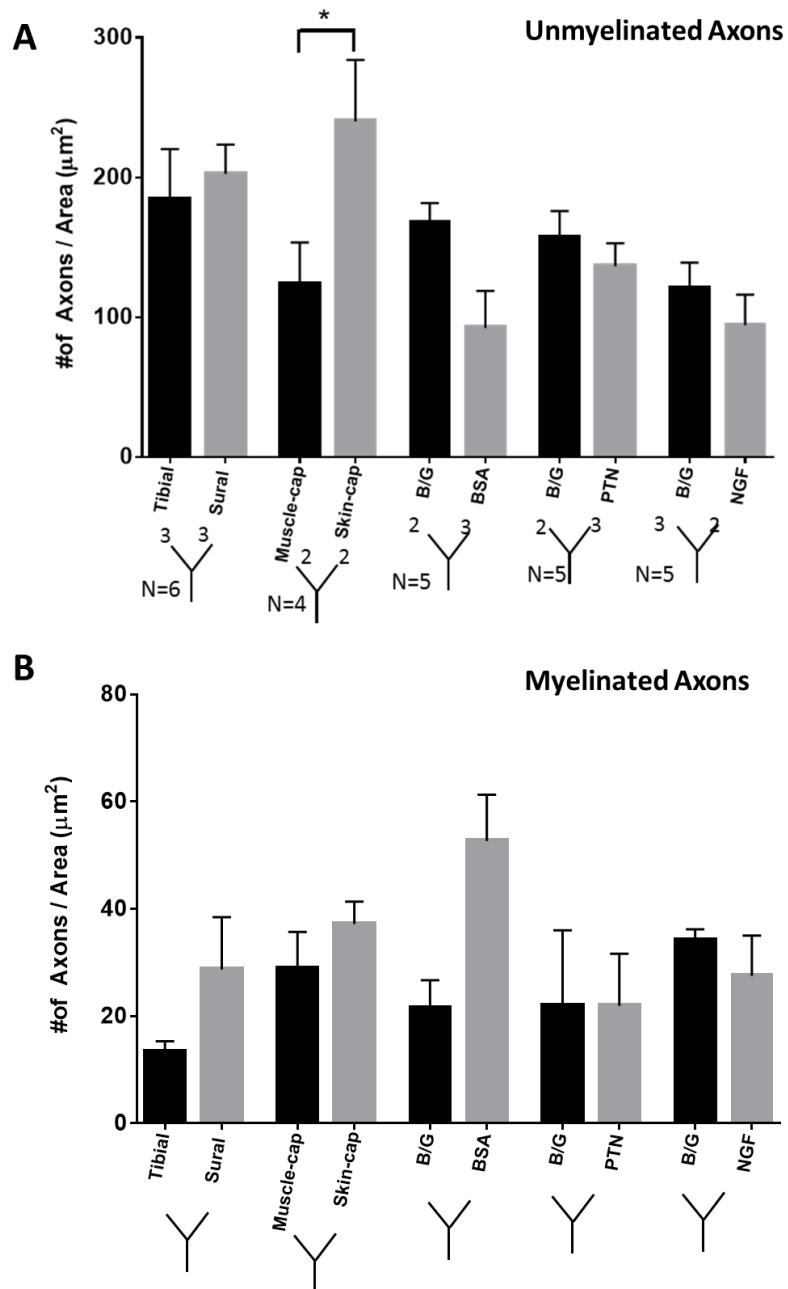


Figure 3.9. Axonal count from motor and sensory compartment for each group. A) Unmyelinated and B) myelinated axon count. Data presented as mean \pm SEM. * indicates $P < 0.05$.

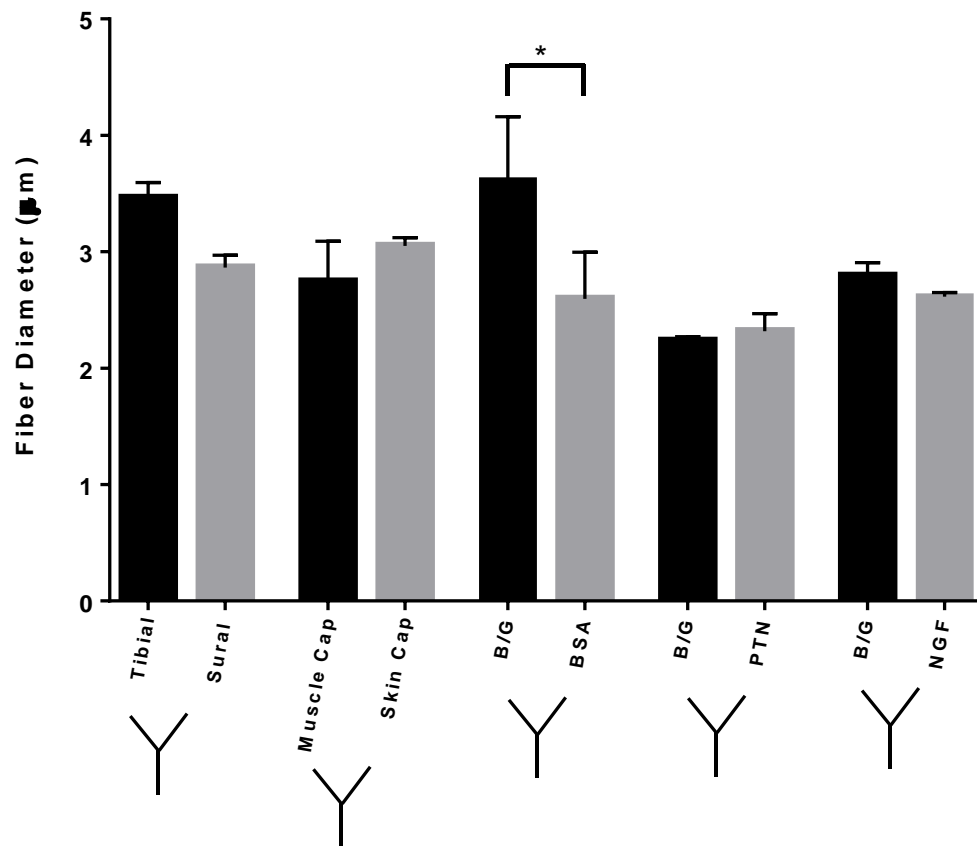


Figure 3.10. Fiber diameter (axon + myelin) for the individual arms of the regenerated arm. Data presented as mean \pm SEM. * indicates $P < 0.05$.

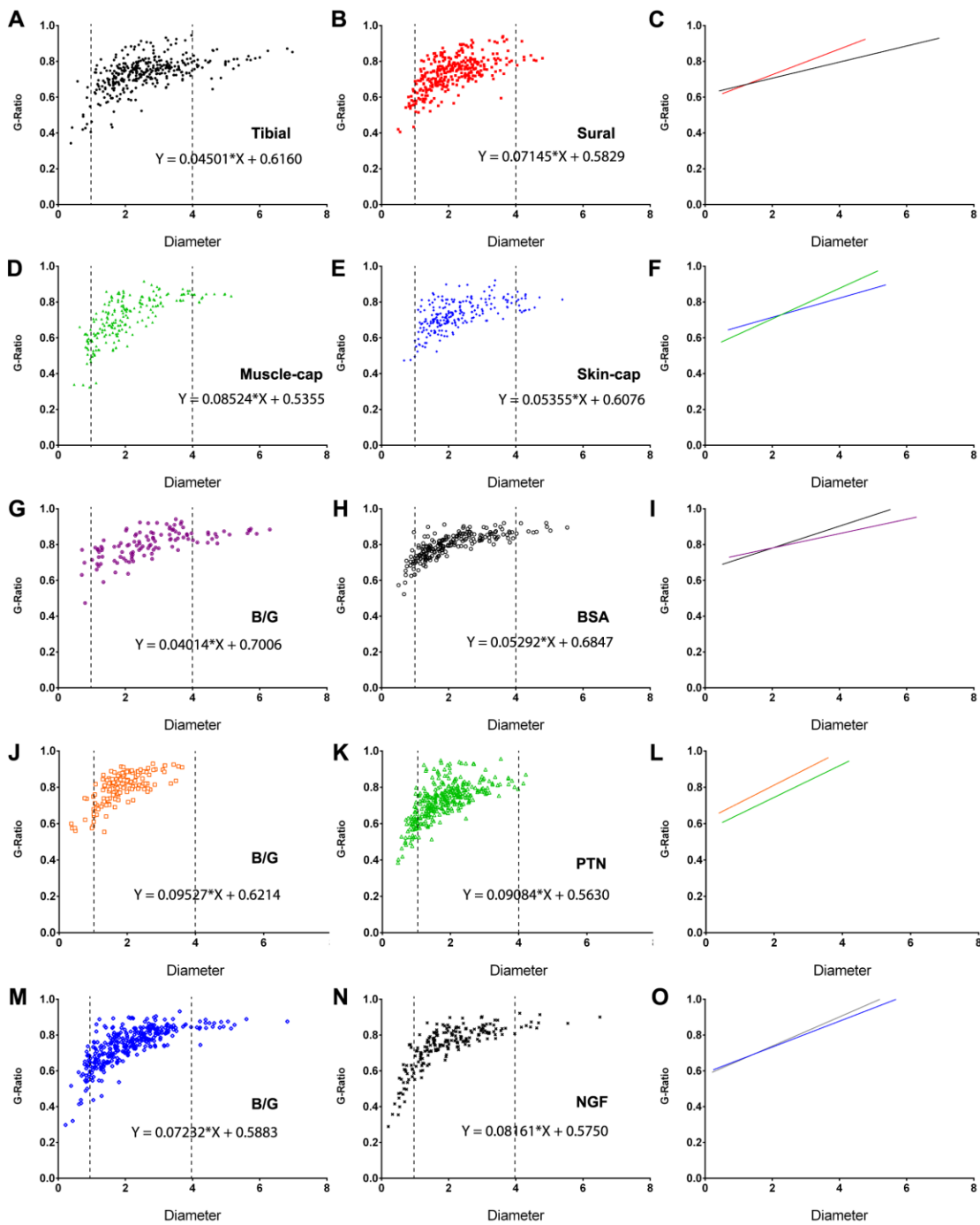


Figure 3.11. Scatter plots of g-ratio as a function of axon diameter. Individual points represent the g-ratio measured for each myelinated axon. (C, F, I, L, O) Linear regression of the best fit per arm per group. The equation for each line presented within the scatter plot.

3.4 Discussion

The present study utilized different combinations of NTFs to entice the regeneration of motor and sensory axon into separate compartments of the Y-conduit. Based on data from previous studies [77], a BDNF/GDNF combination was used to enrich motor neuron regeneration and NGF and PTN was used to entice sensory neuron regeneration. The different combinations for motor and sensory specific attractions were used to modulate the sensory to motor ratio without distal targets. Our data show that the motor compartment had a lower ratio of sensory/motor compared to the sensory compartment. B/G arm showed a low ratio of 4.4 ± 1.0 which was significantly different when compared to the PTN arm having a ratio of 12.7 ± 0.9 (Figure 3.12). However, the overall regenerative capacity for motor neurons was reduced by more than 50% when compared to single attractants. These findings suggest that the application of multiple NTFs can induced a changed in the ratio of sensory and motor neuron regeneration.

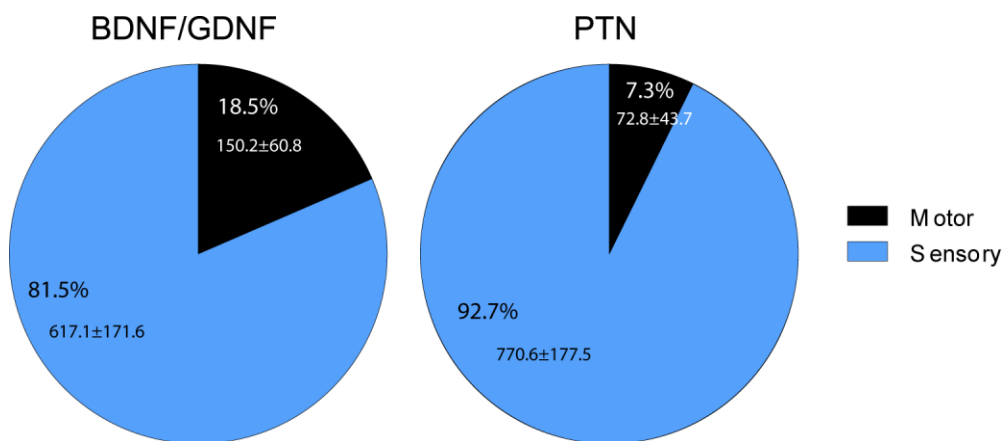


Figure 3.12. Sensory/motor ratio for BDNF/GDNF arm versus PTN showing difference in the percent of motor neuron attracted.

3.4.1 Selectivity using combination of NTFs

During peripheral nerve regeneration, sensory and motor axons are sporadically distributed in the cross sectional area, however, regeneration in continuity with distal targets show motor axons preferentially reinnervate to the muscle branch [99], [154]. The interaction of the regenerating axons with the different growth factors released by the distinct Schwann cell phenotype and end target organs helps in promoting the accuracy in regeneration [86], [152]. This was further validated when muscle connection was prevented and removal of Schwann cells resulted in a loss of regeneration accuracy [155], [156]. These results indicate the role of guidance cues in pathway selection. Here we used a GDNF and BDNF combination to entice motor neuron regeneration and NGF or PTN to induce small caliber sensory neurons. Our data show B/G combination showed no difference in the motor neuron regeneration compared to NGF or PTN. Similarly, small sensory neuron localization in one compartment by NGF could not be established as well. It is known that the receptors for these neurotrophins are differentially expressed following injury, however there is also a degree of overlap as well [86], [157]. After injury, an upregulation of NGF is observed to a larger extent in the dorsal roots than in the ventral roots. Similarly, the high affinity receptor for BDNF, TrkB, is expressed in motor neurons and medium size DRG, and expression is increased following axotomy [158]–[162]. Also, the expression of the low affinity receptor p75 is also increased after injury [163]. Even though an increased expression of these receptors are present in axon subtypes following injury, this current study showed limited selectivity. One factor resulting in the limited enrichment is the cross diffusion of the NTFs in the bifurcation zone. Although a gradient is present with higher concentration at the distal closed end, modeling data from the previous chapter suggests a

mixture of NTF at the bifurcation zone could possibly lead to misdirection during axon elongation.

3.4.2 Regenerative capacity of NTFs in combination

In this present study, the number of motor and sensory neurons that regenerated in the presence of multiple NTFs was drastically reduced. In contrast, previous studies showed multiple growth factors to increase the total amount of regenerated motor and sensory neurons [77]. However, that was not the case in this study which showed a reduction in the regeneration of both motor and sensory neurons. The number of regenerated motor neurons using the tibial and sural branch is expected to be low since the motor neurons that lead to the third branch of the sciatic nerve were not taken into account. The tibial nerve contains 49% of the total motor nerve population in the sciatic compared to the 3% in the sural [145], [164], [165]. Moreover, similar amounts of motor neurons in both compartments suggest preferential motor reinnervation (PMR) did not occur. It is possible this is due to the presence of the conduit and the gap the axons have to cross to reach the distal nerve target. Previous models used to identify PMR were end-to-end repair which suggest that gaps during nerve regeneration can lead to loss of PMR through the mixing of the supportive factors by the Schwann cells in the distal nerve. The increased motor neuron count observed in the muscle-cap compared to the skin-cap suggests the detached muscle secreted trophic factors. However, the lack of motor phenotypic Schwann cells could have limited the enrichment within the compartment.

The limited regeneration potency by multiple NTFs was unexpected; however, the increased concentration of the PLGA particles within the lumen of the conduit could be a factor. The

increased number of particles could act as a barrier and block the pathway for the regenerating axons. Furthermore, PLGA degrades into lactic acid and glycolic acid, and an increased concentration of particles could lead to a more acidic environment [166]. Such environments have been shown to reduce the efficacy of nerve regeneration.

To summarize, the findings of this chapter draw attention to the use of multiple NTFs as a means to modulate the sensory/motor ratio. The muscle-cap and the B/G arms from all experimental groups showed a lower sensory motor ratio compared to their adjacent arms. However, B/G versus PTN combination showed the most prominent difference in the ratio. This shows the feasibility of using NTF combinations and their ability to modulate the ratio of motor and sensory enticement. However, the number of NTFs used in this study likely leads to high PGLA particle concentrations within the Y-conduit resulting in limited neuronal outgrowth. This can possibly be mitigated by refined delivery of NTFs delivered at physiological concentrations with unobstructed delivery method [119]. In peripheral nerve interfacing, a low sensory/motor ratio is preferred as the likelihood of interfacing with a motor axon increase for motor control, whereas high sensory/motor ratio is desirable for stimulation of sensory precepts. However, loss in selectivity in sensory subtypes can possible be mitigated using repulsive cues in one compartment. This will allow axon subtypes to be redirected toward the adjacent chamber resulting in increased axon subtypes.

CHAPTER 4

SEMAPHORIN 3A INHIBITS SMALL DIAMETER AXONS IN A CHOICE ASSAY WITH BDNF AND NGF MOLECULAR ATTRACTANTS

4.1 Introduction

The human hand is populated by an estimated 17,000 touch sensing receptors in the skin that provide information about small slips, skin deformation and limb position [9], [167]. These individual nerve fibers are classified based on conduction velocity and axon diameter which include: Type I includes muscle spindles (Ia) and tendon organs (Ib; 12-20 μm AD and 100 m/s CV), Type II are mechanoreceptors ($A\beta$; 4-12 μm AD, 60 m/s CV), Type III are delta nociceptors ($A\delta$; 1-11 μm AD, 60 m/s CV), and Type IV are C-pain fibers (0.5-1 μm AD, 1-2 m/s CV) [37]. Moreover, there is overlap in axon diameters among the different modality types resulting in no distinction between proprioceptive and large mechanoreceptive afferents [38], [168], [169]. Also, most somatic nerves contain two types of motor axons (α and γ) and five different types of sensory afferents including $A\beta$ proprioceptive axons, high-threshold mechanoreceptors (HTMRs), low-threshold mechanoreceptors (LTMRs), slow-conducting C-nociceptors, and myelinated pain $A\delta$ fibers, all of which are mixed at various proportions and quantities in different nerves [9], [37], [64]. Clearly, interfacing and stimulating a specific sensory modality from mixed sensorimotor somatic nerves presents a great challenge. This is even further complicated by the fact that large myelinated axons (i.e., proprioceptive and motor) are depolarized with smaller electrical currents, while smaller diameter neurons (i.e., pain fibers) require larger depolarizing stimuli. Thus, when stimulating the small caliber fibers, one can expect to non-specifically recruit large-size axons as well [39], [40], [170], [171].

It is known that during development peripheral nerves navigate through a complex environment to reach their target. This is mediated by the receptor-ligand interactions at the growth cone of the axon resulting in cytoskeletal changes that direct the neuron to extend or retreat [49], [50], [172], [173]. The attractive and repulsive cues act as molecular guide posts for the developing axons. These same cues in the adult PNS have been used to enhance regeneration as well as guide regenerating axons to their specific targets [60], [78], [102], [103], [114], [174]–[176]. Individual molecular cues bind the specific receptors on the surface of the growth cone. In the previous chapter, two different types of NTFs were used in the individual arms of the Y-conduit to selectively entice the regeneration of motor neurons in a specific compartment and small caliber sensory neurons in the other. Although, the sensory/motor ratios were modulated, the selectivity of the sensory subpopulation neuron attraction was not achieved. Together these studies indicate that selective guidance of the regenerating axons from a mixed population is feasible, however, it requires additional factors to improve the selective efficacy of enrichment.

In addition to attractants, repellents are also key mediators for axon development and guidance. The Semaphorins family of guidance cues are a large class of protein that are most widely studied. During development Semaphorins are present as either soluble or membrane bound and emit a long or short range repulsive action. They are large proteins consisting of approximately 500 amino acids and divided into eight subclasses with their activity mediated by two receptors, plexin and neuropilin [177]. Most classes of Semaphorins bind to plexin directly, while class 3 (Sema3A) binds to neuropilin first with its complex activating plexin and leading to growth cone

collapse [53], [178]. In the adult PNS, class 3 Semaphorins are upregulated following peripheral nerve injury [179], and interestingly, act as both attractive and repulsive, hence their role has yet to be fully elucidated. However, the role of Sema3A, a member of the Semaphorin family, has been shown to induce turning and growth cone collapse of sensory DRG neurons *in vitro* [42], [180]–[182]. Furthermore, *in vivo* application of NGF attractant in the dorsal column of the spinal cord and exogenous presence Sema3A on the ventral side induced sprouting of NGF responsive axons to the dorsal side while inhibiting its extension towards the ventral side of the spinal cord [43], [114]. Taken together, this advocates the incorporation of both attractive and repulsive cues as a means to refine axon guidance and regeneration. The primary objective of this study is to determine whether the application of both attractive and repulsive cues can further modulate the sensory to motor ratio (S/M) and improve the enrichment of axon subtypes given two different modality attractants.

4.2 Materials and Method

4.2.1 PLGA encapsulation of Sema3A

Recombinant human Semaphorin-3A (Sema3A, 87.3 kD) (Novoprotein, Summit, NJ) protein was encapsulated in biodegradable poly(DL-lactic-co-glycolic acid (PLGA) microparticles using the double emulsion method as described in Chapter 1. Briefly, PLGA 50:50 (Lakeshore Biomaterial, St. Louis, MO) was dissolved in dichloromethane (DCM) 200 mg/ml (Sigma-Aldrich, St. Louis, MO), and mixed with aqueous solutions of 20 ug/ml of recombinant sema3A protein. This solution was then added to polyvinyl alcohol (20 mg/ml) and emulsified. The MP solution was stirred for 1-2 hours to remove excess DCM, centrifuged at 4000 rpm for 15

minutes to pellet the particles and separated from the supernatant. The resulting MPs were transferred to -20°C for 2 hours, to -80°C overnight, freeze dried for 48 hours and stored at -20°C until used. Loading efficacy was calculated at $67 \pm 5\%$.

4.2.2 *In vitro* Y-template fabrication

A polydimethylsiloxane (PDMS) template in the shape of a “Y” was fabricated to test the bioactivity of the Sema3A-MP. Briefly, the elastomer and the curing agent was mixed in a 10 to 1 ratio, then cured in the oven at 60°C for 2 hours. Using a 6.0mm biopsy punch, two holes were made approximately 1.5cm apart. Another hole 1.5 cm below was also made using a 5.0mm biopsy punch creating a 60° angle. Finally, ~2mm canals were cut joining each of the 6.0mm holes connecting to the 5.0mm hole (Figure 4.1). The PDMS Y-template was then attached to a glass cover slip following plasmapheresis treatment and sterilized using ethanol and UV radiation.

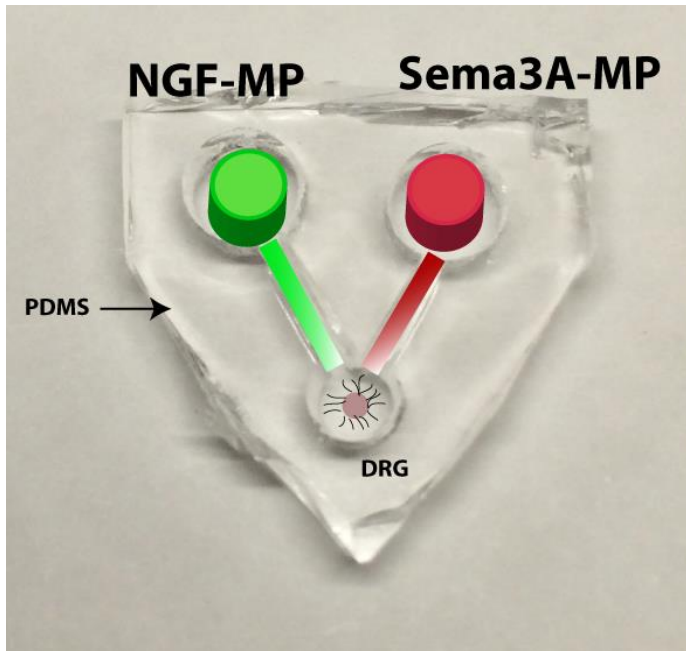


Figure 4.1. *In vitro* Y-template PDMS mold. The 6.0mm holes contain NTF-MP mixed in collagen and the cell chamber (bottom hole) is where the DRG will be place. The canals serve as a pathway for the regenerating axons.

4.2.3 Sema3A-MP bioactivity assay

NTF-MP containing NGF and Sema3A were mixed in 30 μ l of atelomeric chicken collagen (85 % type I, 15 % type II; Millipore; Temecula, CA) and added to the 6.0 mm compartments. The Y-templates were incubated at 37°C with 5% CO₂ for 15 minutes to allow gelation. Embryonic (E15-E18) mice pups were dissected and whole dorsal root ganglia (DRG) were collected in in L-15 Medium (Leibovitz). The DRGs were cleaned of connective tissue and placed in poly-D-lysine (PDL) coated Y-template cell chamber suspended in 10 μ l of atelomeric chicken collagen (Figure 4.1). The explants were incubated at 37°C with 5% CO₂ for 15 minutes to allow gelation before adding 200 μ l of Neurobasal A media (Sigma Aldrich) supplemented with 0.5% penicillin/streptomycin.

4.2.4 DRG choice assay quantification

Seven days following DRG regeneration in the Y-template, the neurite outgrowth site was imaged using the bright field on a Nikon A1R confocal microscope system (Nikon, Inc.). The images were acquired at 20x magnification and the individual images were stitched together within the Nikon's ND Elements software (Nikon, Inc.). Individual axons were traced from the boundary of the DRG to the axon terminal using ImageJ analysis software. Axonal length and degree of turn from each compartment was quantified from 3 DRG treatments.

4.2.5 Y-tube implantation and analysis

Twenty-four adult female Lewis rats were included in the study. The control group received BDNF-MP in one arm and the other NGF-MP (n = 12; Retrograde label 6 animals per NTF arm). The experimental group received a combination of BDNF-MP + Sema3A-MP in one arm and NGF-MP in the other (n = 12; Retrograde label 6 per NTF arm) (Figure 4.2). The surgical implantation, retrograde labeling, CNAP analysis, and quantification were performed similarly as mentioned in Chapter 1. All animal procedures were performed in accordance with the guidelines of the Institutional Animal Care and Use Committees of The University of Texas at Dallas.

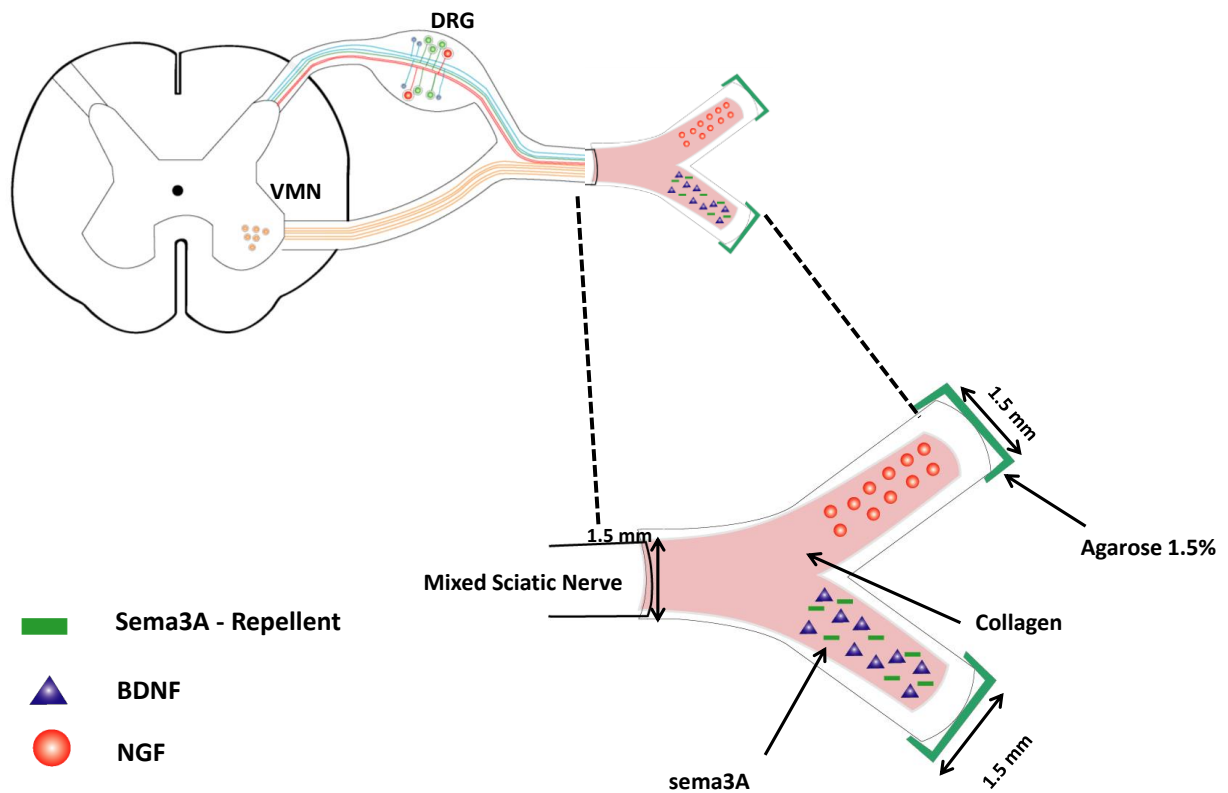


Figure 4.2. Schematic representation of Y-conduit containing attractants and repellent to increased efficacy in axon subtype enrichment.

4.2.6 Statistical analysis

Changes in axonal length and turning *in vitro* were analyzed using student t-test. *In vivo* comparison between experimental groups were compared using one-way ANOVA and Bonferroni's ad-hoc multiple comparison test using Prism 6 software (GraphPad Software Inc.). A $p \leq 0.05$ was considered statistically significant. The data is presented as the mean \pm standard error of mean.

4.3 Results

4.3.1 Axonal turning in the presence of Sema3A *in vitro*

The bioactivity of the Sema3A-MP was tested on DRG explants in a choice assay. The inhibitory effect of the Sema3a in deterring axonal extension towards the chamber was observed (Figure 4.3 A (a1 & a2)). A student t-test analysis showed a statistical significant effect in the axonal turning for NGF versus Sema3A compartment ($P \leq 0.01$, Student t-test). The mean axonal length towards the NGF (43.9 ± 21.9 %) compartment was higher compared to the Sema3A side (29.9 ± 19.7 %) without reaching significance. Similarly, axonal turning was significantly greater in the Sema3A compartment (83.8 ± 32.5 degrees) while the NGF compartment was limited (60.2 ± 23.0 degrees) (Figure 4.3 B & C).

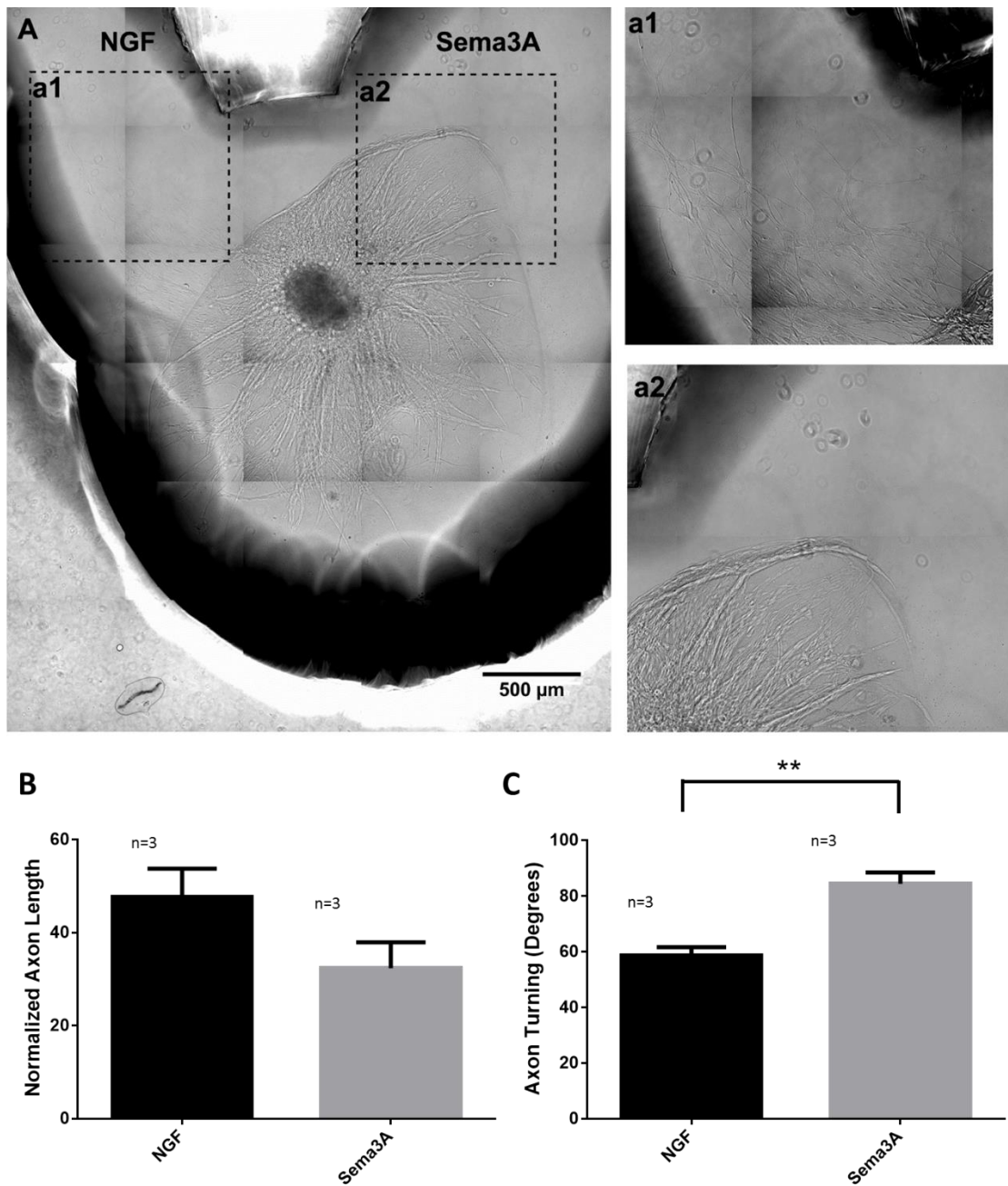
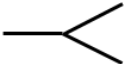
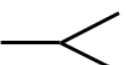


Figure 4.3. Sema3A induced inhibition on DRG neurite outgrowth. A) Bright field image of the DRG axonal extension in the NGF (a1) and Sema3A (a2) chamber. B & C) Normalized axonal length and change in axon turning from the NGF and Sema3A compartments. ** indicates significant difference between the chambers ($P \leq 0.01$). Data present at mean \pm SEM.

4.3.2 Sema3A retains functionality of the regenerated nerves

CNAP analysis from the regenerated Y-nerves in the presence of a repellent retained electrical functionality. Multiple peaks were observed following the activation of all fiber types and the latency was measured from the start of the stimulus. The conduction velocity (CV) was calculated following spike triggered averaging, and the values were categorized into slow (≤ 5 m/s), medium ($5 < x \leq 30$ m/s), and fast (> 30 m/s) (Table 4.1). One hundred percent of the regenerated nerves fascicles show electrical competency with the number of peaks ranging from 1-3. No significant difference in the number of the peaks were observed between the groups.

Table 4.1. CNAP peaks incidences observed within the velocity ranges. ‘+’ indicates one peaks observed within the range. (#) indicates number of animals used to obtain CNAP response.

		Fast ($>30 \text{ ms}^{-1}$)	Medium ($5 < x < 30$)	Slow ($\leq 5 \text{ ms}^{-1}$)
	BDNF (6)	++++	++++++	+++++
	NGF (6)	++++	++++++	++++
	BDNF/Sema3a (6)	++	++++++	+++++
	NGF (6)	+	++++++	++++++

4.3.3 Sema3A does not modulate the S/M neuron ratio

FG+ motor neurons and DRG sensory neurons were quantified from the ipsilateral spinal cord and the L4 and L5 DRGs. The number of regenerated motor neurons ranged from 130-170 using BDNF and NGF attractants, and the number of VMN in the regenerated nerve fascicles were

similar in the BDNF vs. NGF and BDNF+Sema3A vs. NGF (Figure 4.4). The number of regenerated sensory neurons in the BDNF vs. NGF and BDNF/Sema3A vs. NGF groups were quantified and showed similar distribution in both experimental groups (Figure 4.5). Additionally, DRG perikaryal size was also quantified and categorized into small ($< 300 \mu\text{m}^2$), medium ($300 \mu\text{m}^2 < x < 700 \mu\text{m}^2$), and large ($700 \mu\text{m}^2 < x$). The small DRG cell size showed all groups with greater than 20% distribution without reaching significance (Figure 4.5 C). The medium and large size DRG cell body size ranged from 40 – 55% and 17 – 32% respectively (Figure 4.5 C & D). Both groups showed no statistical difference among the arms and across the group.

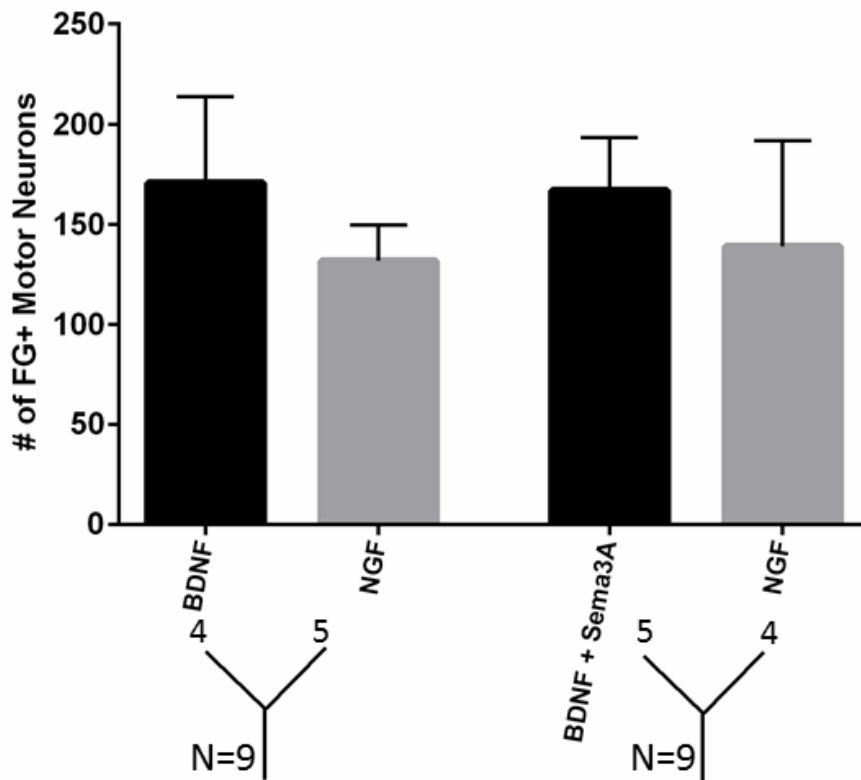


Figure 4.4. FG+ motor neuron counts unaffected by Sema3A repellent and shows individual arms having similar attractive property. Data present as mean \pm SEM.

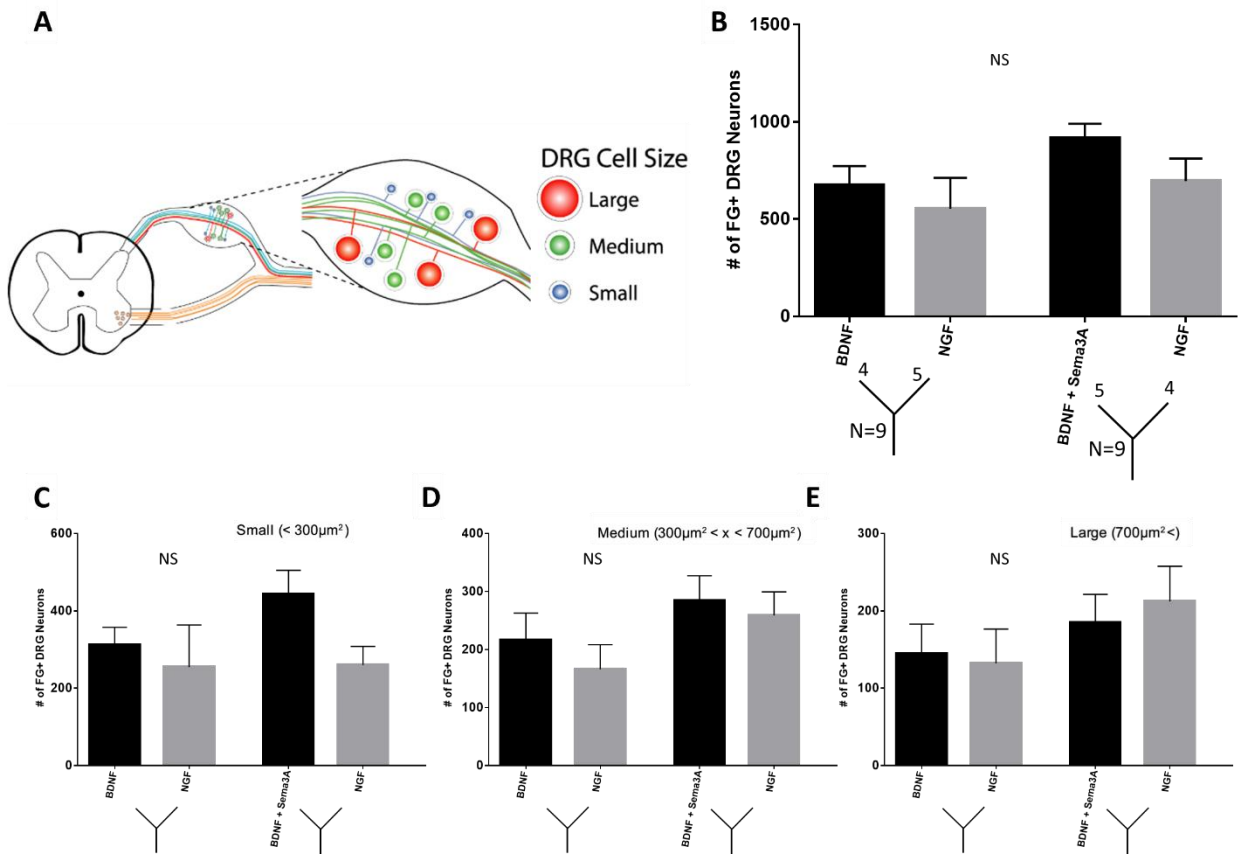


Figure 4.5. DRG perikarya size distribution. A) Schematic representation of small, medium, and large cell distribution located in the DRG. B-D) FG+ cell size distribution quantified from the L4 and L5 DRG categorized into small, medium, and large. Data present as mean \pm SEM. (Figure prepared with the help of Michael Tran.)

The sensory/motor neuron ratio was determined from the positively labeled VMN and DRG sensory neuron in each compartment (Figure 4.6). The mean S/M ratio between the experimental groups ranged from 4.3 – 6.6. Comparison of the individual fascicles in each group showed no significant effect. Additionally, the ratio of BDNF arm (4.3 ± 2.7) compared to the BDNF+Sema3A (6.1 ± 2.6) also showed no difference in the presence of a molecular repellent.

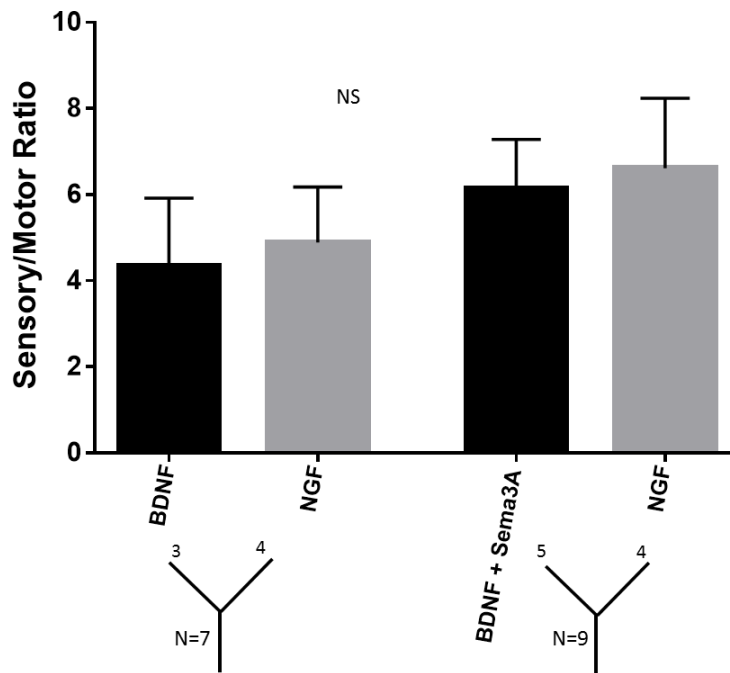


Figure 4.6. Sensory/motor neuron ratio show Sema3A was not effective in altering the ratio in the presence of dual choice molecular attractants.

4.3.4 Axon morphology analysis in the presence of Sema3A

A subset (n =3 Y-nerves per compartment per group) of the individual arms of the regenerated Y-nerves were analyzed for axon type composition and myelination. Evaluation of each Y-nerve showed the presence of normal myelinated and unmyelinated axons with intact perineurium and epineurium (Figure 4.6). The number of unmyelinated and myelinated axon count showed no statistical significance within the arms of the group and across experimental groups (Figure 4.7). Similarly, the myelinated axon count showed no difference between the arms and across experimental groups.

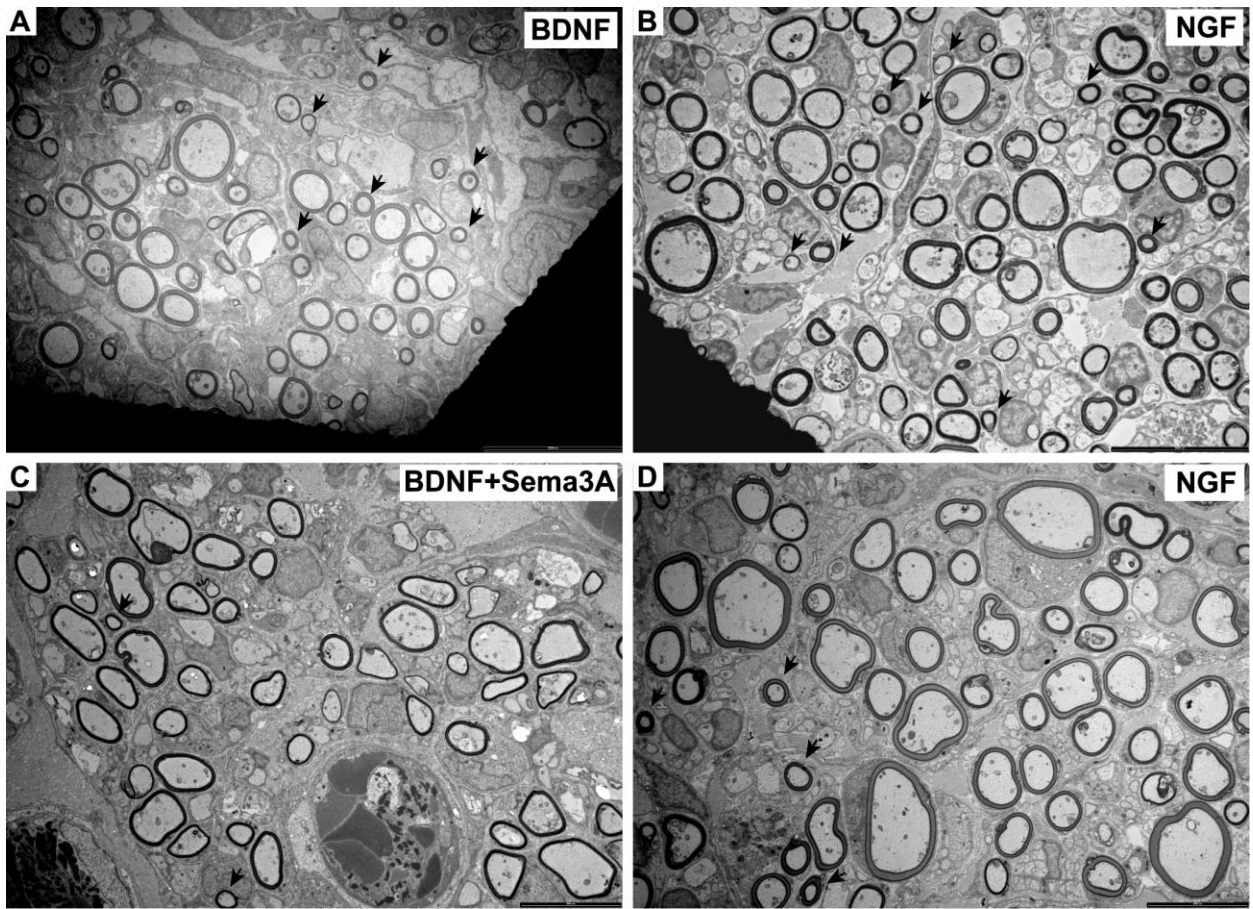


Figure 4.7. Representative EM images from the regenerated arms of the Y-nerve. Arrows designate small myelinated fibers more evident in the group without Sema3A. Scale bar = 10 μ m.

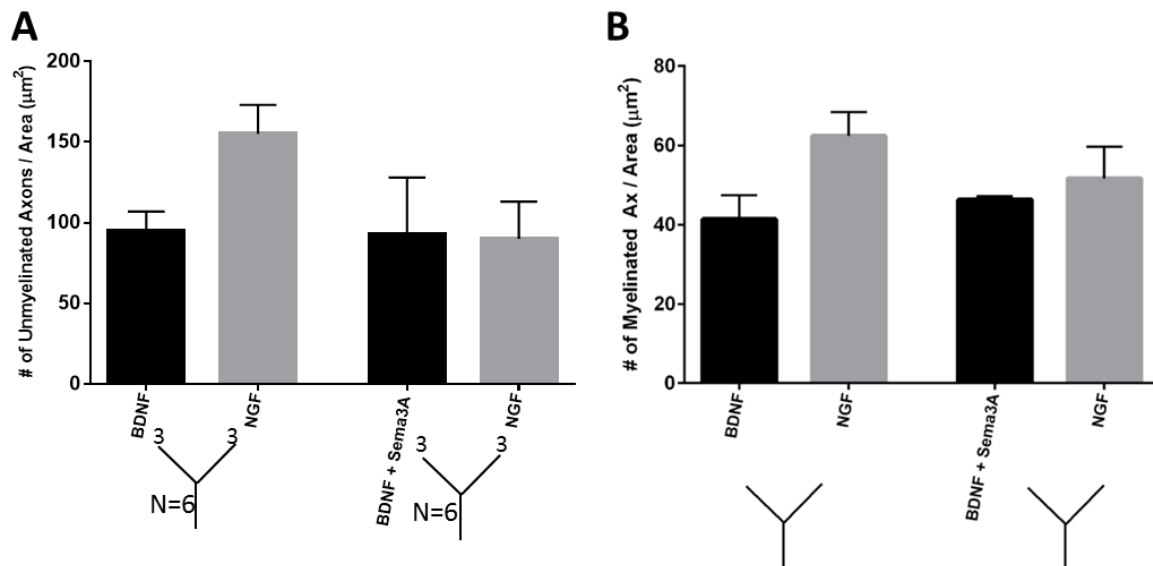


Figure 4.8. Unmyelinated and myelinated axon count. A& B) No difference observed in the unmyelinated and myelinated axon count. Data present as mean \pm SEM.

4.3.5 Sema3A shows inhibitor effect of myelinated axons less than $1\mu\text{m}$

G-ratio as a function of axon diameter was plotted for each regenerated NTF-MP arm, and the relation was best fit using linear regression (Figure 4.8). The BDNF vs. NGF group was showed a steeper slope for NGF with higher myelination for small diameter axons and less myelination for higher axon diameter compared to the BDNF arm. The BDNF + Sema3A vs. NGF group had a similar fit, however observed a limited number of small caliber axons in both the arms of the Sema3A group ($< 1\mu\text{m}$ diameter) (Figure 4.9 D & E). Percent distribution of axons less than $1\mu\text{m}$ showed a significant effect ($\sim 95\%$ decrease) when compared to the BDNF arm without Sema3A using a one-way ANOVA ($P \leq 0.05$; $F = 4.35$; $R^2 = 0.65$) (Figure 4.10). The NGF arm in the Sema3A group had a 41.7% decrease compared to the NGF arm without the Sema3A without

reaching statistical significance. Percent distribution of myelinated axon diameter within the medium ($1 > x \geq 4\mu\text{m}$) and large diameter ($>4\mu\text{m}$) showed no difference.

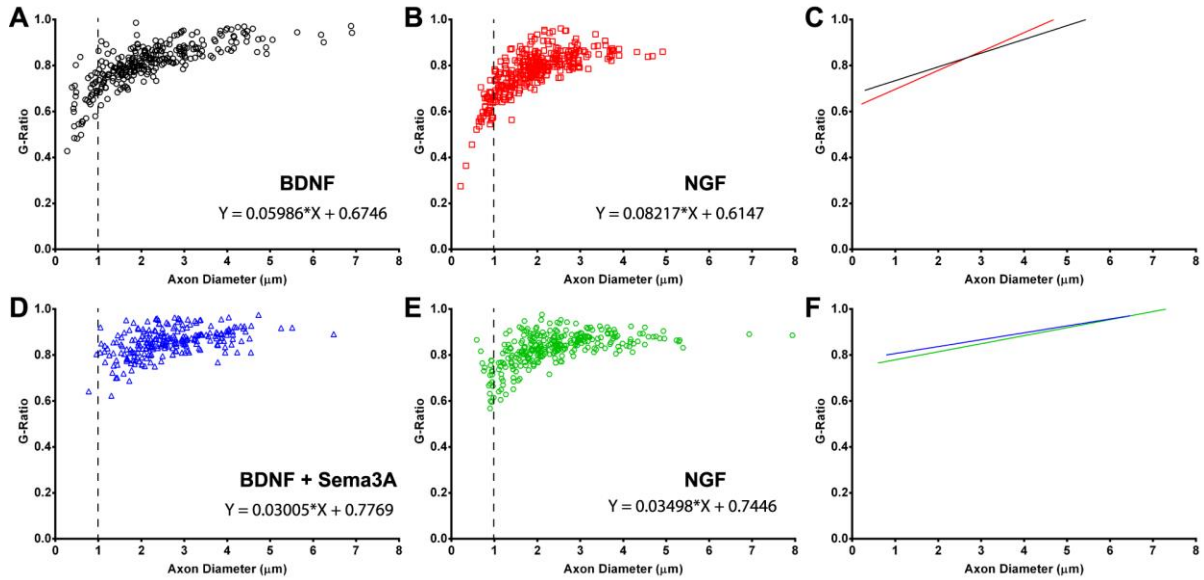


Figure 4.9. Scatter plots of g-ratio as a function of axon diameter. (A-B, D-E) G-ratio versus axon diameter for each regenerated arm ($n = 3$ animals per group). Sema3A group shows limited number of small diameter ($< 1 \mu\text{m}$) compared to the BDNF vs. NGF group. (C & F) Linear regression and equation (below scatter plots) for the individual groups. (Figure prepared with the help of Elaine Ramirez.)

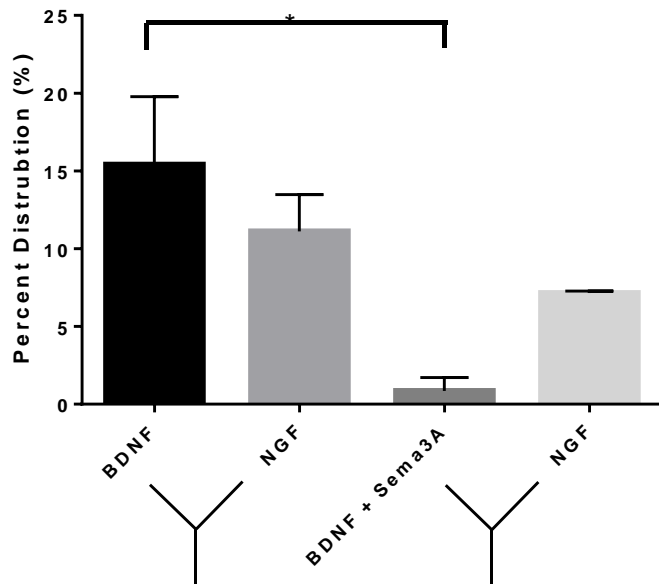


Figure 4.10. Percent distribution of myelinated axon diameter less than 1 μm . BDNF+Sema3A show significant decrease compared to BDNF only arm. * indicates significant difference between the chambers ($P \leq 0.05$, Bonferroni). Data present at mean \pm SEM.

4.4 Discussion

In this study we introduced a combination of chemoattractant and chemorepellent to improve the efficacy of axon subtype enrichment. This was tested using semaphorin3A, a repulsive cue for NGF+ axons that express the receptor neuropilin [178], [181]. Sema3A was introduced into the adjacent compartment of the NGF to direct small diameter axons away from the BDNF+Sema3A chamber. The exogenous application of the Sema3A-MP resulted in a significant reduction in the number of small axons less than 1 μm in diameter. This was verified using axon morphological measurements. However, the effect of Sema3A was also observed in the adjacent arm of the Y-conduit, resulting in a similar response but to a lesser effect in the NGF compartment. Additionally, the presence of Sema3A showed no effect on other axon subtype regeneration or

functionality as both experimental groups had comparable values. These findings demonstrate that mature sensory afferents in the peripheral nerve retain their responsiveness to the Sema3A and can have a trophic effect in a choice assay without distal targets.

4.4.1 Reduced sprouting in the presence of Sema3A

During development growth promoting molecules enable axonal elongation to their appropriate target. The selective expression of repellent cues further mediates that accuracy in path finding for the developing axons [42]. In the developing spinal cord, NGF positive C-fiber (nociceptors) respond to Sema3A, and prevent improper targeting in the dorsal laminae by restricting growth of C-fibers past the designated location. The presence of Sema3A in the adult similarly responds to mature NGF+ sensory afferent and has been shown to impede axonal sprouting in the spinal cord [43]. In this study, we demonstrated a reduced number of small diameter axons following Sema3A expression in the Y-conduits in the peripheral nerve. Scatter plots of g-ratio as a function of axon diameter, revealed limited number of axons less than 1 μm in diameter in both the NTF compartments. Conversely, the non-Sema3A group showed no inhibition of small diameter axons in either of the NTF compartments (Figure 4.9). The reduction in the small diameter myelinated axons suggest that they are A δ fibers. In previous studies, the expression of Sema3A induced a repulsive effect on small A δ fibers in the adult cornea [183]. However, this difference in the number of small fibers in the axon morphometric analysis did not show a similar effect in the distribution of DRG neurons (Figure 4.5). A plausible explanation in the comparable size distribution yet limited small diameter axons in Figure 4.9 could be the inhibition of collateral sprouting from the NGF+ axons. Our *in vivo* data agrees with observation from a similar study showing induced inhibition by Sema3A [43], [114]. Interestingly, the lack

of difference observed in the DRG size distribution suggests that the NTF exerted a strong enough effect to induce axonal elongation, but *Sema3A* was present to minimize axonal sprouting. A delicate balance between the concentration of both the attractant and the repellent is required as demonstrated when higher NGF expression can overcome the inhibitory effect of *Sema3A* [43]. Additionally, the small diameter axons observed in the NGF compartment is also indicative of the cross-diffusion by *Sema3A* to the adjacent compartment, which was also observed in the previous chapters.

Axonal sprouting in an amputee model has been previously reported by calcitonin gene-related peptide (CGRP) positive cells (marker for small caliber peptidergic nociceptors) and isolectin-B4 positive cells (marker for small caliber non-peptidergic nociceptors) [138], [184]. In the current study, FG+ cells in the DRG were stained using CGRP marker to find a correlation. However, the CGRP antibodies failed to stain FG+ cells in all experimental groups, but axonal staining within the DRG was observed (data not shown). A possible explanation is the presence of FG in the cytoplasm or on the cell surface is limiting the binding of the antibody. Additionally, the number of unmyelinated axon count in both the BDNF and BDNF+*Sema3A* compartment was comparable. This could be the presence of non-peptidergic IB4 positive DRG neurons, which are unaffected by *Sema3A*. These particular nociceptors change from NGF+ to IB4 expressing during developmental stages. The number of unmyelinated axon count in the NGF arm of the non-*Sema3A* group was higher compared to the NGF arm of the *Sema3A* group which could suggest the effect of *Sema3A* on the peptidergic axon leading to a lower unmyelinated axon count.

4.4.2 Limited specificity with two attractants

This study aimed to increase sensory axon subtype specificity using two specific NTF. BDNF to attract mechanoreceptors and NGF to entice the regeneration of thermoceptive/nociceptive neurons. However, with single NTFs in each compartment, the specificity was still not attained. The motor neuron enrichment from the BDNF compartments saw ~55% reduction compared to BDNF vs. BSA group from Chapter 1. Small caliber DRG sensory neuron enticement with NGF was also reduced by ~50% compared to the single NTF group from Chapter 1. These observations suggest the presence of NTFs in both compartment of the Y-conduits results in limited specificity.

4.4.3 Conclusion

These experiments demonstrate that exogenous chemorepellents present in the developmental stages can be implement following adult peripheral nerve injury to induce an inhibitory effect. Conversely, this inhibitory effect was not observed in motor neurons as they have been shown to moderately upregulate neuropilin and Plex-A1 mRNA level [185]–[187]. The inhibitory effect of Sema3A on a small axon subtype validate its use to potentially further improve upon the sensory/motor ratio for developing better neural interfaces. One limitation posed during this study is the cross-diffusion between the chambers. To limit the effect of each compartment on axon subtype, improved delivery method of guidance cues will need to be developed or constraint the guidance cues to their specific compartments. Also, Sema3A currently has been shown to only effect small sensory peptidergic fibers, as non-peptidergic nociceptors are

unaffected. Hence, other guidance molecules will need to be tested further in order to better understand axon selective guidance.

CHAPTER 5

5.1 Summary of thesis contribution

In this thesis, we tested the efficacy of using molecular guidance cues to direct the regeneration of a heterogeneously mixed nerve into separate compartments in an *in vivo* choice assay without distal targets. The mixed axon population of the peripheral nerve is a current limiting factor for peripheral nerve interfaces in discriminating motor and sensory subtype neurons. The concept of using molecular guidance cues was tested in this study to increase the probability of interfacing the intended axon subpopulation by modulating the sensory/motor ratio.

In Chapter 2, it was demonstrated that single NTFs were capable of enticing axonal elongation across a gap in an amputee model, and GDNF significantly increased the number of VMN compared to BSA. Furthermore, the regenerated nerve maintained its regenerated state for 45 days and 97% were electrically conductive. However, single NTFs were insufficient in modulating the sensory/motor ratio compared to the BSA control.

Chapter 3 evaluated the efficacy of motor axon guidance molecules (BDNF/GDNF) and sensory axon attractants (NGF or PTN) in altering the sensory/motor ratio. Our results show that B/G combination versus PTN showed a significant difference in the S/M ratio.

In Chapter 4, we introduced a chemorepellent to inhibit the regeneration of small sensory axon subtype. For the first time, we have demonstrated *in vivo*, small diameter A δ fibers can be inhibited following peripheral nerve axotomy and regeneration without distal targets.

The current findings from the Chapters suggest potential combinations of attractants and repellents for future applications. Using GDNF as a motor compartment can improve recording of motor intent, and applying PTN in the adjacent compartment can yield a high sensory to motor ratio. In addition, to minimize evoking unwanted sensations of pain, incorporating Sema3A can result in reduced A δ fibers. This combination of attractants and repellents can ideally provide a split regenerative based neural interface (Figure 5.1). Floating multielectrode arrays placed in the compartments of the Y-conduit will interface with the regenerating axons, and the growth factor combinations will yield a motor and sensory rich compartment.

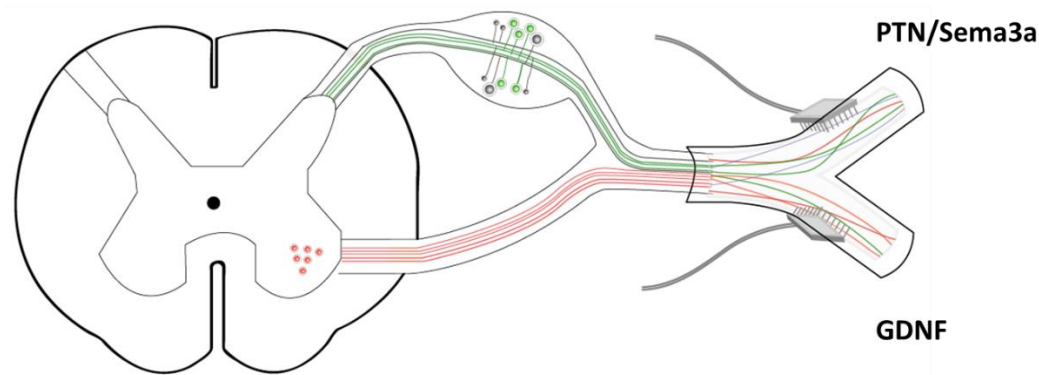


Figure 5.1. Schematic of dual choice guidance cues for a regenerative neural interface.

5.2 Additional considerations for improved enticement of axon subtype regeneration

One of the main limitations faced in this study is the cross-diffusion experienced at the bifurcation of the Y-conduit. Also, the presence of multiple NTFs did not yield an enhanced response as compared to single NTFs. Hence future work will focus on addressing these shortcomings. Some possible directions include:

- Development of a better delivery system for time release NTFs and limiting the cross-diffusion (introduction of semi-permeable barrier).
- Identifying concentrations of NTFs when used in combinations to reduce the inhibitory effect that was observed.
- Incorporate genetically labelled animals with motor and sensory subtype neurons to compensate for limited robustness of retrograde labelling.
- Validate if the modulation of sensory/motor ratio is able to improve the incidence of motor activity recording using neural interface and elicit sensory precept for specific modality. Based on the data obtained, identify or answer what is considered sufficient for motor and/or sensory enrichment.

BIBLIOGRAPHY

- [1] E. J. Lighthelm and S. C. D. Wright, "Lived experience of persons with an amputation of the upper limb," *Int. J. Orthop. Trauma Nurs.*, vol. 18, no. 2, pp. 99–106, Apr. 2016.
- [2] K. Ziegler-graham, E. J. Mackenzie, P. L. Ephraim, T. G. Trivison, R. Brookmeyer, A. Z. K, and M. Ej, "Estimating the Prevalence of Limb Loss in the United States : 2005 to 2050," vol. 89, no. March, pp. 422–429, 2008.
- [3] A. L. Dougherty, C. R. Mohrle, M. R. Galarneau, S. I. Woodruff, J. L. Dye, and K. H. Quinn, "Battlefield extremity injuries in Operation Iraqi Freedom," *Injury*, vol. 40, no. 7, pp. 772–777, Apr. 2016.
- [4] S. Micera and X. Navarro, *Bidirectional interfaces with the peripheral nervous system.*, 1st ed., vol. 86, no. 9. Elsevier Inc., 2009.
- [5] J. a Hoffer and G. E. Loeb, "Implantable electrical and mechanical interfaces with nerve and muscle.," *Ann. Biomed. Eng.*, vol. 8, no. 4–6, pp. 351–60, Jan. 1980.
- [6] L. Resnik, M. R. Meucci, S. Lieberman-Klinger, C. Fantini, D. L. Kelty, R. Disla, and N. Sasson, "Advanced upper limb prosthetic devices: implications for upper limb prosthetic rehabilitation.," *Arch. Phys. Med. Rehabil.*, vol. 93, no. 4, pp. 710–7, Apr. 2012.
- [7] T. R. Farrell and R. F. Weir, "The optimal controller delay for myoelectric prostheses.," *IEEE Trans. Neural Syst. Rehabil. Eng.*, vol. 15, no. 1, pp. 111–8, Mar. 2007.
- [8] C. Cipriani, M. Controzzi, and M. C. Carrozza, "The SmartHand transradial prosthesis.," *J. Neuroeng. Rehabil.*, vol. 8, no. 1, p. 29, Jan. 2011.
- [9] a B. Vallbo and R. S. Johansson, "Properties of cutaneous mechanoreceptors in the human hand related to touch sensation.," *Hum. Neurobiol.*, vol. 3, pp. 3–14, 1984.
- [10] E. V Evarts, "Relation of pyramidal tract activity to force exerted during voluntary movement.," *J. Neurophysiol.*, vol. 31, no. 1, pp. 14–27, 1968.
- [11] P. R. Kennedy and R. A. Bakay, "Restoration of neural output from a paralyzed patient by a direct brain connection.," *Neuroreport*, vol. 9, no. 8, pp. 1707–11, Jun. 1998.
- [12] L. V McFarland, S. L. Hubbard Winkler, A. W. Heinemann, M. Jones, and A. Esquenazi, "Unilateral upper-limb loss: satisfaction and prosthetic-device use in veterans and servicemembers from Vietnam and OIF/OEF conflicts.," *J. Rehabil. Res. Dev.*, vol. 47, no. 4, pp. 299–316, 2010.
- [13] D. J. Tyler, "Neural interfaces for somatosensory feedback: bringing life to a prosthesis,"

Curr. Opin. Neurol., vol. 28, no. 6, pp. 574–581, 2015.

- [14] J. B. Hijjawi, T. a Kuiken, R. D. Lipschutz, L. a Miller, K. a Stubblefield, and G. a Dumanian, “Improved myoelectric prosthesis control accomplished using multiple nerve transfers.,” *Plast. Reconstr. Surg.*, vol. 118, no. 7, pp. 1573–8, Dec. 2006.
- [15] T. a Kuiken, P. D. Marasco, B. a Lock, R. N. Harden, and J. P. a Dewald, “Redirection of cutaneous sensation from the hand to the chest skin of human amputees with targeted reinnervation.,” *Proc. Natl. Acad. Sci. U. S. A.*, vol. 104, no. 50, pp. 20061–6, Dec. 2007.
- [16] A. E. Schultz, P. D. Marasco, and T. A. Kuiken, “Vibrotactile detection thresholds for chest skin of amputees following targeted reinnervation surgery,” *Brain Res.*, vol. 1251, pp. 121–129, 2009.
- [17] P. D. Marasco, A. E. Schultz, and T. a Kuiken, “Sensory capacity of reinnervated skin after redirection of amputated upper limb nerves to the chest.,” *Brain*, vol. 132, no. Pt 6, pp. 1441–8, Jun. 2009.
- [18] L. a Miller, K. a Stubblefield, R. D. Lipschutz, B. a Lock, and T. a Kuiken, “Improved myoelectric prosthesis control using targeted reinnervation surgery: a case series.,” *IEEE Trans. Neural Syst. Rehabil. Eng.*, vol. 16, no. 1, pp. 46–50, Feb. 2008.
- [19] H. Huang, P. Zhou, S. Member, G. Li, and T. A. Kuiken, “An Analysis of EMG Electrode Configuration for Targeted Muscle Reinnervation Based,” vol. 16, no. 1, pp. 37–45, 2008.
- [20] J. Kim, M. Lee, H. J. Shim, R. Ghaffari, H. R. Cho, D. Son, Y. H. Jung, M. Soh, C. Choi, S. Jung, K. Chu, D. Jeon, S.-T. Lee, J. H. Kim, S. H. Choi, T. Hyeon, and D.-H. Kim, “Stretchable silicon nanoribbon electronics for skin prosthesis,” *Nat. Commun.*, vol. 5, p. 5747, 2014.
- [21] L. R. Hochberg, M. D. Serruya, G. M. Friehs, J. a Mukand, M. Saleh, A. H. Caplan, A. Branner, D. Chen, R. D. Penn, and J. P. Donoghue, “Neuronal ensemble control of prosthetic devices by a human with tetraplegia.,” *Nature*, vol. 442, no. 7099, pp. 164–71, Jul. 2006.
- [22] J. D. Simeral, S.-P. Kim, M. J. Black, J. P. Donoghue, and L. R. Hochberg, “Neural control of cursor trajectory and click by a human with tetraplegia 1000 days after implant of an intracortical microelectrode array.,” *J. Neural Eng.*, vol. 8, no. 2, p. 25027, 2011.
- [23] V. S. Polikov, P. A. Tresco, and W. M. Reichert, “Response of brain tissue to chronically implanted neural electrodes.,” *J. Neurosci. Methods*, vol. 148, no. 1, pp. 1–18, Oct. 2005.
- [24] Y. Kim and M. I. Romero-Ortega, “Material considerations for peripheral nerve interfacing,” *MRS Bull.*, vol. 37, no. 6, pp. 573–580, Jun. 2012.

- [25] J. del Valle and X. Navarro, *Interfaces with the peripheral nerve for the control of neuroprostheses.*, 1st ed., vol. 109. Elsevier Inc., 2013.
- [26] K. Horch, S. Meek, T. G. Taylor, and D. T. Hutchinson, "Object discrimination with an artificial hand using electrical stimulation of peripheral tactile and proprioceptive pathways with intrafascicular electrodes.," *IEEE Trans. Neural Syst. Rehabil. Eng.*, vol. 19, no. 5, pp. 483–9, Oct. 2011.
- [27] G. a Clark, N. M. Ledbetter, D. J. Warren, and R. R. Harrison, "Recording sensory and motor information from peripheral nerves with Utah Slanted Electrode Arrays.," *Conf. Proc. IEEE Eng. Med. Biol. Soc.*, vol. 2011, pp. 4641–4, Jan. 2011.
- [28] P. M. Rossini, S. Micera, A. Benvenuto, J. Carpaneto, G. Cavallo, L. Citi, C. Cipriani, L. Denaro, V. Denaro, G. Di Pino, F. Ferreri, E. Guglielmelli, K. P. Hoffmann, S. Raspopovic, J. Rigosa, L. Rossini, M. Tombini, and P. Dario, "Double nerve intraneural interface implant on a human amputee for robotic hand control," *Clin. Neurophysiol.*, vol. 121, no. 5, pp. 777–783, 2010.
- [29] G. S. Dhillon and K. W. Horch, "Direct neural sensory feedback and control of a prosthetic arm," *IEEE Trans. Neural Syst. Rehabil. Eng.*, vol. 13, no. 4, pp. 468–472, 2005.
- [30] D. W. Tan, M. a. Schiefer, M. W. Keith, J. R. Anderson, J. Tyler, and D. J. Tyler, "A neural interface provides long-term stable natural touch perception," *Sci. Transl. Med.*, vol. 6, no. 257, pp. 257–138, Oct. 2014.
- [31] G. Lundborg, L. B. Dahlin, N. Danielsen, R. H. Gelberman, F. M. Longo, H. C. Powell, and S. Varon, "Nerve regeneration in silicone chambers: influence of gap length and of distal stump components.," *Exp. Neurol.*, vol. 76, no. 2, pp. 361–75, May 1982.
- [32] N. Lago, E. Udina, A. Ramachandran, and X. Navarro, "Neurobiological assessment of regenerative electrodes for bidirectional interfacing injured peripheral nerves.," *IEEE Trans. Biomed. Eng.*, vol. 54, no. 6 Pt 1, pp. 1129–37, Jun. 2007.
- [33] K. Garde, E. Keefer, B. Botterman, P. Galvan, and M. I. Romero, "Early interfaced neural activity from chronic amputated nerves.," *Front. Neuroeng.*, vol. 2, no. May, p. 5, Jan. 2009.
- [34] J. L. Seifert, V. Desai, R. C. Watson, T. Musa, Y. Kim, E. W. Keefer, and M. I. Romero, "Regenerative Peripheral Nerve Interfaces Allow Recording of Early Spike Activity Despite Immature Myelination," vol. 20, no. 2, pp. 220–227, 2012.
- [35] V. H. Desai, S. Anand, M. Tran, A. Kanneganti, S. Vasudevan, J. L. Seifert, and J. Cheng, "Chronic Sensory - Motor Activity in Behaving Animals using Regenerative Multi - electrode Interfaces," *36th Annu. Int. Conf. IEEE Eng. Med. Biol. Soc.*, pp. 1973–1976,

2014.

- [36] H. Schmalbruch, “Fiber composition of the rat sciatic nerve,” *Anat. Rec.*, 1986.
- [37] T. Brushart, *Nerve Repair*. Oxford University Press, Inc., 2011.
- [38] V. E. Abraira and D. D. Ginty, “The sensory neurons of touch,” *Neuron*, vol. 79, no. 4, pp. 618–39, Aug. 2013.
- [39] W. M. Grill, S. E. Norman, and R. V Bellamkonda, “Implanted neural interfaces: biochallenges and engineered solutions,” *Annu. Rev. Biomed. Eng.*, vol. 11, pp. 1–24, 2009.
- [40] W. Schady, J. L. Ochoa, H. E. Torebjörk, and L. S. Chen, “Peripheral projections of fascicles in the human median nerve,” *Brain*, vol. 106 (Pt 3), pp. 745–760, 1983.
- [41] T. Masuda, K. Watanabe, C. Sakuma, K. Ikenaka, K. Ono, and H. Yaginuma, “Netrin-1 acts as a repulsive guidance cue for sensory axonal projections toward the spinal cord,” *J. Neurosci.*, vol. 28, no. 41, pp. 10380–5, Oct. 2008.
- [42] E. K. Messersmith, E. D. Leonardo, C. J. Shatz, M. Tessier-Lavigne, C. S. Goodman, and a L. Kolodkin, “Semaphorin III can function as a selective chemorepellent to pattern sensory projections in the spinal cord,” *Neuron*, vol. 14, pp. 949–959, 1995.
- [43] X.-Q. Tang, D. L. Tanelian, and G. M. Smith, “Semaphorin3A inhibits nerve growth factor-induced sprouting of nociceptive afferents in adult rat spinal cord,” *J. Neurosci.*, vol. 24, no. 4, pp. 819–27, Jan. 2004.
- [44] I. Dudanova, G. Gatto, and R. Klein, “GDNF acts as a chemoattractant to support ephrina-induced repulsion of limb motor axons,” *Curr. Biol.*, vol. 20, pp. 2150–2156, 2010.
- [45] B. W. Gallarda, D. Bonanomi, D. Müller, A. Brown, W. A. Alaynick, S. E. Andrews, G. Lemke, S. L. Pfaff, and T. Marquardt, “Segregation of axial motor and sensory pathways via heterotypic trans-axonal signaling,” *Science*, vol. 320, no. 5873, pp. 233–6, Apr. 2008.
- [46] H. M. Young, R. B. Anderson, and C. R. Anderson, “Guidance cues involved in the development of the peripheral autonomic nervous system,” *Auton. Neurosci.*, vol. 112, no. 1–2, pp. 1–14, 2004.
- [47] H. Park and M. M. Poo, “Neurotrophin regulation of neural circuit development and function,” *Nat Rev Neurosci*, vol. 14, no. 1, pp. 7–23, 2013.
- [48] I. Dudanova and R. Klein, “Integration of guidance cues: parallel signaling and crosstalk,” *Trends Neurosci.*, vol. 36, no. 5, pp. 295–304, May 2013.

- [49] B. J. Dickson, "Molecular mechanisms of axon guidance.," *Science*, vol. 298, no. 5600, pp. 1959–64, Dec. 2002.
- [50] C. Plachez and L. J. Richards, "Mechanisms of Axon Guidance in the Developing Nervous System," *Curr. Top. Dev. Biol.*, vol. 69, pp. 267–346, 2005.
- [51] J. Dodd and a Schuchardt, "Axon guidance: a compelling case for repelling growth cones.," *Cell*, vol. 81, pp. 471–474, 1995.
- [52] M. Tessier-Lavigne and C. S. Goodman, "The Molecular Biology of Axon Guidance," *Science (80-.)*, vol. 274, no. 5290, pp. 1123–1133, 1996.
- [53] B. P. Liu and S. M. Strittmatter, "Semaphorin-mediated axonal guidance via Rho-related G proteins.," *Curr. Opin. Cell Biol.*, vol. 13, no. 5, pp. 619–26, Oct. 2001.
- [54] L. N. Gillespie, "Regulation of axonal growth and guidance by the neurotrophin family of neurotrophic factors," *Clin. Exp. Pharmacol. Physiol.*, vol. 30, no. 10, pp. 724–733, 2003.
- [55] E. J. Huang and L. F. Reichardt, "Neurotrophins: roles in neuronal development and function.," *Annu. Rev. Neurosci.*, vol. 24, pp. 677–736, 2001.
- [56] V. M. Verge, K. a Gratto, L. a Karchewski, and P. M. Richardson, "Neurotrophins and nerve injury in the adult.," *Philos. Trans. R. Soc. Lond. B. Biol. Sci.*, vol. 351, no. 1338, pp. 423–30, Mar. 1996.
- [57] R. y Cajal, "Degeneration and Regeneration of the Nervous System," vol. 2, 1928.
- [58] R. Levi-Montaclini, "The nerve growth factor 35 years later.," *Science (80-.)*, vol. 237, pp. 1154–62, 1987.
- [59] K. Bartkowska, K. Turlejski, and R. L. Djavadian, "Neurotrophins and their receptors in early development of the mammalian nervous system," *Acta Neurobiol. Exp. (Wars)*, vol. 70, no. 4, pp. 454–467, 2010.
- [60] A. Markus, T. D. Patel, and W. D. Snider, "Neurotrophic factors and axonal growth.," *Curr. Opin. Neurobiol.*, vol. 12, no. 5, pp. 523–31, Oct. 2002.
- [61] M. D. Taylor, R. Vancura, J. M. Williams, J. T. Riekhof, B. K. Taylor, and D. E. Wright, "Overexpression of neurotrophin-3 in skeletal muscle alters normal and injury-induced limb control.," *Somatosens. Mot. Res.*, vol. 18, no. 4, pp. 286–94, 2001.
- [62] J. Kucera, G. Fan, R. Jaenisch, S. Linnarsson, and P. Ernfors, "Dependence of developing group Ia afferents on neurotrophin-3," *J. Comp. Neurol.*, vol. 363, pp. 307–320, 1995.
- [63] G. K. Essick and B. B. Edin, "Receptor encoding of moving tactile stimuli in humans. II. The mean response of individual low-threshold mechanoreceptors to motion across the

- receptive field.," *J. Neurosci.*, vol. 15, no. January, pp. 848–864, 1995.
- [64] M. D. Boada, T. T. Houle, J. C. Eisenach, and D. G. Ririe, "Differing neurophysiologic mechanosensory input from glabrous and hairy skin in juvenile rats.," *J. Neurophysiol.*, vol. 104, no. 6, pp. 3568–75, Dec. 2010.
 - [65] W. Luo, H. Enomoto, F. L. Rice, J. Milbrandt, and D. D. Ginty, "Molecular identification of rapidly adapting mechanoreceptors and their developmental dependence on ret signaling.," *Neuron*, vol. 64, no. 6, pp. 841–56, 2009.
 - [66] P. Carroll, G. R. Lewin, M. Koltzenburg, K. V Toyka, and H. Thoenen, "A role for BDNF in mechanosensation.," *Nat. Neurosci.*, vol. 1, no. 1, pp. 42–46, 1998.
 - [67] a M. LeMaster, R. F. Krimm, B. M. Davis, T. Noel, M. E. Forbes, J. E. Johnson, and K. M. Albers, "Overexpression of brain-derived neurotrophic factor enhances sensory innervation and selectively increases neuron number.," *J. Neurosci.*, vol. 19, no. 14, pp. 5919–5931, 1999.
 - [68] Y. Honma, M. Kawano, S. Kohsaka, and M. Ogawa, "Axonal projections of mechanoreceptive dorsal root ganglion neurons depend on Ret.," *Development*, vol. 137, no. 14, pp. 2319–28, Jul. 2010.
 - [69] W. D. Snider, "Functions of the Neurotrophins What the Knockouts Are Teaching Us," *Cell*, vol. 77, pp. 627–638, 1994.
 - [70] I. Fariñas, C. K. Yoshida, C. Backus, and L. F. Reichardt, "Lack of neurotrophin-3 results in death of spinal sensory neurons and premature differentiation of their precursors," *Neuron*, vol. 17, no. 6, pp. 1065–1078, 1996.
 - [71] R. a Oakley, F. B. Lefcort, P. Plouffe, a Ritter, and E. Frank, "Neurotrophin-3 promotes the survival of a limited subpopulation of cutaneous sensory neurons.," *Dev. Biol.*, vol. 224, no. 2, pp. 415–27, Aug. 2000.
 - [72] F. Wang, D. P. Julien, and A. Sagasti, "Somatosensory peripheral axon guidance and morphogenesis," vol. 7, no. 4, pp. 388–394, 2013.
 - [73] M. Fitzgerald, G. C. Kwiat, J. Middleton, and a Pini, "Ventral spinal cord inhibition of neurite outgrowth from embryonic rat dorsal root ganglia.," *Development*, vol. 117, pp. 1377–1384, 1993.
 - [74] G. Lundborg, F. M. Longo, and S. Varon, "Nerve regeneration model and trophic factors in vivo.," *Brain Res.*, vol. 232, no. 1, pp. 157–61, Jan. 1982.
 - [75] I. Allodi, E. Udina, and X. Navarro, "Specificity of peripheral nerve regeneration: interactions at the axon level.," *Prog. Neurobiol.*, vol. 98, no. 1, pp. 16–37, Jul. 2012.

- [76] M. Richner, M. Ulrichsen, S. L. Elmegaard, R. Dieu, L. T. Pallesen, and C. B. Vaegter, "Peripheral Nerve Injury Modulates Neurotrophin Signaling in the Peripheral and Central Nervous System," *Molecular Neurobiology*, 2014.
- [77] J. G. Boyd and T. Gordon, "Glial cell line-derived neurotrophic factor and brain-derived neurotrophic factor sustain the axonal regeneration of chronically axotomized motoneurons in vivo," *Exp. Neurol.*, vol. 183, pp. 610–619, 2003.
- [78] R. M. Lindsay, "Nerve growth factors (NGF, BDNF) enhance axonal regeneration but are not required for survival of adult sensory neurons.," *J. Neurosci.*, vol. 8, no. July, pp. 2394–2405, 1988.
- [79] G. Terenghi, "Peripheral nerve regeneration and neurotrophic factors.," *J. Anat.*, vol. 194, pp. 1–14, Jan. 1999.
- [80] G. D. Sterne, R. a. Brown, C. J. Green, and G. Terenghi, "Neurotrophin-3 delivered locally via fibronectin mats enhances peripheral nerve regeneration," *European Journal of Neuroscience*, vol. 9, no. 7, pp. 1388–1396, 1997.
- [81] A. W. English, W. Meador, and D. I. Carrasco, "Neurotrophin-4/5 is required for the early growth of regenerating axons in peripheral nerves.," *Eur. J. Neurosci.*, vol. 21, no. 10, pp. 2624–34, 2005.
- [82] R. Heumann, D. Lindholm, C. Bandtlow, M. Meyer, M. J. Radeke, T. P. Misko, E. Shooter, and H. Thoenen, "Differential regulation of mRNA encoding nerve growth factor and its receptor in rat sciatic nerve during development, degeneration, and regeneration: role of macrophages.," *Proc. Natl. Acad. Sci. U. S. A.*, vol. 84, no. 23, pp. 8735–9, 1987.
- [83] M. Meyer, I. Matsuoka, C. Wetmore, L. Olson, and H. Thoenen, "Enhanced synthesis of brain-derived neurotrophic factor in the lesioned peripheral nerve: different mechanisms are responsible for the," *J Cell Biol*, vol. 119, no. 1, pp. 45–54, 1992.
- [84] P. Naveilhan, W. M. ElShamy, and P. Ernfors, "Differential regulation of mRNAs for GDNF and its receptors Ret and GDNFR alpha after sciatic nerve lesion in the mouse," *Eur J Neurosci*, vol. 9, no. 7, pp. 1450–1460, 1997.
- [85] G. W. Glazner, S. Lupien, J. A. Miller, and D. N. Ishii, "Insulin-like growth factor II increases the rate of sciatic nerve regeneration in rats.," *Neuroscience*, vol. 54, no. 3, pp. 791–7, 1993.
- [86] a Höke, R. Redett, H. Hameed, R. Jari, C. Zhou, Z. B. Li, J. W. Griffin, and T. M. Brushart, "Schwann cells express motor and sensory phenotypes that regulate axon regeneration.," *J. Neurosci.*, vol. 26, no. 38, pp. 9646–55, Sep. 2006.
- [87] R. Mi, W. Chen, and A. Höke, "Pleiotrophin is a neurotrophic factor for spinal motor

- neurons.,” *Proc. Natl. Acad. Sci. U. S. A.*, vol. 104, no. 11, pp. 4664–9, Mar. 2007.
- [88] J. Jungnickel, K. Gransalke, M. Timmer, and C. Grothe, “Fibroblast growth factor receptor 3 signaling regulates injury-related effects in the peripheral nervous system,” *Mol. Cell. Neurosci.*, vol. 25, no. 1, pp. 21–29, 2004.
 - [89] R. R. Islamov, V. Chintalgattu, E. S. Pak, L. C. Katwa, and A. K. Murashov, “Induction of VEGF and its Flt-1 receptor after sciatic nerve crush injury,” *Neuroreport*, vol. 15, no. 13, pp. 2117–2121, 2004.
 - [90] A. F. Dawood, P. Lotfi, S. N. Dash, S. K. Kona, K. T. Nguyen, and M. I. Romero-Ortega, “VEGF Release in Multiluminal Hydrogels Directs Angiogenesis from Adult Vasculature In Vitro,” *Cardiovasc. Eng. Technol.*, vol. 2, no. 3, pp. 173–185, Sep. 2011.
 - [91] T. W. Gould and H. Enomoto, “Neurotrophic modulation of motor neuron development.,” *Neuroscientist*, vol. 15, no. 1, pp. 105–16, Feb. 2009.
 - [92] S. Tham, B. Dowsing, D. Finkelstein, R. Donato, S. S. Cheema, P. F. Bartlett, and W. A. Morrison, “Leukemia inhibitory factor enhances the regeneration of transected rat sciatic nerve and the function of reinnervated muscle.,” *J. Neurosci. Res.*, vol. 47, no. 2, pp. 208–15, Jan. 1997.
 - [93] M. Kirsch, U. Terheggen, and H. D. Hofmann, “Ciliary neurotrophic factor is an early lesion-induced retrograde signal for axotomized facial motoneurons,” *Mol. Cell. Neurosci.*, vol. 24, no. 1, pp. 130–138, 2003.
 - [94] P. G. Murphy, J. Grondin, M. Altares, and P. M. Richardson, “Induction of Interleukin-6 in Axotomized,” vol. 15, no. July, pp. 5130–5138, 1995.
 - [95] G. Lundborg, “Tissue Specificity in Nerve Regeneration,” *J. Plast. Reconstr. Surg.*, vol. 20, pp. 279–283, 1986.
 - [96] M. J. Politis, K. Ederle, and P. S. Spencer, “Tropism in nerve regeneration in vivo. Attraction of regenerating axons by diffusible factors derived from cells in distal nerve stumps of transected peripheral nerves.,” *Brain Res.*, vol. 253, no. 1–2, pp. 1–12, Dec. 1982.
 - [97] J. Weis and J. M. Schröder, “Differential effects of nerve, muscle, and fat tissue on regenerating nerve fibers in vivo.,” *Muscle Nerve*, vol. 12, no. 9, pp. 723–34, Sep. 1989.
 - [98] S. E. Mackinnon, A. L. Dellon, G. Lundborg, A. R. Hudson, and D. A. Hunter, “A study of neurotrophism in a primate model.,” *J. Hand Surg. Am.*, vol. 11, no. 6, pp. 888–94, Nov. 1986.
 - [99] T. M. Brushart, “Preferential reinnervation of motor nerves by regenerating motor

axons.,” *J. Neurosci.*, vol. 8, no. 3, pp. 1026–31, Mar. 1988.

- [100] T. M. Brushart, M. Aspalter, J. W. Griffin, R. Redett, H. Hameed, C. Zhou, M. Wright, a Vyas, and a Höke, “Schwann cell phenotype is regulated by axon modality and central-peripheral location, and persists in vitro.,” *Exp. Neurol.*, vol. 247, pp. 272–81, Sep. 2013.
- [101] J.-H. Hsieh, W.-M. Lin, H. Chiang, L.-Y. Chang, C.-T. Wu, C.-M. Pu, J.-T. Wu, and S.-T. Hsieh, “Patterns of target tissue reinnervation and trophic factor expression after nerve grafting.,” *Plast. Reconstr. Surg.*, vol. 131, no. 5, pp. 989–1000, May 2013.
- [102] X. Hu, J. Cai, J. Yang, and G. M. Smith, “Sensory axon targeting is increased by NGF gene therapy within the lesioned adult femoral nerve.,” *Exp. Neurol.*, vol. 223, no. 1, pp. 153–65, May 2010.
- [103] M. I. Romero, N. Rangappa, M. G. Garry, and G. M. Smith, “Functional regeneration of chronically injured sensory afferents into adult spinal cord after neurotrophin gene therapy.,” *J. Neurosci.*, vol. 21, no. 21, pp. 8408–16, Nov. 2001.
- [104] P. Lotfi, K. Garde, A. K. Chouhan, E. Bengali, and M. I. Romero-Ortega, “Modality-specific axonal regeneration: toward selective regenerative neural interfaces.,” *Front. Neuroeng.*, vol. 4, no. October, p. 11, Jan. 2011.
- [105] R. Klein, “Role of neurotrophins in mouse neuronal development.,” *FASEB J.*, vol. 8, no. 10, pp. 738–44, Jul. 1994.
- [106] M. D. Wood, H. Kim, A. Bilbily, S. W. P. Kemp, C. Lafontaine, T. Gordon, M. S. Shoichet, and G. H. Borschel, “GDNF released from microspheres enhances nerve regeneration after delayed repair.,” *Muscle Nerve*, vol. 46, no. 1, pp. 122–4, Jul. 2012.
- [107] T. Gordon, O. Sulaiman, and J. G. Boyd, “Experimental strategies to promote functional recovery after peripheral nerve injuries.,” *J. Peripher. Nerv. Syst.*, vol. 8, no. 4, pp. 236–50, Dec. 2003.
- [108] J. G. Boyd and T. Gordon, “A dose-dependent facilitation and inhibition of peripheral nerve regeneration by brain-derived neurotrophic factor.,” *Eur. J. Neurosci.*, vol. 15, no. 4, pp. 613–26, Feb. 2002.
- [109] E. G. Fine, I. Decosterd, M. Papaloïzos, A. D. Zurn, and P. Aebischer, “GDNF and NGF released by synthetic guidance channels support sciatic nerve regeneration across a long gap.,” *Eur. J. Neurosci.*, vol. 15, no. 4, pp. 589–601, Feb. 2002.
- [110] R. a Oakley, F. B. Lefcort, D. O. Clary, L. F. Reichardt, D. Prevet, R. W. Oppenheim, and E. Frank, “Neurotrophin-3 promotes the differentiation of muscle spindle afferents in the absence of peripheral targets.,” *J. Neurosci.*, vol. 17, no. 11, pp. 4262–74, Jun. 1997.

- [111] J. C. de Nooij, S. Doobar, and T. M. Jessell, "Etv1 inactivation reveals proprioceptor subclasses that reflect the level of NT3 expression in muscle targets.," *Neuron*, vol. 77, no. 6, pp. 1055–68, Mar. 2013.
- [112] C. R. Matheson, J. Carnahan, J. L. Urich, D. Bocangel, T. J. Zhang, and Q. Yan, "Glial cell line-derived neurotrophic factor (GDNF) is a neurotrophic factor for sensory neurons: comparison with the effects of the neurotrophins.," *J. Neurobiol.*, vol. 32, no. 1, pp. 22–32, 1997.
- [113] W. P. Rakowicz, C. S. Staples, J. Milbrandt, J. E. Brunstrom, and E. M. Johnson, "Glial cell line-derived neurotrophic factor promotes the survival of early postnatal spinal motor neurons in the lateral and medial motor columns in slice culture.," *J. Neurosci.*, vol. 22, no. 10, pp. 3953–3962, 2002.
- [114] X.-Q. Tang, P. Heron, C. Mashburn, and G. M. Smith, "Targeting sensory axon regeneration in adult spinal cord.," *J. Neurosci.*, vol. 27, no. 22, pp. 6068–78, May 2007.
- [115] J. L. Seifert, V. Desai, R. C. Watson, T. Musa, Y. T. Kim, E. W. Keefer, and M. I. Romero, "Normal molecular repair mechanisms in regenerative peripheral nerve interfaces allow recording of early spike activity despite immature myelination," *IEEE Trans. Neural Syst. Rehabil. Eng.*, vol. 20, no. 2, pp. 220–227, 2012.
- [116] N. Alsmadi, "Growth factor enticement of nerve regeneration. Phd dissertation," University of Texas at Arlington, 2014.
- [117] Y. Hong, J. Guan, K. L. Fujimoto, R. Hashizume, A. L. Pelinescu, and W. R. Wagner, "Tailoring the degradation kinetics of poly(ester carbonate urethane)urea thermoplastic elastomers for tissue engineering scaffolds," *Biomaterials*, vol. 31, no. 15, pp. 4249–4258, 2010.
- [118] J. Guan, K. L. Fujimoto, M. S. Sacks, and W. R. Wagner, "Preparation and characterization of highly porous, biodegradable polyurethane scaffolds for soft tissue applications," *Biomaterials*, vol. 26, no. 18, pp. 3961–3971, 2005.
- [119] N. Z. Alsmadi, L. S. Patil, E. M. Hor, P. Lofti, J. M. Razal, C.-J. Chuong, G. G. Wallace, and M. I. Romero-Ortega, "Coiled polymeric growth factor gradients for multi-luminal neural chemotaxis," *Brain Res.*, vol. 1619, pp. 72–83, 2015.
- [120] S. Ramanujan, A. Pluen, T. D. McKee, E. B. Brown, Y. Boucher, and R. K. Jain, "Diffusion and convection in collagen gels: implications for transport in the tumor interstitium.," *Biophys. J.*, vol. 83, no. 3, pp. 1650–1660, 2002.
- [121] M. B. BORNSTEIN, "Reconstituted rattail collagen used as substrate for tissue cultures on coverslips in Maximow slides and roller tubes.," *Lab. Invest.*, vol. 7, no. 2, pp. 134–137, 1958.

- [122] J. D. Murray, *Mathematical Biology Vol. II : Spatial Models and Biomedical Applications*. Secaucus, NJ, USA: Springer, 2003.
- [123] S. a. Schnell, W. a. Staines, and M. W. Wessendorf, "Reduction of Lipofuscin-like Autofluorescence in Fluorescently Labeled Tissue," *J. Histochem. Cytochem.*, vol. 47, no. 6, pp. 719–730, Jun. 1999.
- [124] M. Abercrombie, "Estimation of nuclear population from microtome sections," *Anat. Rec.*, 1946.
- [125] a a Harper and S. N. Lawson, "Conduction velocity is related to morphological cell type in rat dorsal root ganglion neurones.," *J. Physiol.*, vol. 359, pp. 31–46, 1985.
- [126] R. S. Scroggs and A. P. Fox, "Calcium current variation between acutely isolated adult rat dorsal root ganglion neurons of different size," *Physiology*, pp. 229–246, 1992.
- [127] M. J. Groves, T. Christopherson, B. Giometto, and F. Scaravilli, "Axotomy-induced apoptosis in adult rat primary sensory neurons," *J. Neurocytol.*, vol. 26, no. 9, pp. 615–624, 1997.
- [128] S. Lisney, "Regeneration of unmyelinated axons after injury of mammalian peripheral nerve," *Q. J. Exp. Physiol.*, vol. 3, pp. 757–784, 1989.
- [129] M. Richner, M. Ulrichsen, S. L. Elmegaard, R. Dieu, L. T. Pallesen, and C. B. Vaegter, "Peripheral Nerve Injury Modulates Neurotrophin Signaling in the Peripheral and Central Nervous System.," *Mol. Neurobiol.*, Apr. 2014.
- [130] M. Ikeda and Y. Oka, "The relationship between nerve conduction velocity and fiber morphology during peripheral nerve regeneration," *Brain Behav.*, vol. 2, no. 4, pp. 382–390, 2012.
- [131] S. Raspopovic, M. Capogrosso, F. M. Petrini, M. Bonizzato, J. Rigosa, G. Di Pino, J. Carpaneto, M. Controzzi, T. Boretius, E. Fernandez, G. Granata, C. M. Oddo, L. Citi, A. L. Ciancio, C. Cipriani, M. C. Carrozza, W. Jensen, E. Guglielmelli, T. Stieglitz, P. M. Rossini, and S. Micera, "Restoring natural sensory feedback in real-time bidirectional hand prostheses.," *Sci. Transl. Med.*, vol. 6, no. 222, p. 222ra19, Feb. 2014.
- [132] C. M. Oddo, S. Raspopovic, F. Artoni, A. Mazzoni, G. Spigler, F. Petrini, F. Giambattistelli, F. Vecchio, F. Miraglia, L. Zollo, G. Di Pino, D. Camboni, M. C. Carrozza, E. Guglielmelli, P. M. Rossini, U. Faraguna, and S. Micera, "Intraneural stimulation elicits discrimination of textural features by artificial fingertip in intact and amputee humans," *Elife*, vol. 5, pp. 1–27, 2016.
- [133] G. a. Clark, S. L. Schister, N. M. Ledbetter, D. J. Warren, F. Solzbacher, J. D. Wells, M. D. Keller, S. M. Blair, L. W. Rieth, and P. R. Tathireddy, "Selective, high-optrode-count,

artifact-free stimulation with infrared light via intrafascicular Utah slanted optrode arrays,” 2012, vol. 8207, p. 820751.

- [134] B. R. Dowden, M. a Frankel, R. a Normann, and G. a Clark, “Non-invasive method for selection of electrodes and stimulus parameters for FES applications with intrafascicular arrays.,” *J. Neural Eng.*, vol. 9, no. 1, p. 16006, Feb. 2012.
- [135] a Branner and R. a Normann, “A multielectrode array for intrafascicular recording and stimulation in sciatic nerve of cats.,” *Brain Res. Bull.*, vol. 51, no. 4, pp. 293–306, Mar. 2000.
- [136] G. S. Dhillon, S. M. Lawrence, D. T. Hutchinson, and K. W. Horsch, “Residual function in peripheral nerve stumps of amputees: implications for neural control of artificial limbs.,” *J. Hand Surg. Am.*, vol. 29, no. 4, pp. 605–15–8, Jul. 2004.
- [137] T. Gordon, “The physiology of neural injury and regeneration: The role of neurotrophic factors.,” *J. Commun. Disord.*, vol. 43, no. 4, pp. 265–73, 2010.
- [138] N. Lago and X. Navarro, “Evaluation of the long-term regenerative potential in an experimental nerve amputee model.,” *J. Peripher. Nerv. Syst.*, vol. 12, no. 2, pp. 108–20, Jun. 2007.
- [139] Y. Sakai, M. Ochi, Y. Uchio, K. Ryoke, and S. Yamamoto, “Prevention and treatment of amputation neuroma by an atelocollagen tube in rat sciatic nerves.,” *J. Biomed. Mater. Res. B. Appl. Biomater.*, vol. 73, no. 2, pp. 355–60, May 2005.
- [140] N. Danielsen, B. C. Shyu, L. B. Dahlin, G. Lundborg, and S. A. Andersson, “Absence of ongoing activity in fibres arising from proximal nerve ends regenerating into mesothelial chambers.,” *Pain*, vol. 26, no. 1, pp. 93–104, Jul. 1986.
- [141] B. Blondet, “Pleiotrophin Cellular Localization in Nerve Regeneration after Peripheral Nerve Injury,” *J. Histochem. Cytochem.*, vol. 53, no. 8, pp. 971–977, 2005.
- [142] P. Ernfors, a Henschen, L. Olson, and H. Persson, “Expression of nerve growth factor receptor mRNA is developmentally regulated and increased after axotomy in rat spinal cord motoneurons.,” *Neuron*, vol. 2, pp. 1605–1613, 1989.
- [143] M. Taniuchi, H. B. Clark, and E. M. Johnson, “Induction of nerve growth factor receptor in Schwann cells after axotomy.,” *Proc. Natl. Acad. Sci. U. S. A.*, vol. 83, no. 11, pp. 4094–8, 1986.
- [144] H. Kashiba, B. Hyon, and E. Senba, “Glial cell line-derived neurotrophic factor and nerve growth factor receptor mRNAs are expressed in distinct subgroups of dorsal root ganglion neurons and are differentially regulated by peripheral axotomy in the rat.,” *Neurosci. Lett.*, vol. 252, no. 2, pp. 107–10, Aug. 1998.

- [145] J. Badia, A. Pascual-Font, M. Vivó, E. Udina, and X. Navarro, "Topographical distribution of motor fascicles in the sciatic-tibial nerve of the rat.," *Muscle Nerve*, vol. 42, no. 2, pp. 192–201, Aug. 2010.
- [146] H. Funakoshi, J. Frisé, G. Barbany, T. Timmusk, O. Zachrisson, V. M. K. Verge, and H. Persson, "Differential expression of mRNAs for neurotrophins and their receptors after axotomy of the sciatic nerve," *J. Cell Biol.*, vol. 123, no. 2, pp. 455–465, 1993.
- [147] L. Novikov, L. Novikova, and J.-O. Kellerth, "Brain-derived neurotrophic factor promotes axonal regeneration and long-term survival of adult rat spinal motoneurons in vivo," *Neuroscience*, vol. 79, no. 3, pp. 765–774, 1997.
- [148] J. D. Stewart, "Peripheral nerve fascicles: anatomy and clinical relevance.," *Muscle Nerve*, vol. 28, no. 5, pp. 525–41, Nov. 2003.
- [149] R. D. Madison, M. V. Sofroniew, and G. A. Robinson, "Schwann cell influence on motor neuron regeneration accuracy," *Neuroscience*, vol. 163, no. 1, pp. 213–221, 2009.
- [150] J. M. Lee, P. Tos, S. Raimondo, M. Fornaro, I. Papalia, S. Geuna, and M. G. Giacobini-Robecchi, "Lack of topographic specificity in nerve fiber regeneration of rat forelimb mixed nerves.," *Neuroscience*, vol. 144, no. 3, pp. 985–90, Mar. 2007.
- [151] Y. Iwabuchi, Y. Maki, T. Yoshizu, and H. Narisawa, "Lack of topographical specificity in peripheral nerve regeneration in rats.," *Scand. J. Plast. Reconstr. Surg. Hand Surg.*, vol. 33, no. 2, pp. 181–5, Jun. 1999.
- [152] G. A. Robinson and R. D. Madison, "Manipulations of the mouse femoral nerve influence the accuracy of pathway reinnervation by motor neurons," *Exp. Neurol.*, vol. 192, no. 1, pp. 39–45, 2005.
- [153] T. Gordon, "The role of neurotrophic factors in nerve regeneration.," *Neurosurg. Focus*, vol. 26, no. 2, p. E3, Feb. 2009.
- [154] M. E. Brushart, "Motor Axons Preferentially Reinnervate," vol. 13, no. June, pp. 2730–2738, 1993.
- [155] T. Uschold, G. A. Robinson, and R. D. Madison, "Motor neuron regeneration accuracy: Balancing trophic influences between pathways and end-organs," *Exp. Neurol.*, vol. 205, no. 1, pp. 250–256, 2007.
- [156] R. D. Madison, G. A. Robinson, and S. R. Chadaram, "The specificity of motor neurone regeneration (preferential reinnervation)," *Acta Physiol.*, vol. 189, no. 2, pp. 201–206, 2007.
- [157] I. Allodi, E. Udina, and X. Navarro, "Specificity of peripheral nerve regeneration:

- interactions at the axon level.,” *Prog. Neurobiol.*, vol. 98, no. 1, pp. 16–37, Jul. 2012.
- [158] X. Mu, I. Silos-Santiago, S. L. Carroll, and W. D. Snider, “Neurotrophin receptor genes are expressed in distinct patterns in developing dorsal root ganglia.,” *J. Neurosci.*, vol. 13, no. 9, pp. 4029–41, Sep. 1993.
- [159] P. Ernfors, C. M. Rosario, J. P. Merlio, G. Grant, H. Aldskogius, and H. Persson, “Expression of mRNAs for neurotrophin receptors in the dorsal root ganglion and spinal cord during development and following peripheral or central axotomy.,” *Brain Res. Mol. Brain Res.*, vol. 17, no. 3–4, pp. 217–26, Mar. 1993.
- [160] N. R. Kobayashi, A. M. Bedard, M. T. Hincke, and W. Tetzlaff, “Increased expression of BDNF and trkB mRNA in rat facial motoneurons after axotomy.,” *Eur. J. Neurosci.*, vol. 8, no. 5, pp. 1018–29, May 1996.
- [161] F. Piehl, J. Frisén, M. Risling, T. Hökfelt, and S. Cullheim, “Increased trkB mRNA expression by axotomized motoneurons.,” *Neuroreport*, vol. 5, no. 6, pp. 697–700, Feb. 1994.
- [162] J. G. Boyd and T. Gordon, “The neurotrophin receptors, trkB and p75, differentially regulate motor axonal regeneration,” *J. Neurobiol.*, vol. 49, no. 4, pp. 314–325, 2001.
- [163] S. O. Yoon, P. Casaccia-Bonofil, B. Carter, and M. V Chao, “Competitive signaling between TrkA and p75 nerve growth factor receptors determines cell survival.,” *J. Neurosci.*, vol. 18, no. 9, pp. 3273–3281, 1998.
- [164] J. E. Swett, R. P. Wikholm, R. H. Blanks, a L. Swett, and L. C. Conley, “Motoneurons of the rat sciatic nerve.,” *Exp. Neurol.*, vol. 93, no. 1, pp. 227–52, Jul. 1986.
- [165] D. A. Chad, U. DeGirolami, and J. Zivin, “Motor fibers in sural nerve,” *Acta Neuropathol.*, vol. 71, pp. 338–340, 1986.
- [166] P. Gentile, V. Chiono, I. Carmagnola, and P. Hatton, “An Overview of Poly(lactic-co-glycolic) Acid (PLGA)-Based Biomaterials for Bone Tissue Engineering,” *Int. J. Mol. Sci.*, vol. 15, no. 3, pp. 3640–3659, Feb. 2014.
- [167] J. Dargahi and S. Najarian, “Human tactile perception as a standard for artificial tactile sensing--a review.,” *Int. J. Med. Robot.*, vol. 1, no. 1, pp. 23–35, 2004.
- [168] F. Marmigère and P. Ernfors, “Specification and connectivity of neuronal subtypes in the sensory lineage.,” *Nat. Rev. Neurosci.*, vol. 8, no. 2, pp. 114–27, Feb. 2007.
- [169] A. W. Harrington and D. D. Ginty, “Long-distance retrograde neurotrophic factor signalling in neurons.,” *Nat. Rev. Neurosci.*, vol. 14, no. 3, pp. 177–87, Mar. 2013.
- [170] A. Branner, R. B. Stein, E. Fernandez, Y. Aoyagi, and R. a Normann, “Long-term

stimulation and recording with a penetrating microelectrode array in cat sciatic nerve.,” *IEEE Trans. Biomed. Eng.*, vol. 51, no. 1, pp. 146–57, Jan. 2004.

- [171] L. Djouhri, X. Fang, S. Koutsikou, and S. N. Lawson, “Partial nerve injury induces electrophysiological changes in conducting (uninjured) nociceptive and nonnociceptive DRG neurons: Possible relationships to aspects of peripheral neuropathic pain and paresthesias.,” *Pain*, vol. 153, no. 9, pp. 1824–36, Sep. 2012.
- [172] A. M. McCormick and N. D. Leipzig, “Neural regenerative strategies incorporating biomolecular axon guidance signals,” *Ann. Biomed. Eng.*, vol. 40, no. 3, pp. 578–597, 2012.
- [173] D. Bagnard, *Axon Growth and guidance*. 2007.
- [174] X. Navarro, M. Vivó, and A. Valero-Cabré, “Neural plasticity after peripheral nerve injury and regeneration.,” *Prog. Neurobiol.*, vol. 82, no. 4, pp. 163–201, Jul. 2007.
- [175] S. Y. Fu and T. Gordon, “The cellular and molecular basis of peripheral nerve regeneration.,” *Mol. Neurobiol.*, vol. 14, no. 1–2, pp. 67–116, 1997.
- [176] B. R. Seckel, “Enhancement of peripheral nerve regeneration.,” *Muscle nerve*, vol. 13, no. 9, pp. 785–800, 1990.
- [177] “Unified nomenclature for the semaphorins/collapsins. Semaphorin Nomenclature Committee.,” *Cell*, vol. 97, no. 5, pp. 551–2, May 1999.
- [178] F. Nakamura, R. G. Kalb, and S. M. Strittmatter, “Molecular basis of semaphorin-mediated axon guidance.,” *J. Neurobiol.*, vol. 44, no. 2, pp. 219–29, Aug. 2000.
- [179] J. Ara, P. Bannerman, A. Hahn, S. Ramirez, and D. Pleasure, “Modulation of sciatic nerve expression of class 3 semaphorins by nerve injury.,” *Neurochem. Res.*, vol. 29, no. 6, pp. 1153–9, Jun. 2004.
- [180] A. Kaselis, R. Treinys, R. Vosyliute, and S. ??atkauskas, “DRG axon elongation and growth cone collapse rate induced by Sema3A are differently dependent on NGF concentration,” *Cell. Mol. Neurobiol.*, vol. 34, no. 2, pp. 289–296, 2014.
- [181] V. D. Dontchev and P. C. Letourneau, “Nerve growth factor and semaphorin 3A signaling pathways interact in regulating sensory neuronal growth cone motility.,” *J. Neurosci.*, vol. 22, no. 15, pp. 6659–6669, 2002.
- [182] Y. Wanigasekara and J. R. Keast, “Nerve growth factor, glial cell line-derived neurotrophic factor and neurturin prevent semaphorin 3A-mediated growth cone collapse in adult sensory neurons,” *Neuroscience*, vol. 142, no. 2, pp. 369–379, 2006.
- [183] D. L. Tanelian, M. A. Barry, S. A. Johnston, T. Le, and G. M. Smith, “Semaphorin III can

repulse and inhibit adult sensory afferents in vivo.,” *Nat. Med.*, vol. 3, no. 12, pp. 1398–401, 1997.

- [184] C. Witzel, C. Rohde, and T. M. Brushart, “Pathway sampling by regenerating peripheral axons,” *J. Comp. Neurol.*, vol. 485, no. 3, pp. 183–190, 2005.
- [185] F. De Winter, A. J. G. D. Holtmaat, and J. Verhaagen, “Neuropilin and class 3 semaphorins in nervous system regeneration.,” *Adv. Exp. Med. Biol.*, vol. 515, pp. 115–39, 2002.
- [186] R. J. Pasterkamp, R. J. Giger, and J. Verhaagen, “Regulation of semaphorin III/collapsin-1 gene expression during peripheral nerve regeneration.,” *Exp. Neurol.*, vol. 153, no. 2, pp. 313–27, Oct. 1998.
- [187] I. Gavazzi, J. Stonehouse, A. Sandvig, J. N. Reza, L. S. Appiah-Kubi, R. Keynes, and J. Cohen, “Peripheral, but not central, axotomy induces neuropilin-1 mRNA expression in adult large diameter primary sensory neurons.,” *J. Comp. Neurol.*, vol. 423, no. 3, pp. 492–9, Jul. 2000.

BIOGRAPHICAL SKETCH

Sanjay Anand received his BS in Biomedical Engineering from the Georgia Institute of Technology in Atlanta, Georgia in 2009. After graduation, he continued to work in Dr. Ravi Bellamkonda's research lab as a Research Technologist for another 1.5 years. Sanjay then pursued his Doctoral degree in the joint Bioengineering program between The University of Texas at Arlington, The University of Texas Southwestern Medical Center and The University of Texas at Dallas. His research focused on using developmental guidance cues to modulate the axonal composition of peripheral nerves for improved neural interfaces. During this graduate work he presented his work in multiple national meetings and received the GAANN Fellowship to aid in his doctoral work. Sanjay was invited as a guest speaker at Plexon Inc. Workshop in 2013. Sanjay is a member of a number of scientific organizations including BMES student chapter and SfN Dallas chapter, among others. His goal is to work on cutting edge neural interfacing technology and to develop more intuitive prosthesis.

CURRIVULUM VITAE

EDUCATION:

University of Texas at Dallas
Ph.D. in Bioengineering

Richardson, TX
December 2016

Georgia Institute of Technology
B.S. in Biomedical Engineering

Atlanta, GA
December 2009

PUBLICATIONS:

Anand, S, Desai, V, Vasudevan, S, Nguyen, D, Tran, M, Myint, N, Alsmadi, N, Kanneganti, A, Hong, Y, Cheng, J, Keefer, E and Romero-Ortega, MI (2016) Sensory to motor ratio modulation using dual attractants in a *in vivo* choice assay. (*In print*)

Gu L, Uhelski ML, **Anand S**, et al. (2015) Pain Inhibition by Optogenetic Activation of Specific Anterior Cingulate Cortical Neurons. Price TJ, ed. *PLoS ONE*. 10(2)

Desai, V.H.; **Anand, S.**; Tran, M.; Kanneganti, A.; Vasudevan, S.; Seifert, J.L.; Cheng, J.; Keefer, E.W.; Romero-Ortega, M.I., "Chronic sensory-motor activity in behaving animals using regenerative multi-electrode interfaces," *Engineering in Medicine and Biology Society (EMBC), 2014 36th Annual International Conference of the IEEE*, vol., no., pp.1973,1976, 26-30 Aug. 2014

Kanneganti A, **Anand S**, Desai V, Kim YT, Keefer E, Romero-Ortega MI (2012) "Closed-loop Peripheral Nerve Interfacing through Regenerative Multielectrode Arrays" 17th Annual Meeting of the International Functional Electrical Stimulation Society, Banff, Alberta. Sept 9-12. (Peer Reviewed)

Karumbaiah, L., S. E. Norman, N.B. Rajan, **Anand S**, et al. (2012). "The upregulation of specific interleukin (IL) receptor antagonists and paradoxical enhancement of neuronal apoptosis due to electrode induced strain and brain micromotion." *Biomaterials* **33**(26): 5983-5996.

Karumbaiah, L., **Anand, S**, et al. (2011). "Targeted downregulation of N-acetylgalactosamine 4-sulfate 6-O-sulfotransferase significantly mitigates chondroitin sulfate proteoglycan-mediated inhibition." *Glia* **59**(6): 981-996.

PROFESSIONAL AND ACADEMIC CONFERENCE PRESENTATIONS:

Anand S, Desai VH, et al. Sensory and Motor Enrichment using Molecular Guidance Cues (Neural Interface Conference 2014)

Tran M, **Anand S**, Desai VH et al. Functional Regeneration of Axons into Surrogate Muscle and Skin Targets (Synapse Conference, NC 2014)

Nguyen DH, **Anand S** et al. Peripheral nerve guidance using muscle and skin targets for neural interface (ACES 2014)

Anand S, Kanneganti A, et al. Modality Specific Neural Interface in the Peripheral Nervous System (ACES 2011)

Anand S, Kanneganti A, Desai V et al. Regenerative Multi-Electrode Interfacing of the Tibial Nerve (Neural Interface Conference 2012)

Anand S, Desai V et al. Modality Specific Neural Interfacing in the PNS (Podium Talk - BMES 2012)

Lohitash Karumbaiah, Sharon Norman, Nithish Rajan, **Sanjay Anand**, Ravi Bellamkonda. Stretch Induced Astroglial Stress Negatively Regulates Neuronal Growth (Termis 2010)

Karumbaiah, L., **Anand S**. et al. Chondroitin sulfate-4,6 glycosaminoglycan significantly inhibits rat embryonic day 18 (E18) cortical neurons in vitro and chondroitin 4,6 sulfotransferase mRNA is over-expressed after CNS injury (SFN 2010)

AWARDS AND HONORS:

GAANN Fellowship	Fall 2012 – Spring 2014
Stem Scholarship	Fall 2011 – Spring 2014
HOPE Scholarship	Fall 2005 – Spring 2009
Dean's List	Fall 2005 – Fall 2007
President's Undergraduate Research Award	Fall 2009

TEACHING POSITIONS:

Graduate Teaching Assistant:

BE 5382 Laboratory Principles -Physiology (University of Texas at Arlington)

Fall 2013; Spring 2014

- Designed experiments to measure different types of physiological activity (EMG, EEG, ECG, EGG etc.) within the human body.

BMEN 3330 Engineering Physiology of the Human Body (University of Texas at Dallas)

Fall 2014 & 2015

- Assisted students in understanding engineering components of the human body and delivered lectures on individual physiological systems.

BMEN 4330 Advanced Eng. Physiology of the Human Body (University of Texas at Dallas)
Spring 2015

- Help design/teach course to complement latest research on bioengineering components and relate to human physiological systems.

SKILLS AND TECHNIQUES:

Lab Procedures: *In vitro* cell culture (Rat/mice – DRG, Spinal Cord, Cortex), Bradford assays, Spot/Stripe Assay, Silver Stain assay, western blotting, RiboGreen assay, Protein patterning, RT-PCR, Electrophysiology neural recording, *In vivo* animal surgery, immunohistochemistry, Microparticle fabrication

Equipment: Bright field/fluorescent/Confocal microscope, MicroFab JetLab II, Confocal microscopy, Plexon Electrophysiology Recording,

Software: Microsoft Office, Visual Basics, MATLAB, Simulink, ImageJ, LabVIEW, HTML, SolidWorks, Media Cybernetics Image-Pro, Prism, Adobe Illustrator/Photoshop, SketchUp